BIPEDAL ROBOTIC WALKING ON GRANULAR MATERIAL: AN INERTIAL AND KINEMATIC CONTROL APPROACH

A Thesis
Presented to
The Academic Faculty

By

Jonathan R. Gosyne

In Partial Fulfillment
of the Requirements for the Degree
Master of Science in the
School of Mechanical Engineering

Georgia Institute of Technology

December 2018

BIPEDAL ROBOTIC WALKING ON GRANULAR MATERIAL: AN INERTIAL AND KINEMATIC CONTROL APPROACH

Approved by:

Dr. Daniel I. Goldman, Advisor
School of Physics
Georgia Institute of Technology

Dr. Gregory S. Sawicki
School of Mechanical Engineering
Georgia Institute of Technology

Dr. Anirban Mazumdar
School of Mechanical Engineering
Georgia Institute of Technology

Date Approved: November 14, 2018

As each has received a gift, use it to serve one another, as good stewards of God's varied grace

1 Peter 4:10, ESV

To Uncle Subesh and Aunty Debbie

ACKNOWLEDGEMENTS

During my time at Georgia Tech, I have been blessed with the privilege and honour of being surrounded by intelligent, driven and supportive mentors and peers. I would like to thank Dr. Daniel Goldman for his constant stream of advice, guidance and mentorship, and Dr. Christian Hubicki for his encouragement, mentorship and direction over the course of this project. I would also like to extend my heartfelt thanks to Dr. Gregory Sawicki and Dr. Anirban Mazumdar for their time spend on the thesis reading committee, and Dr. Aaron Ames for his collaboration on this project.

I have found that the CRAB Lab is nothing short of a magnet for incredible people, and would like to extend my gratitude to each and every member for their support throughout the entirety of this process. I would like to give special thanks to Enes Aydin for his incredible systems engineering expertise, and his seemingly never-ending source of unique and challenging perspectives, as well as Dr. Yasemin Aydin for her patience and wealth of technical advice, particularly as I sought to climb a bit of a learning curve during the foundational parts of this project. I would also like to thank Margot Paez, Will Savoie, Kelimar Diaz, Xiaobin Xiong and Seth Daly for their technical input, as well as Ian Tomkinson and Kehinde Aina for their friendship and witty, thought provoking conversation. And of course, I would like to thank Victoria Joh for her love and never ending support from the very beginning of this project.

TABLE OF CONTENTS

LIST OF TABLES

LIST OF FIGURES

SUMMARY

Bipedal robotic locomotion in granular media presents a unique set of challenges at the intersection of granular physics and robotic locomotion. In this project, we performed a series of systematic design implementations, trials and experiments to enable a 7 degree-of-freedom planar biped walker to robustly traverse granular inclines. We hypothesize that, through the optimization of open loop gait, variation of inertial properties, and development of contact area control, a robust locomotion system for biped robotic locomotion on granular media can be identified.

While the balancing and locomotion of biped systems has been widely studied for decades, these systems are typically in the context of body-based balancing on hard ground. Such schemes largely encompass control based on body and joint torques as a way to stabilize the biped system. However, when faced with complex, highly non-linear complex matter, such as granular material, these techniques alone are insufficient. This thesis discusses the development of a gait system and control scheme that encompasses static inertial changes through torso re-positioning, and dynamic contact area variation, to allow for robust, steady gait over granular media.

This thesis contains six main chapters, each focusing on pertinent points concerning the biped walker, Chapter 1 begins with an overview of our problem space, relevant work within it, and our key motivations. Chapter 2 then focuses on our system design, test bed specification and engineering requirements. After this, Chapter 3 covers the biped's electrical design, While chapter 4 covers the mechanical design of the system. Once the electrical and mechanical aspects are discussed, chapter 5 highlights the software approach used to govern the system. Finally, chapter 6 contains observations and our experimental design and results, and future directions. These results provide increased insight into the design, sensitivity and robustness of gaits on granular material, as well as the kinematic, inertial and geometric changes necessary for stable locomotion on complex media.

CHAPTER 1
INTRODUCTION

1.1 Robophysics - The Intersection of Robotics and Physics

Robots are amazing tools that can be used for a wide variety of applications. From early automata as far back as the Roman empire, to state-of-the-art systems that are barely distinguishable from their human creators [1], robotic systems have never ceased to capture human fascination. A key feature of distinction between robotic and biological systems however, is that of autonomy. Even though this gap continues to close, robotic systems, unlike animals, require input to produce commanded motion. Similarly, robotic systems have sensory mechanisms that require analysis and interpretation. This however, can be advantageous to scientists and researchers, in that they are able to manipulate inputs and measure the resulting outputs; this would be incredibly difficult to do with biological organisms in a controlled, repeatable manner. This has been done for organisms such as turtles, rattlesnakes, lizards, and even humanoids [2–4]. From this, the importance of a robophysical approach can be seen in the study of biped robotics over complex terrain. Systematic studies and robust experimentation can help us better characterize the behaviour and boundary interaction of bipeds, both robotic and biological, and will allow us to create more informed solutions for applications in health care, agriculture, defence, and beyond.

1.2 Objective

A solid robophysical model is imperative in designing a hypothesis, an experiment, and obtaining a meaningful set of results. As such, this thesis will first discuss and document the development of a robophysical model of a biped robotic system. This is explored particularly through the lens of electrical, mechanical and software perspectives. This will

then allow us to make observations and glean insights about the implementation of gait over granular media. After this, we will then examine the experimental design, in which we optimize gaits for the walker when locomoting up a granular incline. This thesis will also document and provide a preliminary analysis for the experimental results and, finally, this document seeks to make meaningful observations from the use of a bio-inspired geometric and inertial control to augment our optimal gait. This is accomplished through the use of robust sensing and will provide a comparative analysis of open loop and controlled gait designs. Using this analysis, we will then comment on future directions.

1.3 Bipedal Locomotion on Sand

1.3.1 Biological Locomotion

Biological locomotion in sand has been found to manifest itself in many ways across countless species of organisms [2]. When more specifically focusing on biped locomotion, however, we can, for the sake of thesis, think of these systems as belonging to certain broad categories, as seen in fig. 1.1 and table 1.1. Conventionally, biped human walking in sand is achieved through manipulation of body weight distribution, intrusion angle, and intrusion forces [5]. One key point to note in this case is that humans have a high enough mass to enable this sort of intrusion behaviour. However, when systems with very low mass to contact areas are examined [6, 7], we find that these organisms, such as the sidewinder rattlesnake or zebra tailed lizard, have developed unique geometric adaptations to produce effective locomotion in complex environments. Since the robot walker discussed in this thesis is a low-mass system, it is quite insightful to consider these low mass systems as biological inspiration, in addition to conventional bipeds.

1.3.2 Robotic Locomotion

Historically, the key idea used to allow locomotion of biped robots has been to find methods that allow for the maintenance of dynamic stability of the system. This has been used

Table 1.1: A table showing examples of biological systems that ambulate on granular material, classified according to mass and speed.

	Low Speed	High Speed
High Mass	Human	Common Ostrich
Low Mass	Sidewinder Rattlesnake	Zebra Tailed Lizard

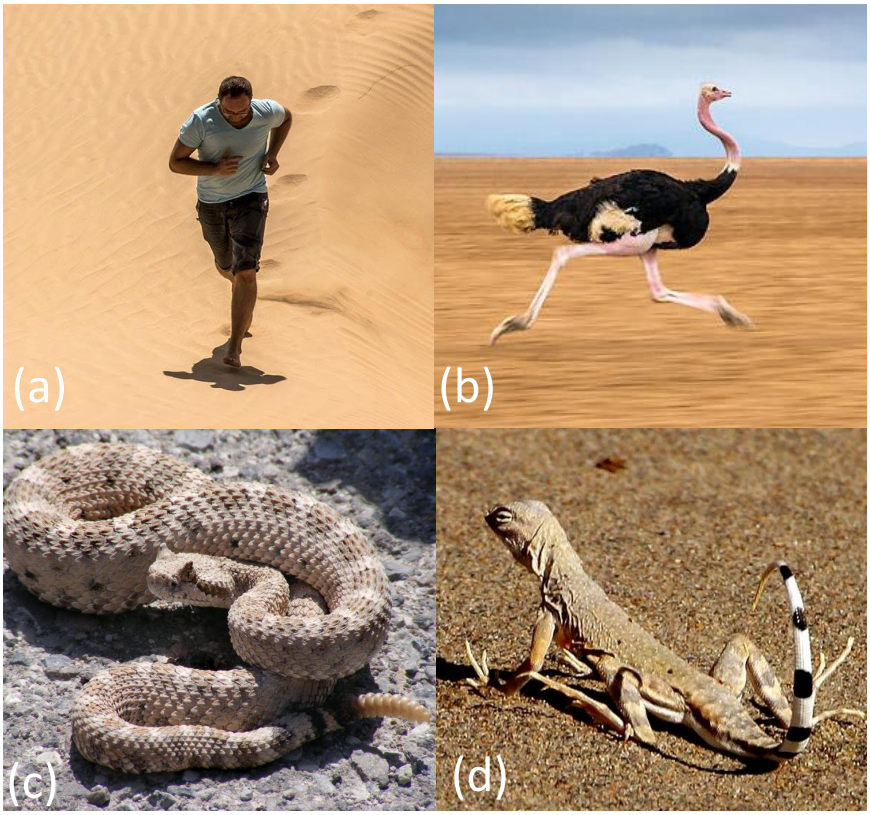

Figure 1.1: (a) shows human walking on sand, an example of a high mass, low speed system on granular material. (Photo Courtesyn BRL Sports) (b) shows an ostrich, *Struthio camelus*, a high mass, high speed system. (Photo Credit Klein Hubert). Both of these rely heavily on inertial biological control. (c) and (d) show the Sidewinder Rattlesnake, *Crotalus cerastes* and the Zebra Tailed Lizard, *Callisaurus draconoides*. These are examples of low mass systems that travel at low and high speed respectively. (Photo Credit: Wikipedia)

for decades, across as wide range of applications, as seen in Fig. 1.2. Such schemes usually entail the robot's gait being generated and controlled within a dynamically or quasi-statically stable area on the ground surface [8–18]. To this effect, many robots have made use of systems such as Hybrid Zero Dynamics (HZD) [8], Zero Moment Point (ZMP) [9], and other methods of manipulating parameters in order to maintain the dynamic stability of the system, in order to generate planar, or even three-dimensional paths. However, these have largely been in the context of flat footed walking over flat ground. Thus, in order to better study the phenomena of bipedal walking over granular material, it is necessary for us to consider the use of a specialized biped robot and system that can better allow the study of slip types, slip detection, and as a result, the necessary adjustments, that are necessary for biped locomotion over complex, granular material.

1.3.3 Granular Media

As stated above, granular material was the choice of complex matter used in the experiments that are detailed in this thesis [19]. Perhaps one of the most interesting features of this type of material is that during legged locomotion, the material can display properties of both solids and fluids [7]. While the study of Rheology and Terradynamics are exciting, developing fields with numerous practical application, predictive models are still not well understood. Thus, the systematic experimentation and characterization discussed in this thesis allows us to increase the scope of understanding in this area.

1.4 Background and Relevant Work

Perhaps one of the most intuitive and widely implemented methods of controlling biped robotic systems is through the use of inertial feedback, particularly in terms of acceleration and position feedback. This has been implemented as a highly effective solution that can account for environmental disturbances, and is usually achieved by installing inertial measurement units (IMU's) at strategic points on the head or body of the system. Much like

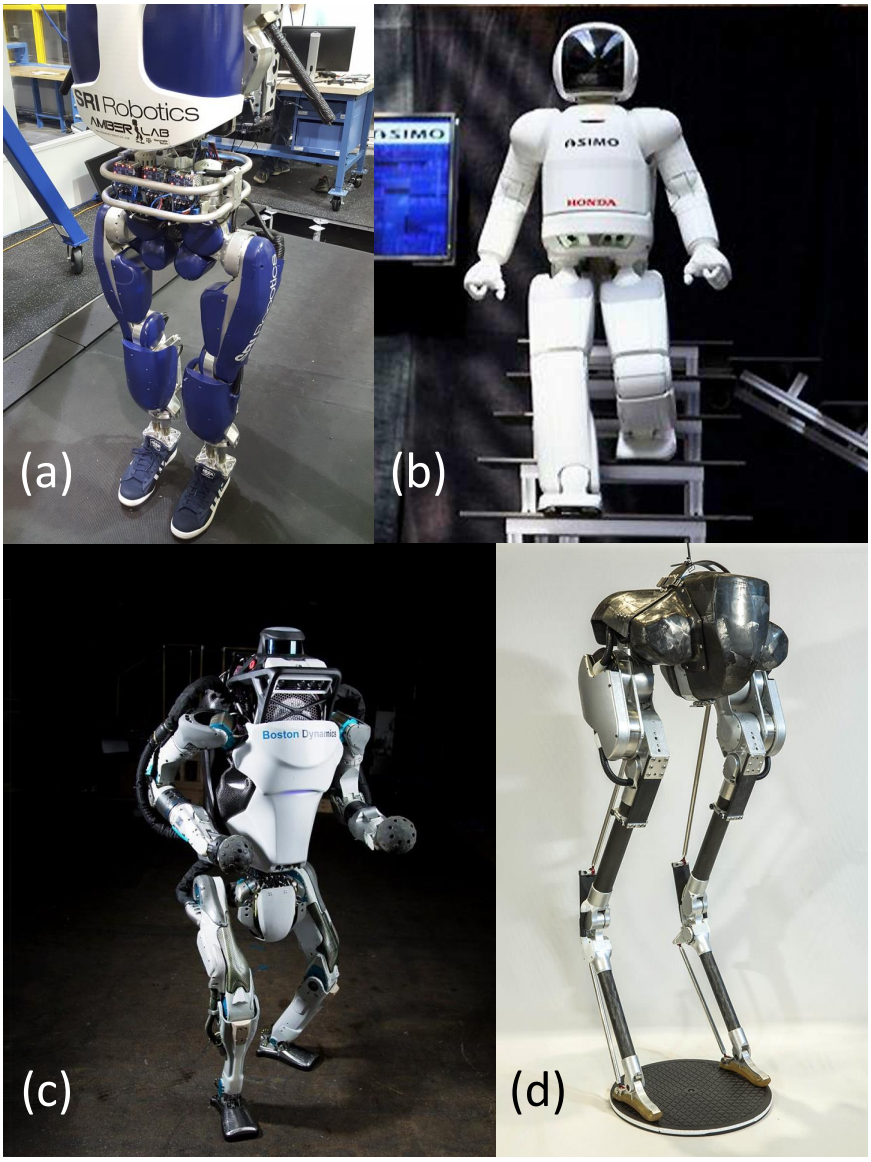

Figure 1.2: Various walking robot systems. (a) shows Durus, a humanoid robot that uses dynamic stabilization techniques similar to biological systems. Photo courtesy AMBER Lab (b) shows Asimo, perhaps the most popular biped robot. Similar to the robot used in this study, Asimo uses Zero Moment Point Walking as the preferred method for generating stable gaits. Photo courtesy Honda Robotics. (c) The Atlas systems is currently one of the most advanced biped robotic systems and is a good example of the robustness of bipeds when bio-inspired sensor fusion is implemented. Photo Courtesy Boston Dynamics (d) shows the Cassie robot, an example of non-human bio-inspiration in biped robotic design.Photo Courtesy Agility Robotics

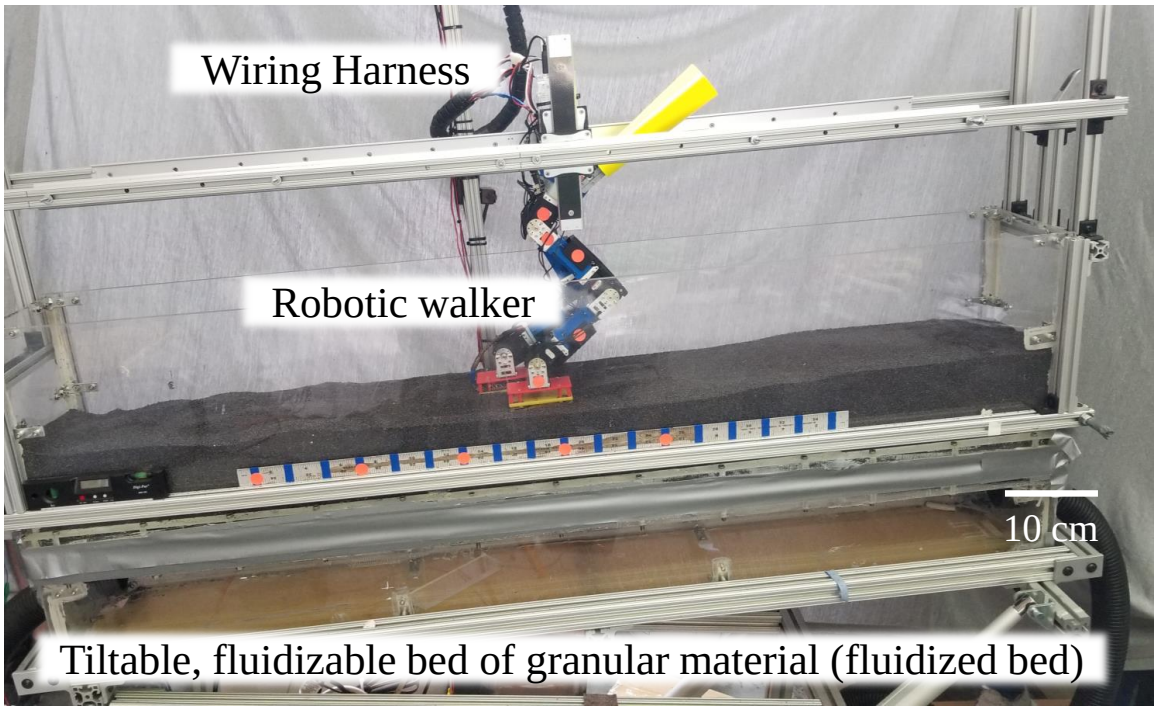

Figure 1.3: A picture showing the primary granular test bed setup used for experimentation.

in biological systems, sensory data is fed into a control center that then signals motion or re-positioning of the torso or appendages as necessary [12]. However, most use cases of inertial control tend to be over terrain with predictive material properties [2]. Thus, because of the unpredictable non-linearities associated with granular media, for instance sand, it is important that we also lean heavily on the control and manipulation of the geometry and kinematics of the system [4].

When examining the mechanics of biped locomotion, we see that typical bipedal walking has an alternating single and double support phase (SSP and DSP) [3], which is well studied for ground where a robot's feet do not have complex interactions with the substrate on which it ambulates. These interactions may include, but are not limited to penetration or slip on the boundary of the surface. For biological systems, these complex surfaces are typically accounted for through sensing and processing of the resulting forces on the plantar surface of the foot, using input as a feed-forward into a complex, proprioceptive feedback system [1, 20–24]. In addition, biological systems are able to augment their locomotion

though the use of visual and memory-based cues. Much in line with this complex biological model, previous work has in fact showed that it is difficult to enable and optimize walking in a robotic system over sand without estimation of the complex force interactions that occur at the surface [2, 7].

Once again ,when we look to biological systems, one of the key corrections that bipeds make, when using position and boundary force information, is that of kinematic repositioning [5, 25]. This supports the idea that adjusting the gait kinematics can allow slope climbing on complex terrain for biped robots. This was previously investigated for simulated human gait through variation of the parameters of step height, center of mass (CoM) height and step length [13]. These use simulated vestibular IMU input to control torso position, as well as a simulated kinesthetic sense through force and torque sensors to govern joint positions. The focus was a kinesthetic augmentation of the vestibular sense to provide stability when walking over complex terrain, and served as a good indicator of gait adjustments for uphill gait design.

While force feedback [5] from the foot contact on a sandy surface is incredibly important for CoM stabilization of a human subject, this feedback serves as a means to an end. There needs to be significantly different gait patterns due to unique effects of walking on a changing substrate compared to the typical levels of energetics and mechanical work done for biped gait over flat ground. This is much in line with the findings of our experimental trials discussed later in this thesis and also supports other work [2, 7], that suggests that instantaneous force feedback was necessary for robust dynamic balancing in biped walking over complex terrain. This therefore serves to reinforce the need for robust analysis of feedback from the plantar surface of biped systems.

Once again, examining the literature, it is apparent that the force feedback from biological systems alters the system response from both an inertial and geometric perspective [6, 7]. As mentioned above, for the scope of this thesis, we will consider biological systems on granular media as either high or low mass. We see than systems with higher mass, or more

accurately those with higher plantar pressure, tend to utilize inertial control as a primary mechanism for balance and locomotion [5]. This is due to their higher mass causing higher level of compaction, and then providing a semi-rigid platform on which it can push off [2, 3, 5]. However, low mass systems may not be able to efficiency effect the say manner of platform generation, and thus have to take advantage of geometric properties as a way of overcoming the challenge of locomotion [6]. This geometric approach served as a large source of inspiration in the experiments described in this thesis.

In order to traverse a slope or inclined surface, the regular ZMP equation must be modified. This is because of the need to accommodate the fact that in any given phase where both feet make contact with the surface, one leg will be higher than the other [14]. Since traditional ZMP trajectories assume the contact point of both feet must be coplanar [14, 15], we considered the uphill trajectories of the robot to be along a virtual slope.

As can be seen, the study of walking on granular material is an area that is still novel, with many potential research directions spanning many disciplines. This thesis will begin to explore inertial, geometric and kinematic factors in biped gait design, and interesting observations and phenomena on which future work can be built.

CHAPTER 2
SYSTEM DESIGN

To be able to conduct a set of trials, we must first have a robust platform on which we base our experiments. This chapter discusses the general approach of the system design, including the robot walker and the test bed as seen in Fig 2.1 [4]. Through the examination of design constraints and choices, we will provide a basis for more detailed discussion of the electrical, mechanical, and software components in the chapters to come.

2.1 Design Objectives

To begin the design and implementation of a system, a set of parameters was identified in the design that allowed for effective operation and meaningful experimentation. These included: safety, autonomy, robustness, durability, repeatability, translatability, and maintainability. These are summarized in Table 2.1.

2.1.1 Safety

As stated above, it was of key importance that the robot system be safe for handing by the operator, as well as non-hazardous to others and the surrounding environment. To achieve this a number of measures were implemented. To begin, the robot was designed without any sharp edges that would come into direct contact with the operators. This was to ensure safe handling of the robot between experiments.

From an electrical standpoint, multiple safety measures were implemented to avoid harm to operators and the environment. Firstly, all wires were properly insulated and kept away from moisture to avoid electrical hazards. As seen in Fig. 2.2, a master safety switch was included in the experimental setup. This allowed a quick, easy way to cut power to the system in case of emergency.

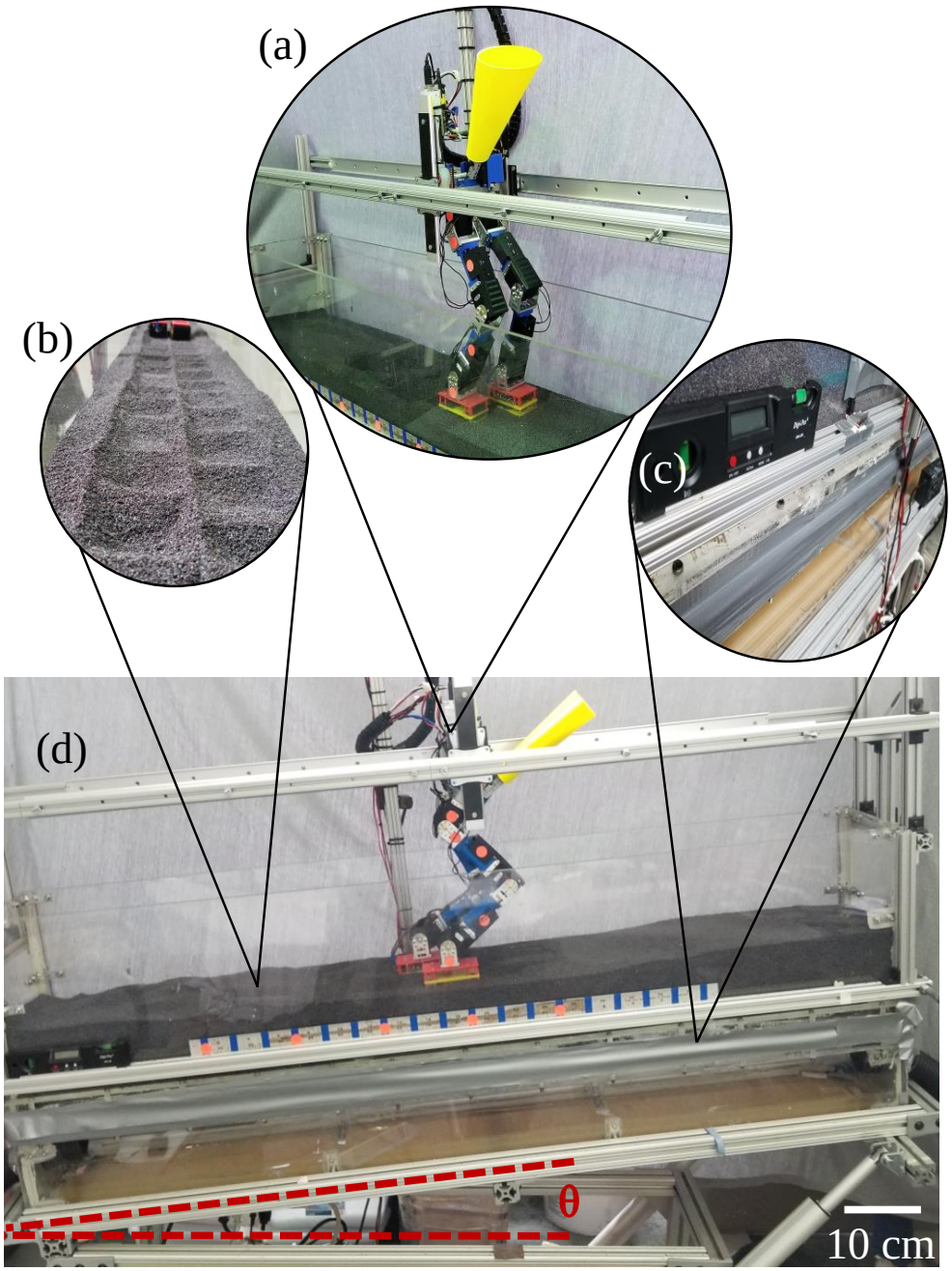

Figure 2.1: (a) A picture of the 7 degree of freedom planar biped robotic walker used during the experimental trials. (b) Staircase tracks made in the poppyseed bed, reflecting the type of gait design methods used. Poppy seeds were used to simulate coarse sand in order to avoid excess wear on the biped walker. (c) Microcontroller and leveling system for the testbed that controlled slope angle. (d) The robot constrained to the sagittal plane during an experimental trial on the bed.

Table 2.1: A table summarizing the different design requirements considered when developing or augmenting the robot system.

Design Requirement	Detailed Description
Safety	The robot must be constructed in such a way that ensures that it will not cause harm to the operator, surrounding individuals, or the environment in which it is tested.
Autonomy	For certain aspects of the experiment, the robot should be able to read in, interpret data, and react without the need for operator intervention.
Robustness	The robot should be resistant to damage from tipping, slipping or falling over at moderate to high speed, and should maintain a similar level of performance before and after a failure.
Durability	The robot should be able to run repeated trials without significant loss of performance due to wear and tear of its constituent parts.
Repeatability	Robot should be able to perform the same task in a repeatable manner within a very small margin of error.
Translatability	The robot and system should be designed in such a way to allow for implementation on different platforms, be they larger, smaller, or of similar scale.
Maintainability	The system should be able to be easily repaired or augmented through the use of easily attainable, readily available components

Additionally, the system incorporated a fuse system, as seen in Fig. 2.3, attached to the bed actuator, to stop uncontrolled elevation in the event of a power surge. This was also coupled with isolated power supplies with common grounds (Fig. 2.4) to avoid excess current pull and heat generation on any one supply. Apart from this, the robot also included

Figure 2.2: A picture showing the emergency cutoff switch

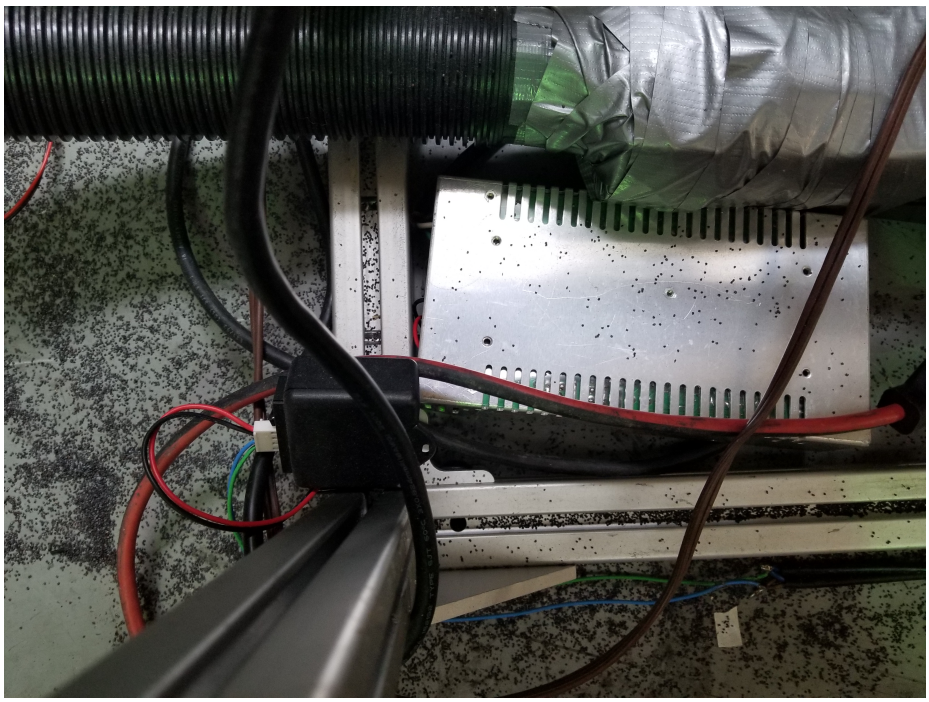

Figure 2.3: A picture showing remote receptor and fuse

a strain-based servo power release (Fig. 2.5) that would disengage when excess strain was placed on the servo wires. As shown in Fig. 2.6, meticulous cable management was also employed to avoid snag, tangling and shear of power and communication wires.

Apart from these, there were safety measures put in place by the software interface. The robot had a stall torque that was programmed to be lower than that which could cause significant operator injury. Additionally, emergency shutdown protocol were enacted when the torque output or temperatures of the motors became too high.

Another noteworthy safety mechanism that was built into the foot's construction was break-free connections between the linear actuators and the toe/heel units. In the even of too high of a moment being applied to the linear actuator, the tip of the toe/heel unit was designed to split, causing a drop in the levels of normal torque on the actuator itself. This can be seen in Fig 2.7.

The test bed also had multiple safety features built into its structure and function. These will be further discussed in section 2.2, where the bed is discussed in further detail.

Figure 2.4: A picture showing the power supply array

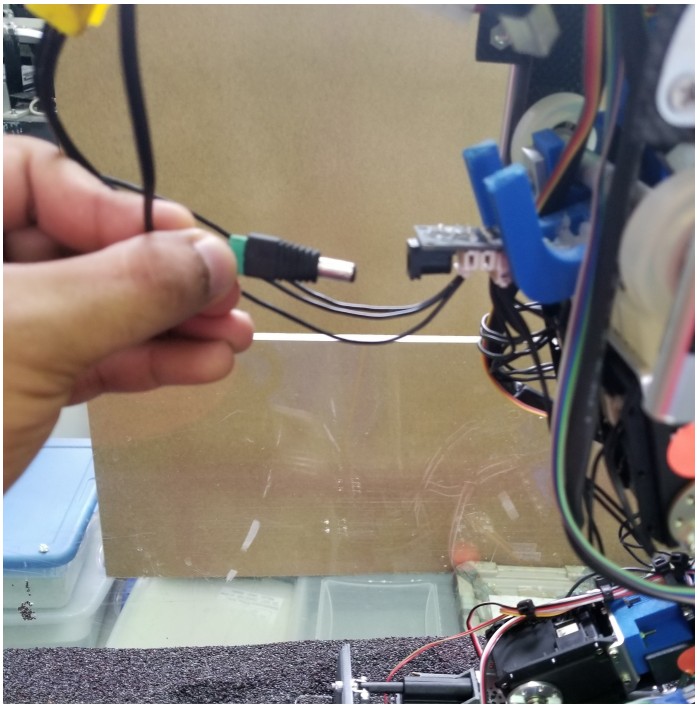

Figure 2.5: A picture showing the strain-based release

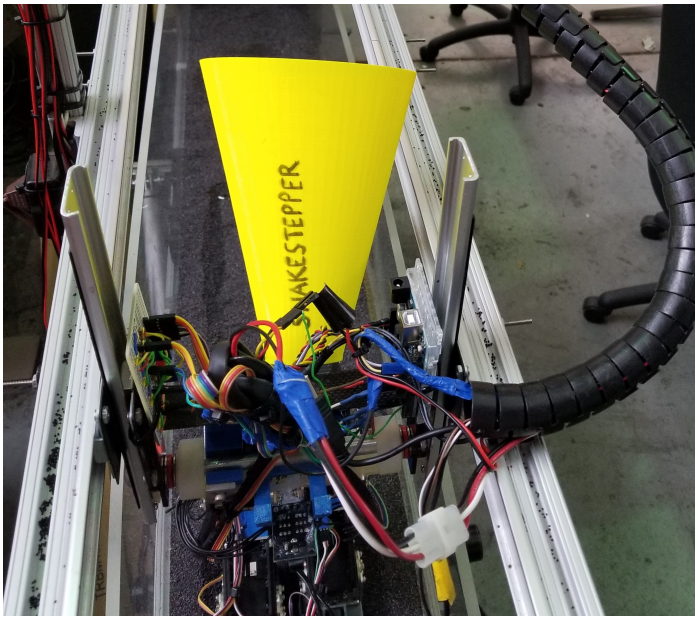

Figure 2.6: A picture showing cable harness and cable management onboard the robot

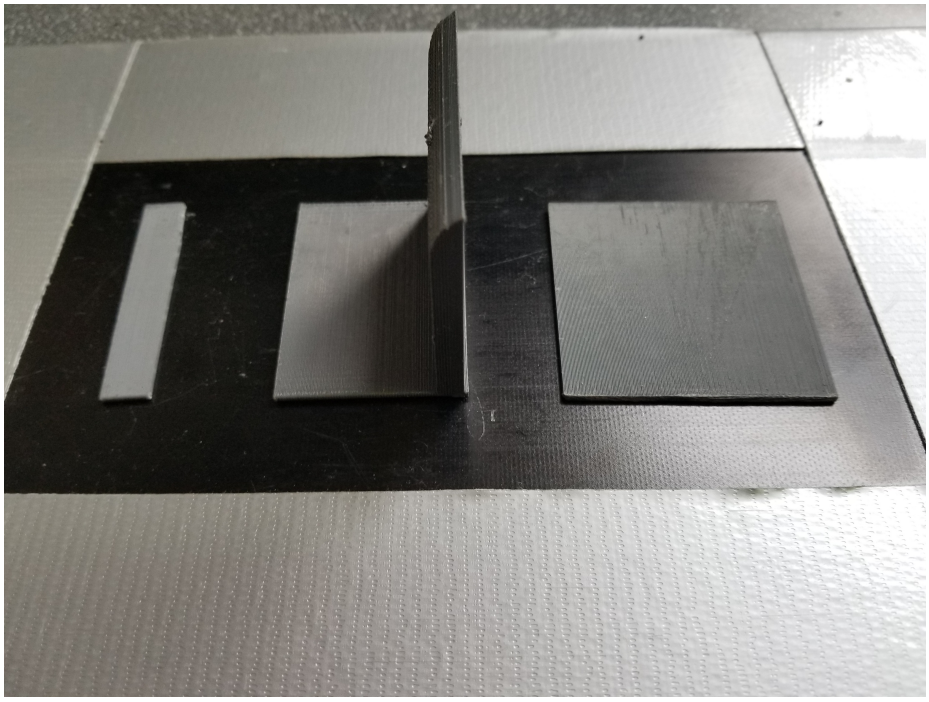

Figure 2.7: A picture showing splitting of the heel/toe mechanism due to moment application

2.1.2 Autonomy

As previously stated, over the course of the experiment, it was necessary for the robot to interpret data, and react without the need for operator intervention. In lieu of a fully automated system, small changes were implemented to better automate the system; one step that was taken to make the robot ”smart” was to then incorporate instantaneous slope angle feedback into the system. An Inertial Measurement Unit (IMU) was installed on the bed to automatically input an angle to the biped code before each trial, at which point it would react accordingly (Fig. 2.8). When compared to the analogue leveling system, the accuracy of the automated system was found to be within $\pm 5^{\circ}$.

2.1.3 Robustness

As mentioned in table 2.1, the robot was repeatedly put in situations where system failure was analyzed. Over the course of thousands of trials, the robot was subject to tipping and

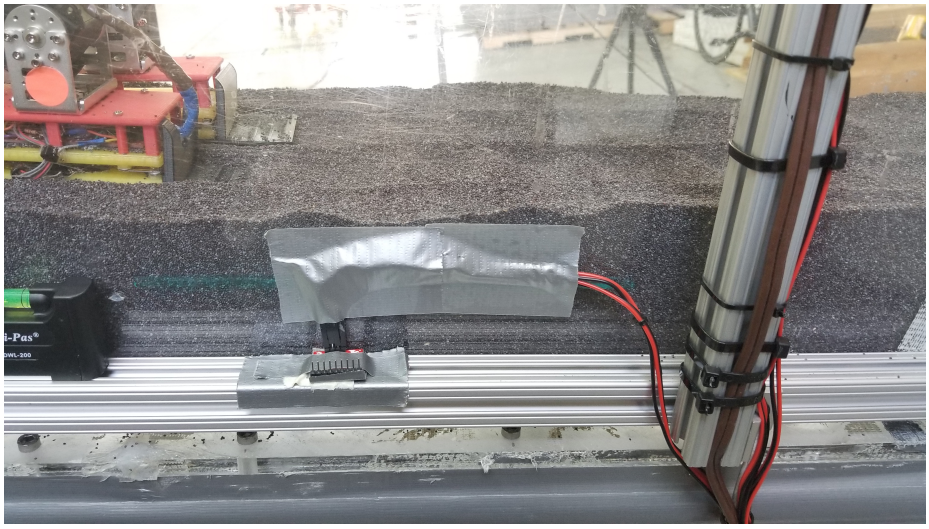

Figure 2.8: A picture showing the IMU Automation System on the test bed

slipping failure over hard and soft ground, as well as unpredictable high velocity impacts from servo sputter. As such, the system was constructed in such a way to be adequately strong and resistant to fracture. A key way that components were protected was through the use of protective shielding on the legs of the robot. This protected the wiring running to and from the feet, and reduced the number of poppy seeds lodged in the servo motors. Similarly, all of the wiring itself was coated and fastened to avoid detachment and malfunction.

2.1.4 Durability

The durability of the system was an important factor that was considered during robot design. Because of the high volume and long hours of the trials being run, it was necessary to develop the electrical and mechanical system in such a way to endure high levels of fatigue. To achieve this, the components were chosen such that they operated well within the bounds of their range. Circuity was securely attached to the robot, voltage regulation was used on the power supplies, and vulnerable mechanical parts were shielded. Regular maintenance of parts was done in conjunction with the above to extend part life to well beyond the scope of the experiments covered in this thesis.

2.1.5 Repeatability

For an experiment to be valid, there needs to be some level of repeatablility. Given a set of initial conditions, the robot should be able to reproduce similar results within a very small margin of error. The parts used in the system were chosen, as stated above and below, to have a high level of durability and maintainability. They were also chosen to allow for similar performance levels throughout the part life, as well as when components were replaced.

2.1.6 Translatability

One of the inspirations for doing this project lies in the idea of studying trends in locomotion to develop a theory of behaviour and control. As such, the robot needed to be designed in such a way that its scheme could be easily adaptable to other, more complex biped systems.

2.1.7 Maintainability

The issue of maintainability is incredibly important when attempting to efficiently conduct an experiment. Early in the design process, it became a matter of utmost importance to use components that were readily available from reputable online distributors, electronics dealers or hardware stores. This ensured the ability to obtain the necessary components for upgrade and repair of the system in a quick, cost efficient manner. Additionally, a large portion of the robot's body utilized 3D printed components, which allowed for rapid design, prototyping, and implementation of robot parts.

2.2 Test Bed Design

The main area in which the robot was operated was, as mentioned above, a test bed of granular material. This was designed in such a way to allow for safe, easy operation, and

to planarize the system to allow for simplified data analysis.

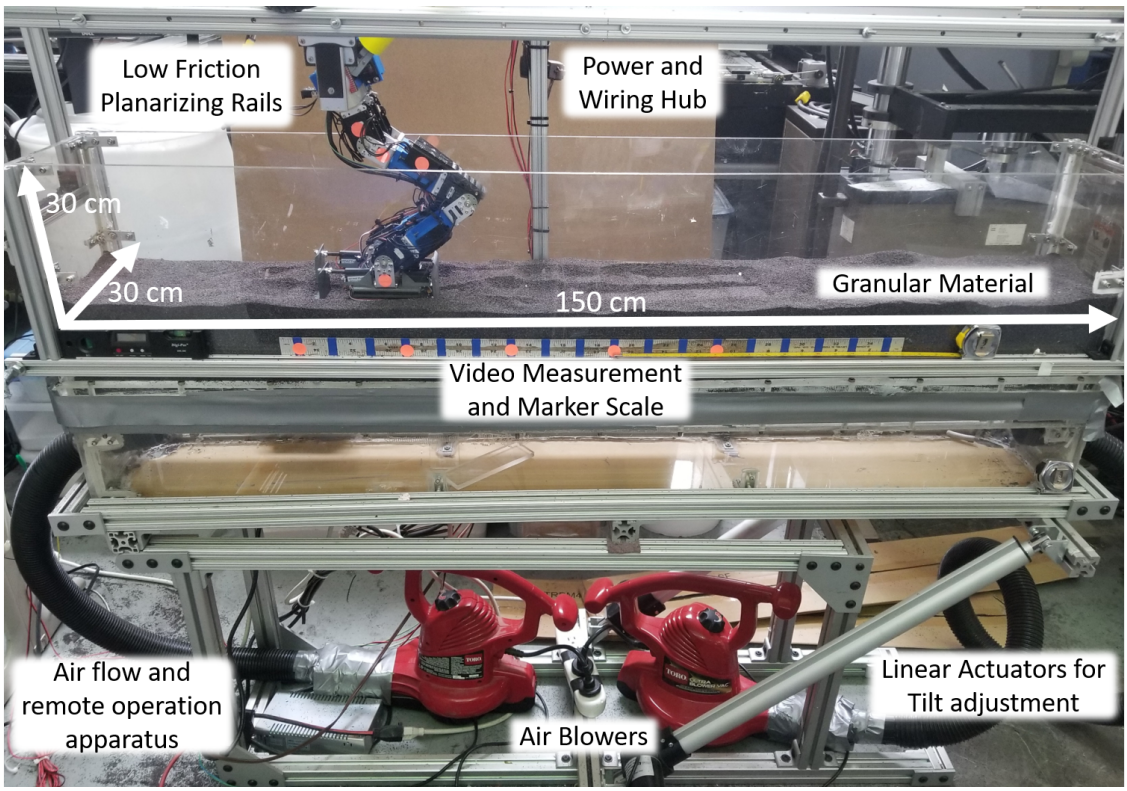

Figure 2.9: An annotated picture showing the test bed apparatus used in the experiments.

2.2.1 Design Overview

The key motivation in designing a test bed system was to allow for the walking robot to run large numbers of trials in a repeatable, reliable manner over extended periods of time. The test bed itself was constructed primarily out of aluminum 6061, and can be seen in Fig. 2.9. This served as a rigid platform on which additional components could be placed. The aluminum was used to construct two main components: the base and the granular bed. The base of the test bed housed electronics, such as the fuse, remote control receptor, emergency stop switch, and power distribution hubs. Additionally, it also served as a containment unit for the blowers that will be discussed further in this subsection. With respect to power and signal distribution, a harness containing all power and signal wires

was run from the base to the top of the system to counteract the gravitational effect of wire weight on the robot. Connected by a hinge and pair of high powered linear actuators, the base of the test bed was attached to the top, granular bed section. The poppy seeds themselves were housed in a plexiglass containment unit, while the low friction tracks for the robot were constructed using carbon fiber and aluminum, and ran parallel to the top of the plexiglass. Housed right outside of the plexiglass containment unit was the inertial measurement system, which allowed for position feedback from the granular bed. The low friction tracks ran the length of the test bed, and were the key mechanism for planarizing the robot walker. This allowed us to eliminate yaw and roll from the system, and let us focus primarily on pitch stabilization. A main feature of the system was the ability to fluidize the bed of poppy seeds, leaving a uniform, loosely packed surface. To achieve this, air was blown from the two blowers on either side of the test bed into a fluid chamber under the poppy seeds, as seen in 2.9. Once the air entered the chamber, it was forced upward through a mesh and semi-permeable membrane to cause aeration and fluidization of the granular material. To contain air flow, silicone caulk was used as a sealant, and bolts were used for reinforcement.

2.2.2 Poppy Seeds as Simulated Sand

When considering locomotion of organisms on granular material, the material itself presents an amazing amount of complexity. For this thesis, we attempted to recreate the behaviour of sand through the use of poppy seeds. We are interested in the reactionary properties of granular material when an external force is applied; of particular importance is that granular material itself can behave like a solid under compaction conditions, but can also exhibit fluid properties. In nature, while granular material may manifest itself in different forms, from sand to snow, to mud, it has been found that for small, regular particles, the fluid behavior of any granular material is approximately equivalent for the distinct cases of loose and tight compaction states. [7]. This being considered, since poppy seed pro-

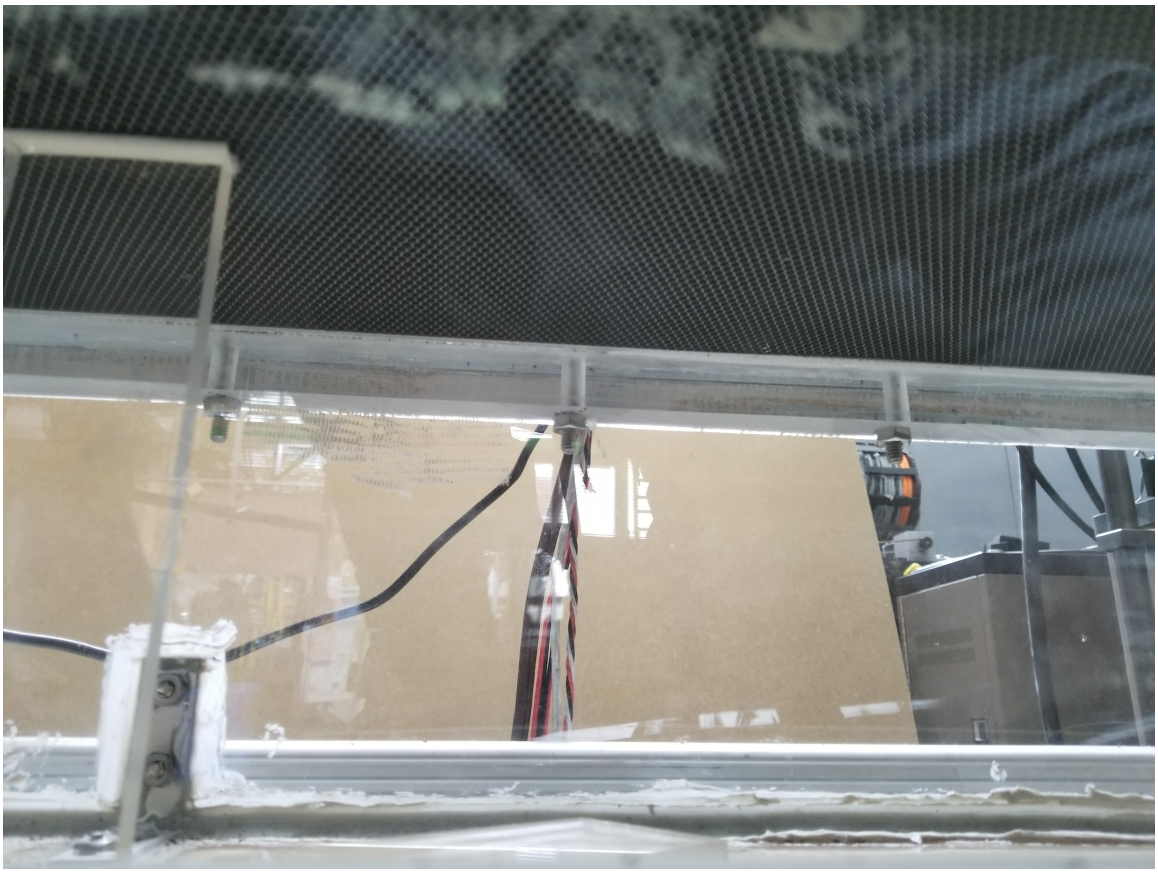

Figure 2.10: A picture showing the fluid chamber and mesh used under the poppy seed bed. This served as a mechanism to fluidize and then loosely pack the test bed.

duce less abrasion on robot components, and are readily available in large volumes at local agriculture depots, they became a natural choice for our simulated granular media.

2.2.3 Fluidization and Compaction

The primary group of experiments in this thesis were conducted using loosely packed material. During prototyping, granular material was also manually compacted to better simulate hard ground. Future plans include the installation of a compaction motor system on the test bed.

Figure 2.11: A picture showing the intrusion of footsteps into the granular surface.

2.2.4 Planarization and Directionality

As mentioned above, the system allowed for bidirectional planarization, and thus, the elimination of roll and yaw from the system. This was important because it allowed us to focus on the pitch aspect of the control scheme without needing to designate time and resources toward three dimensional control. We theorize that similar methods found for a two dimensional, planar case can be applied to a full scale three dimensional model.

CHAPTER 3
ELECTRICAL DESIGN

This chapter discusses the design and implementation of the electrical and electromechanical systems involved in the construction and operation of the biped walker. It is broken up into four main areas: microcontrollers, sensors, actuators and power systems, with each being discussed with respect to their iterative design and the final system.

3.1 Microcontrollers

While much of the joint angle trajectory computations for the biped gait are performed on a remote PC (discussed further in Chapter 5), for in-the-loop sensing and control, we required a microcontroller unit. This is a small, single-unit, low power computing system that allows for rapid processing of inputs and outputs, and can be embedded on another device. When choosing the appropriate device for this project, five microcontrollers were considered: the Arduino Uno, Arduino Due, MintDuino, Raspberry Pi and the BeagleBone Black [26]. These devices were chosen because of their relatively low cost, ease of access, and availability of open source and manufacturer support when designing a control system. The summary of the specification of each microcontroller can be seen in table 3.1.

From the table, we see that the Arduino Uno and the MintDuino were the most cost effective options, with the Raspberry Pi and the BeagleBone controller being the most powerful. Given that the reaction time needed to be within approximately 0.1 second to estimate biological behavior, the memory and processing speed of all of the controllers met our minimum standards. This, coupled with the fact that the Arduino Uno, unlike the MintDuino, was plug-and-play, caused the Uno to be our initial front-runner in the selection process. Processing capability aside, the Arduino Due and the BeagleBone had the best input and output support; it is because of this that the Raspberry Pi became unfeasible

Table 3.1: A table summarizing the specifications of the various microcontrollers considered for the design of the biped system.

	Arduino Uno	Arduino Due	MintDuino	Raspberry Pi	BeagleBone Black
Price:	29.99	49.99	24.99	39.99	59.99
Processor:	ATmega328	32-bit SAM3X8E ARM Cortex-M3	ATmega328	Intel Quark SoC X1000	Sitara AM3359A ARM Cortex-A8
Processor:	16 MHz	84 MHz	16 MHz	700 MHz	1 GHz
Analog Pins:	6	12	6	None (no on-board ADC)	7
Digital Pins:	14 (6 PWM)	54 (12 PWM)	14 (6 PWM)	8 Digital GPIO	65 GPIO (8 PWM)
Memory:	SRAM 2KB - EEPROM 1KB	SRAM - 96 KB	SRAM 2KB - EEPROM 1KB	RAM 512MB	DRAM 512MB DDR3L, eMMC 2GB
Language:	Arduino / C Variant	Arduino / C Variant	Arduino / C Variant	Linux compatible	Linux compatible
Programmer:	USB, ISP	USB, ISP	FDTI Friend	Linux-compatible	Linux-compatible
Assembly:	Assembled	Assembled	Kit	Assembled	Assembled

due to the lack of input and output pins, and the absence of analogue pins completely. As discussed later in the chapter, the system had a minimum requirement of 5 PWM pins, 4 dedicated digital pins, and 6 dedicated analogue pins. The Arduino Uno once again met our minimum requirements, and allowed seamless plug-and-play support for many of the sensors used. Another key advantage of using Arduino products is their ability to use serial input and output, a major advantage when cross-platform communication (such as with MATLAB) is required. In the future, the Arduino Due may be used for making the system independent of the remote PC, however, for the scope of this thesis, we found the Arduino Uno to be more than sufficient.

3.2 Sensors

In order to appropriately adapt to its environment, the biped walking robot was equipped with sensors that allowed information to be taken in, processed, and then converted to a form that could be used as a reference input to our control schemes. These sensors are discussed in this section.

3.2.1 Hip Joint Magnetometer and Pitch Sensor

As will be discussed in chapter 6, the torso position itself was not the input that we chose to have as a reference for our controller. However, it was still beneficial to have extra information about the position of the hip joints at any given time, in order to paint a picture for the operator as to how well a given control scheme worked. As such, a magnetometer and hip pitch sensor were attached to the hip of the robot. Given that the ZMP should facilitate walking with a hip angle of 90°, any major deviation from this would be easily detectable on, for instance, a 0° to 180° graphical readout. For this application, we chose the Sparkfun LSM9D50 as the IMU of choice to supply this information. The LSM9D50, as seen in Fig. 3.1 is a nine degree of freedom unit, and was chosen because of its affordability and compatibility with the Arduino Uno

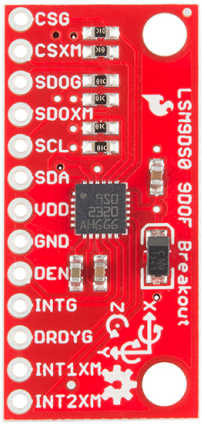

Figure 3.1: Picture showing the pins of the of the IMU pitch and roll sensor on the poppy seed bed

3.2.2 Bed Pitch and Roll Sensor

Similar to the hip, an IMU was attached to the bed itself to gauge the slope angle at any given time. This is further explored in section 2.2, however, the LSM9D50 Unit shown in Fig. 3.1 was also used, particularly because of existing infrastructure in the code to facilitate seamless integration. Unlike the hip IMU however, the pitch was isolated, and was actually used as the reference input to the torso controller, in order to dictate the slope dependent torso posture. This control is explored further in section 6.1.9.

3.2.3 Strain Gauges

Strain gauges are precisely calibrated resistance-based sensors that are used for force and torque measurement applications. As seen in Fig. 3.2, the strain gauge is typically bonded onto a surface through the use of high strength adhesive. At this point, when there is deflection, there will be a minute compression or tension of the gauge, causing it to lengthen or shorten. The unit is made up of resistive material, and as such, this lengthening and shortening causes small changes in resistance. Thus, when a voltage is applied across the gauge, these changes in resistance result in small fluctuations in voltage; these can

Figure 3.2: Picture showing a strain gauge bonded to a force plate-cantilever assembly

be plotted against the force causing the deflection, effectively making a force plate. This calibration can then be used in a microcontroller, such as the Arduino Uno, to create a force reference input.

In our biped system, the primary stability control mechanism is at the foot level, using force based control. As such, because of the precision and low cost of the strain gauges, it was a natural first choice in the initial force sensing foot design. However, because of some of the disadvantages of the system, it was ultimately not chosen as the force transduction device used in the final foot design. The factors that were weighed into this initial decision are outlined below.

Advantages of Strain Gauges

Some key advantages of strain gauges are:

1. Strain gauges tend to be very light and thus do not change the dynamics of the system that with which it interacts.

2. These are quite simple, passive transduction systems, and have a very high bandwidth, sensitivity, and measurable load, depending on the material to which they are bonded.

3. Strain gauges tend to be very accurate, and can be used for high precision applications

4. Strain gauges are quite affordable, and readily available for purchase at many online retailers.

Disadvantages of Strain Gauges

Some key disadvantages of strain gauges are:

1. Strain gauges tend to be sensitive to disturbance in their connection wires, simply due to the fact that they are resistance based, with small changes in wire position causing false strain readings. This was a problem in the case of a system that constantly moved and fell.

2. Strain gauges also can be difficult to bond to a surface, and require significantly more time and expertise to install

3. strain gauges have to be calibrated based on the material to which they are bonded, as well as after major impacts

4. Strain gauges also have to be doubled to compensate for temperature effects.

3.2.4 Force Sensitive Resistors

A Force Sensitive Resistor (FSR) is a device that changes its resistance based on the amount of compression applied to its surfaces. In general, these devices are made of two separate active layers, separated by a spacer. As the FSR is compressed more and more, and the layers get closer together, causing the semi-conductive material between them to conduct more, and therefore lowering resistance. This response is typically linear, and the shape of the FSR is typically retained or restored using air cushioning and venting. As seen in Fig. 3.3, an Interlink 402 38mm$\times$38mm FSR was chosen for each heel and toe. The comparison of this device's performance, as well as all details concerning calibration and robustness testing are examined below.

Advantages

1. FSR's are thin, flexible and allow for unobtrusive integration into a pressure-sensitive system

2. FSR's come in a variety of shapes and sizes that can be customized based on the shape of the surface itself

3. FSR's are typically more robust to destructive force, due to them being contact-based instead of resistance-based

4. FSR's are also quite affordable, and readily available for purchase at many online retailers.

5. Unlike strain gauges, FSR's require significantly less signal conditioning to produce a force signal.

6. FSR's are easier to replace and clean than strain gauges, which are single use.

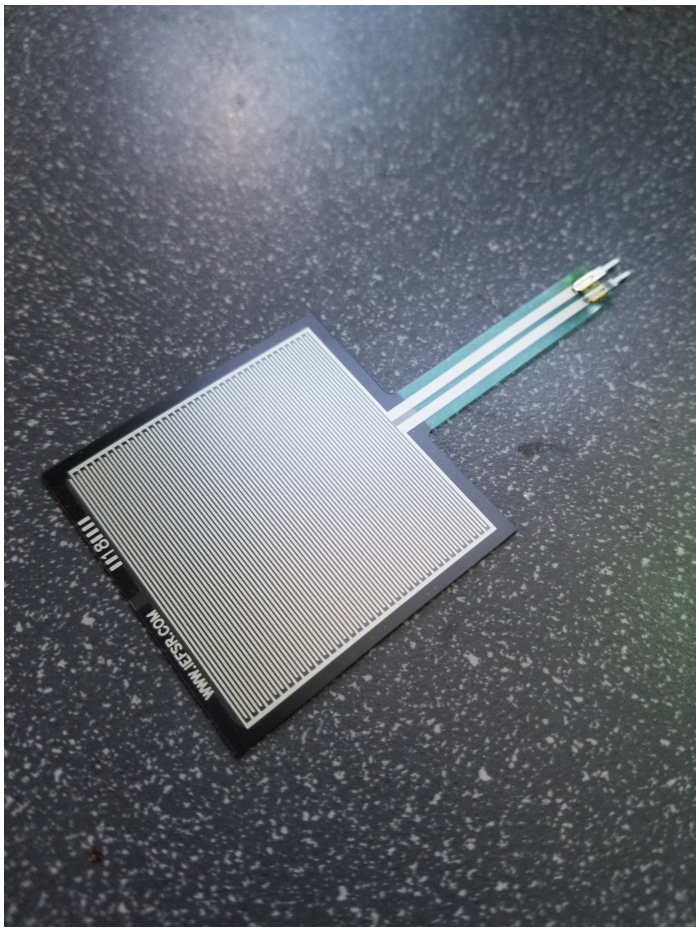

Figure 3.3: Picture showing the force sensitive resistor used in the heels and toes

Disadvantages

1. Perhaps the main disadvantage of the FSR is accuracy. These devices tend to be far less accurate than strain gauges, with accuracy of about $\pm 5\%$ as opposed to approximately $\pm 0.2\%$ for strain gauges.

Comparison to Strain Gauges

Ultimately, the deciding factor for the FSR over the strain gauge was the robustness of the transduction device. When designing for a device that is constantly disturbed and perturbed, the FSR allowed for a system that was tougher and more easily maintainable than that with the strain gauges.

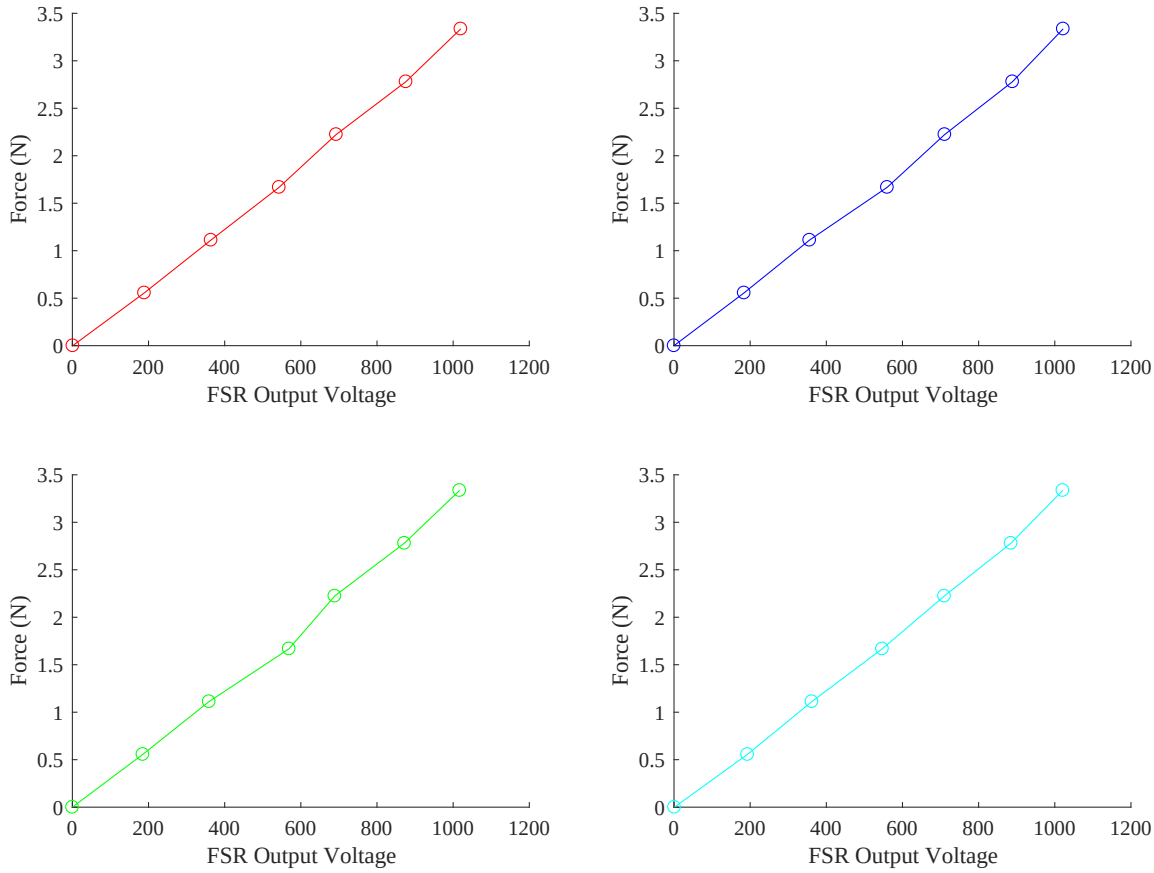

Figure 3.4: A figure showing the calibration curves for each of the force sensitive resistors in the heels and toes of the biped. A set of standard weights were applied with even pressure across the surface of the FSR, and the voltages were recorded with a voltmeter

Calibration and Characterization

Given that the FSR's were chosen over the strain gauges, it was then necessary to properly calibrate each resistor. For each device, standard weights between 0N and 3.34N were applied to each resistor. Using a 5V supply from the Arduino Uno, the corresponding voltages were recorded as shown in Fig. 3.4. These datasets were then used to determine Force-voltage equations for each FSR. These force values would serve as the eventual reference input to the controller discussed in section 6.1.9.

After this initial calibration, it was then necessary to ensure that the FSR's were not susceptible to drift (Fig. 3.5). As such, each FSR was connected to a common ground and

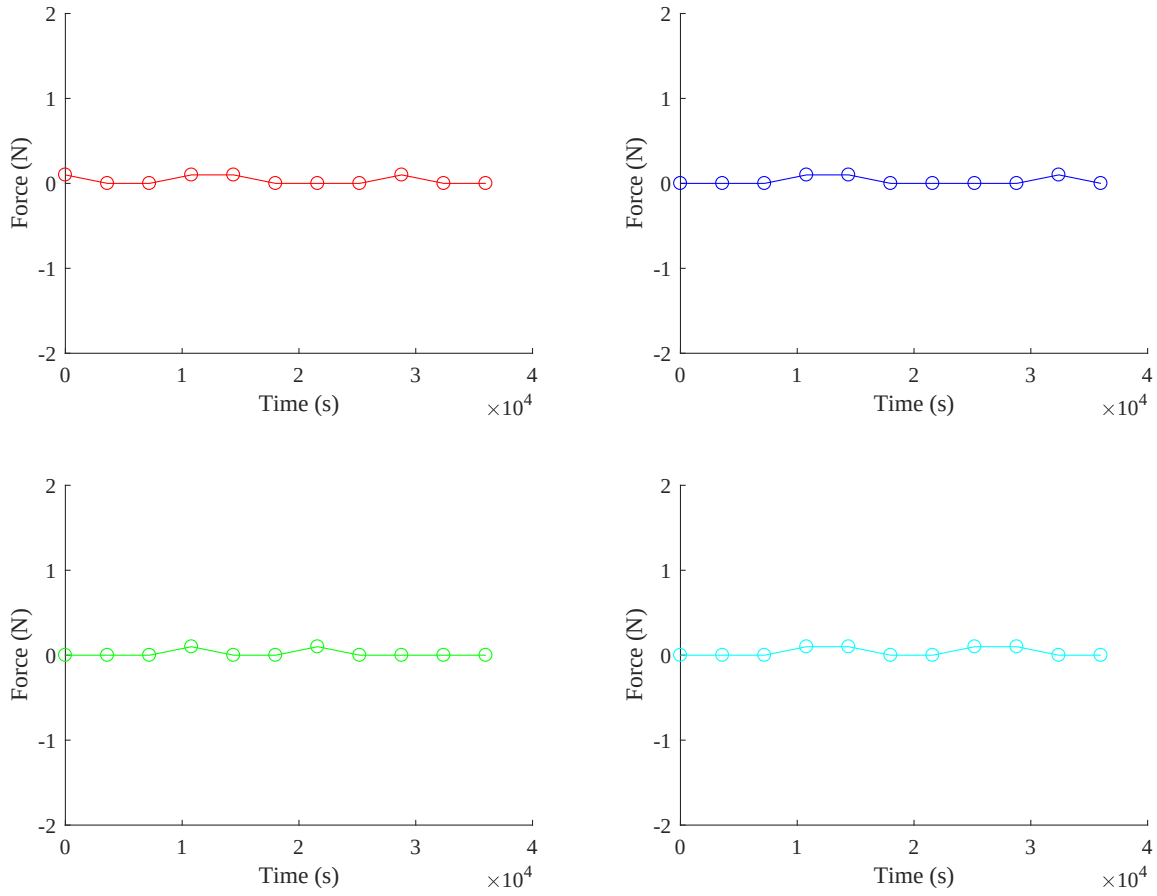

Figure 3.5: A graph showing the readings of each of the FSR's over time. This was done to ensure that the system was not susceptible to drift.

a 5V power supply, and force readings were taken every hour for 10 hours. For the 8N range of the FSR, drift was limited to $\pm$0.05N, or 1.25% of the range, a figure which we found to be quite reasonable.

It should be noted that this drift test was done for a static situation, and as such, to once again test the system for robustness and repeatability, it became necessary to test each foot for a dynamic case. To achieve this, the center point (or the ankle) of each foot was marked as 0, with the toe direction being positive, and the heel direction being negative. starting from the zero point, 5mm increments were indicated on the surface of each foot until arriving at 50mm at the tip of the toe. Similarly, 5mm decrements were indicated

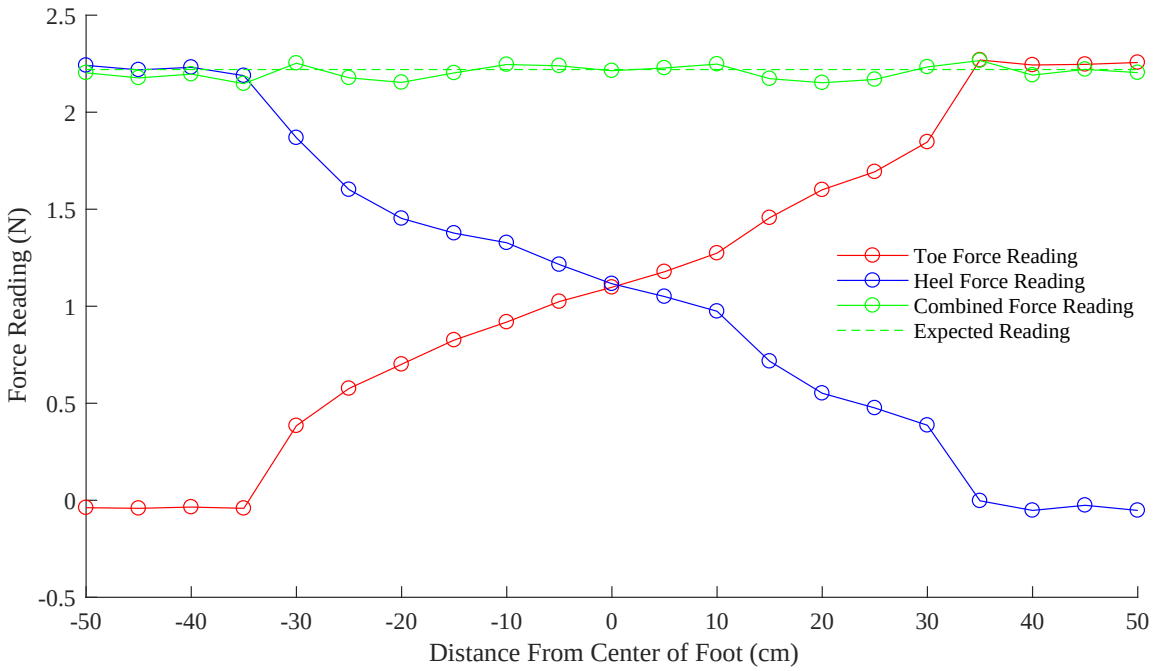

Figure 3.6: A graph showing the loading of a 2.22N weight at various distances, starting from the tip of the heel to the tip of the toe for the left foot of the system. As can be seen, the combined forces provide a good estimation of the applied force. The plateaus occur when only one FSR is being loaded due to crossbar deflection.

until arriving at -50mm at the tip of the heel. For each case, as seen in Figs. 3.6 and 3.7, a standard weight of 2.2N was placed at each interval, recording the heel and toe forces in each instance. We expected, in the case of proper calibration, that sum of the heel and toe forces at any given time would result in the total weight applied to the foot surface. As expected, this is true for both figures. It should be noted, that because flexible bushings were used to attach the bottom surface of the foot to the layer that contained the FSR's, there was a small plateau at the extreme corners of each graph, where the bushings allowed the unloaded side to completely break contact with its corresponding FSR. This design is further discussed in chapter 4.

Once FSR's are properly calibrated, they can prove to be incredibly powerful tools. Figure 3.8 shows the resolution of moments about the toes and heels, as well as graphs showing the ratio of the toe and heel forces. This is important, in that we can actually use

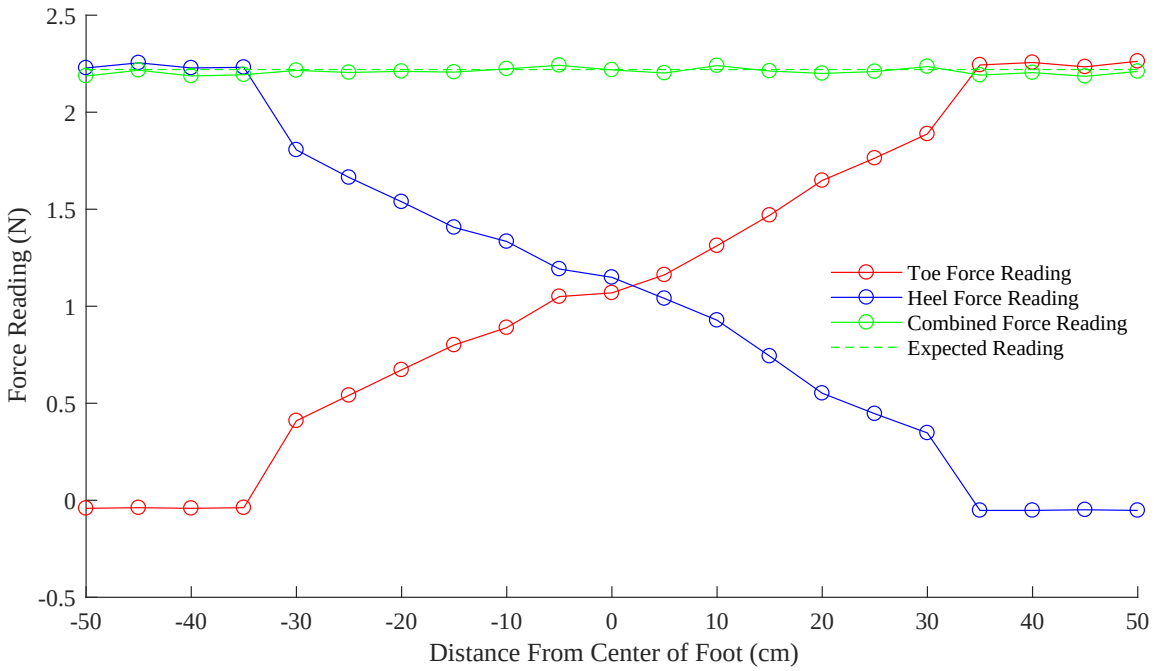

Figure 3.7: A graph showing the loading of a 2.22N weight at various distances, starting from the tip of the heel to the tip of the toe for the right foot of the system. As can be seen, the combined forces provide a good estimation of the applied force. The plateaus occur when only one FSR is being loaded due to crossbar deflection.

this information to find the position of the equivalent resultant force on the surface of the foot, and use this as an indication of the displacement of the zero moment point. In the final design, this was adapted to be a force difference, as opposed to a ratio, however, it still allowed for effective control based on uneven distribution of force on the robot's foot.

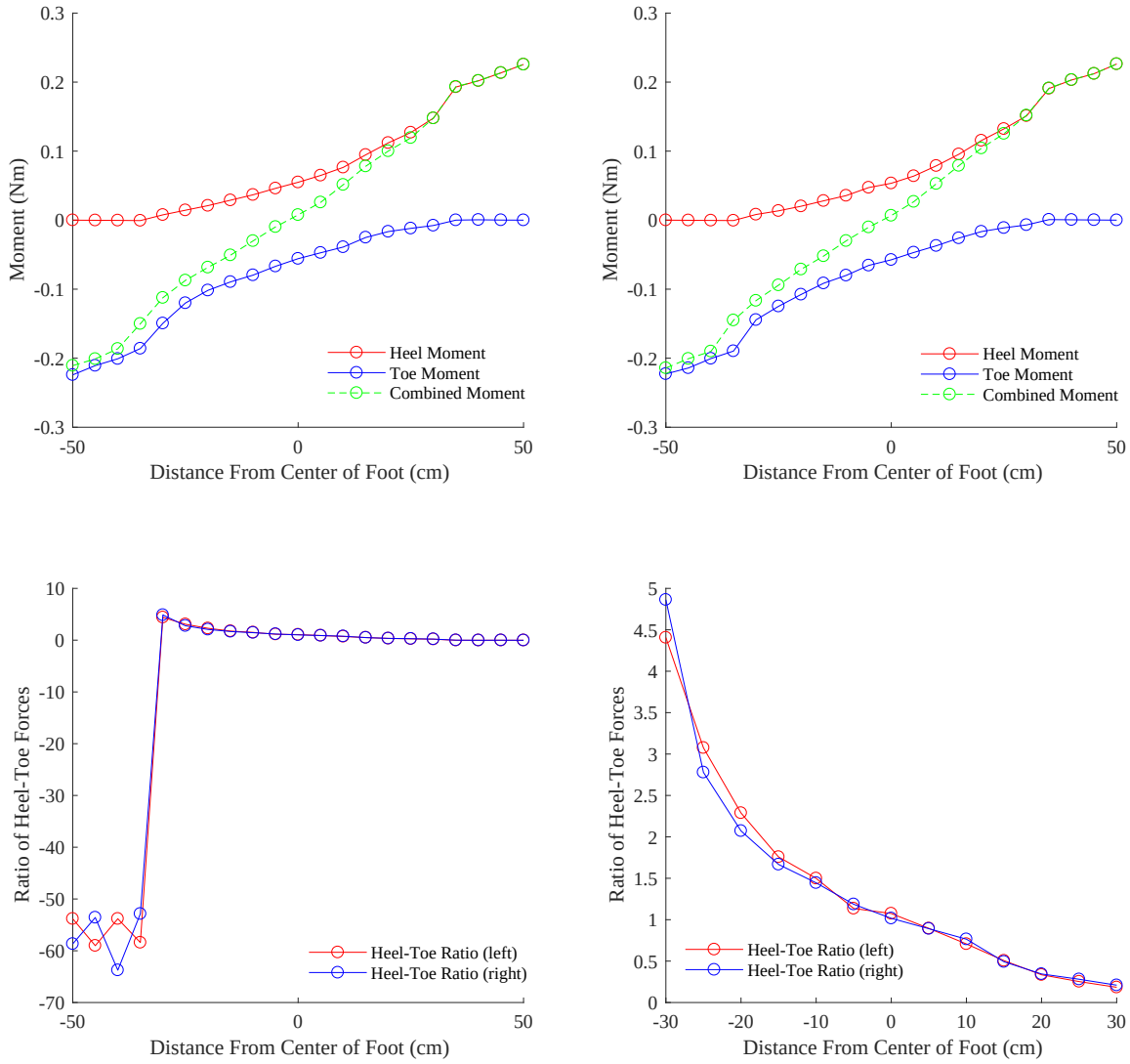

Figure 3.8: The top figures in this plot show the moments about the heels and toes when a 2.22N force is loaded from the tip of the heel to the tip of the toes, for the left and right feet respectively. The bottom left figure shows an initial attempt at using the heel/toe ratio to estimate the position of the equivalent force on the foot. Because of the FSR plateauing, this is difficult, and thus, a zoomed in model from the points between the plateaus are shown in the bottom right.

Figure 3.9: Picture showing one of the six MX-64A actuators used in constructing the legs of the robot system

3.3 Actuators

In most biped robotic system, actuators that make up the joints are perhaps the single most important electromechanical component. For the planar biped walker, three main types of actuators were used: smart servomotors, high torque servos, and linear actuators. Each of these is discussed in further detail below.

3.3.1 Robotis MX-64A Servos

For the hip, knee and ankle joints of each leg, a Dynamixel MX64A servomotor, shown in Fig 3.9, was used. This particular device was chosen for a number of reasons. First and foremost among these was the torque output of the servo. The MX64A is able to produce torques of up to 7.3Nm at 14.8V before stalling, which is well within the estimated 3Nm

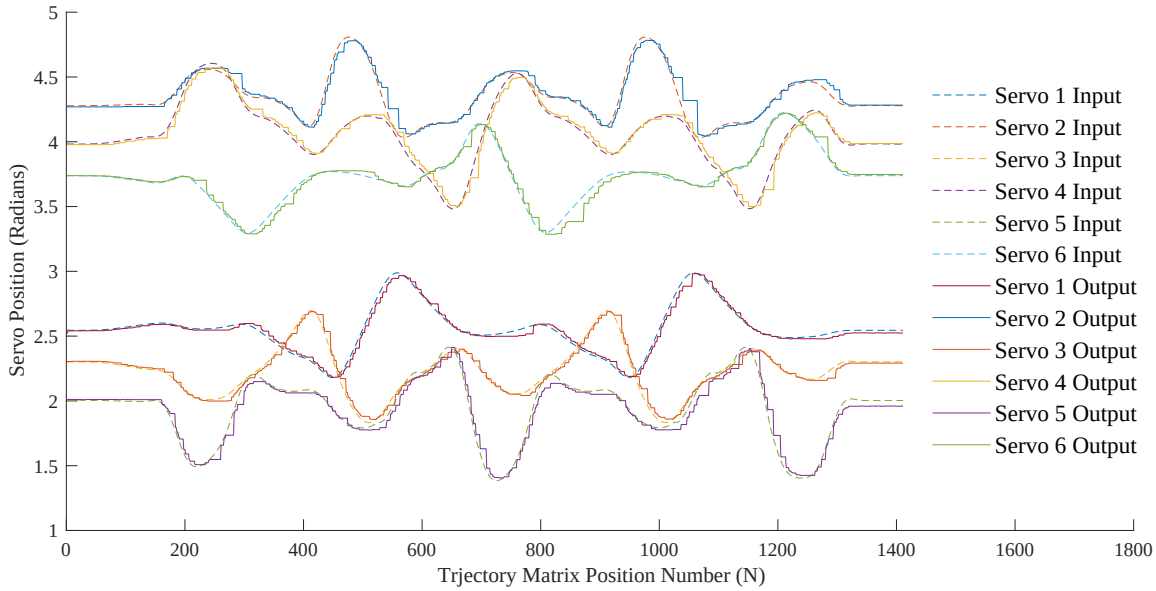

Figure 3.10: A figure showing the encoder tracking test of the MX64 servos. This was done in order to ensure that the robot was able to accurately follow the gait trajectory, and that the on-board servo control system was functioning properly.

of torque at the ankle joint, based on the robot geometry. After this, the MX64A had the key advantage of running a Cortex-M3 microprocessor on each unit, allowing for on-board PID control, without the need for adjustment through external joint position control. Another feature that made the MX64A a favourable choice was the inclusion of a contactless absolute encoder. During gait experimentation, this encoder was used to ensure that the servos were following their intended trajectories, and that the PID gains were appropriate. An example of this encoder output can be seen in Fig. 3.10.

3.3.2 HiTech High Torque Torso Servo

The torso was attached to the hips using a HiTech HS-M7990TH High Torque Servo, which produced approximately 4.5Nm of torque before stalling. While this not may have been as much as the MX64A servos, it should be noted that the torso servo is significantly smaller, simply due to the size constrains of the robot itself. We found this value to be sufficient, due to the fact that the torso servo control system was designed to operate at fairly low

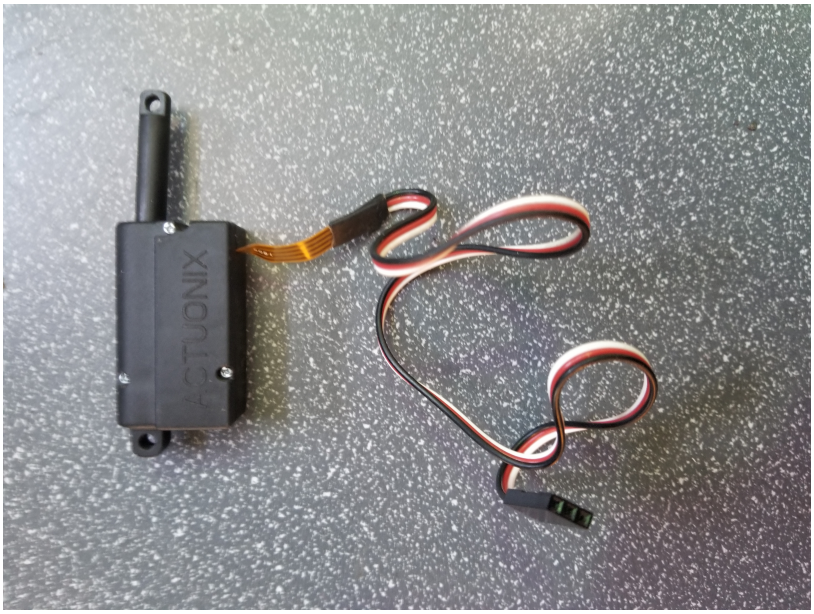

Figure 3.11: Picture showing one of the four Firgelli PQ12 Linear actuators used in constructing the foot of the robot

speed, with an estimated resistant torque of approximately 1Nm.

3.3.3 Firgelli Linear Actuators

A linear actuator is an actuator that moves in a straight line, as oppose to the circular motion of conventionally designed servomotors like the HiTech or the MX64A. These actuators played a key role in the design of the feet, in that they allowed for the rapid expansion and contraction according to the force profiles fed into the controller. In order to design such a system, we required the smallest possible actuator with feedback capability, and as such, the Firgelli PQ12-P by Actuonix Motion Devices (Fig. 3.11) was a natural choice. As seen in Fig. 3.12, this was anchored to the foot itself, with a +5.8V, GND, and signal wires running into the harness and Arduino Uno.

This Firgelli actuator system served as a means to expand the foot surface when faced with unusual force differentials. This is the basis of the foot control scheme discussed in section 6.1.9, however, a graph showing the preliminary testing of this system can be seen in Fig. 3.13.

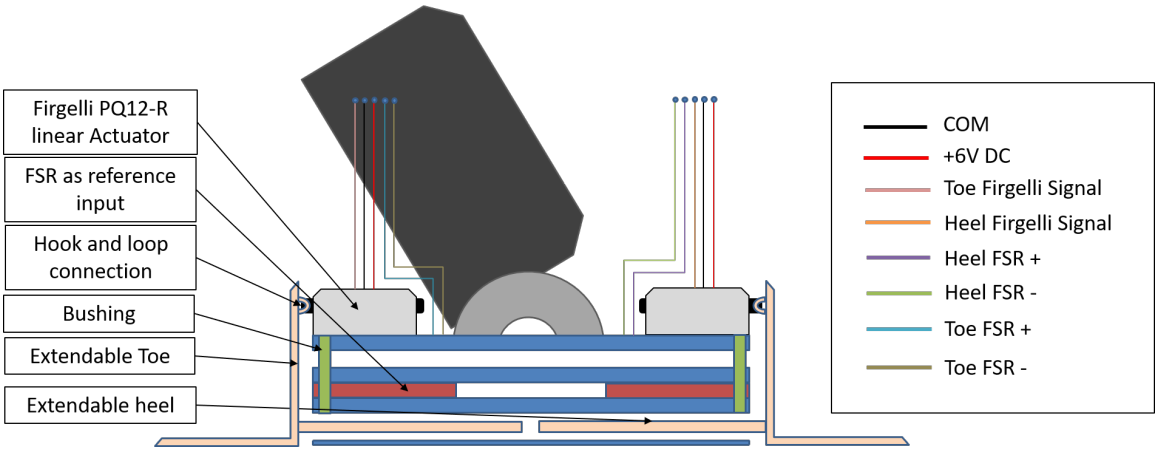

Figure 3.12: A schematic showing the wiring setup for the actuated foot/FSR assembly. This was run through a harness under the plating.

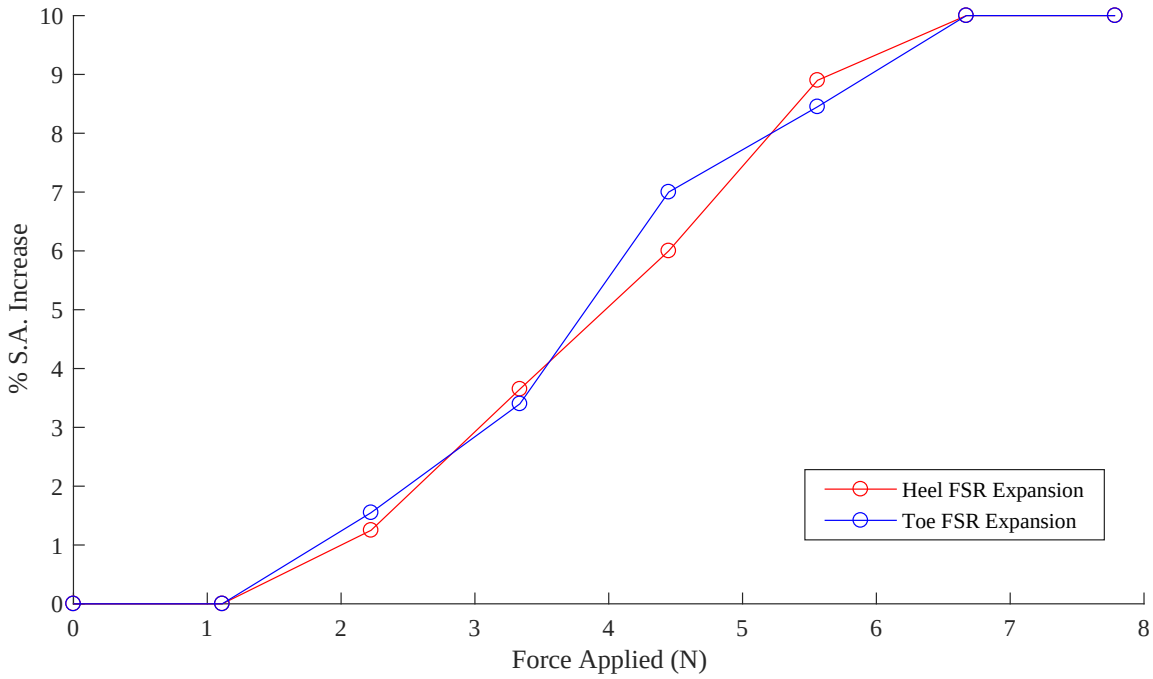

Figure 3.13: A graph showing the percentage expansion of each of the FSR-Heel and FSR-Toe combinations for one of the feet.

3.4 Power Systems

As seen in the sections above, various sensors and electromechanical devices were utilized in the construction of the biped walker. These require specific voltages and currents to operate, and as such, power distribution systems were designed within the confines of the requirements established in section 2.1. These are further explored below.

3.4.1 Harness System

In order to distribute power and communicate with the remote desktop, a harness was used, as seen in Fig. 3.14. This contained the following connections: +14.8V for the MX64A servomotors, +6v for the HiTech high torque servo, +5.8V for the Firgelli actuators, 5V for the Arduino, 3.3V for the Bed and Hip IMU's, and a common ground, GND. Additionally, it contained a TTL signal distributor for the MX64A servos to communicate with MATLAB, and a USB serial communication connection for the Arduino to communicate with the Arduino IDE window on the remote PC. Lastly, it contained signal jumpers from the Arduino Uno to the HiTech servo and the Bed IMU.

3.4.2 Battery Pack vs. Tether

Because of the high number of trials performed in a given time frame, the need to power multiple components at various voltages at any given time, the lack of use outside a predefined enclosure, the need for low mass, and the preexistence of a harness for communication with the remote desktop, we chose to run a tethered power system instead of a battery.

3.4.3 Linear Actuator Power Distribution Circuit

As shown in Fig. 3.15, a circuit was build that served multiple purposes. Firstly, it served as a power distribution hub for the linear actuator, and channelled a single +5.8V rail and common GND rail into each individual actuator. Apart from this, it served as a signal

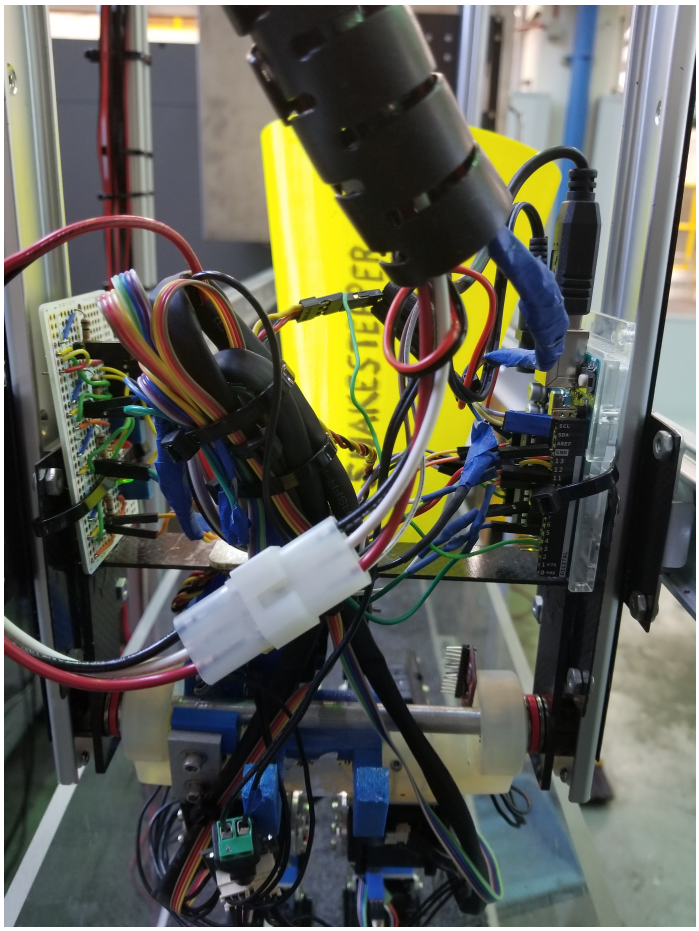

Figure 3.14: Picture showing main harness used to supply power and signal to and from the system.

bus; this circuit received force signals from the FSR's and sent them to the Arduino for processing. After this, it received controlled position signal outputs from the Arduino and relayed these to the Firgelli Actuators. This was necessary due to lack of a dedicated feedback signal from the actuators, however, during trials, the system functioned without the need for additional feedback.

3.4.4 Overview of Strain Gauge Circuit

A picture of the initial strain gauge circuit can be seen in Fig. 3.16. In order to actually measure the strain voltage from a strain gauge, it needed to be first connected to a signal conditioning circuit that was capable of measuring very small differences in strain, resis-

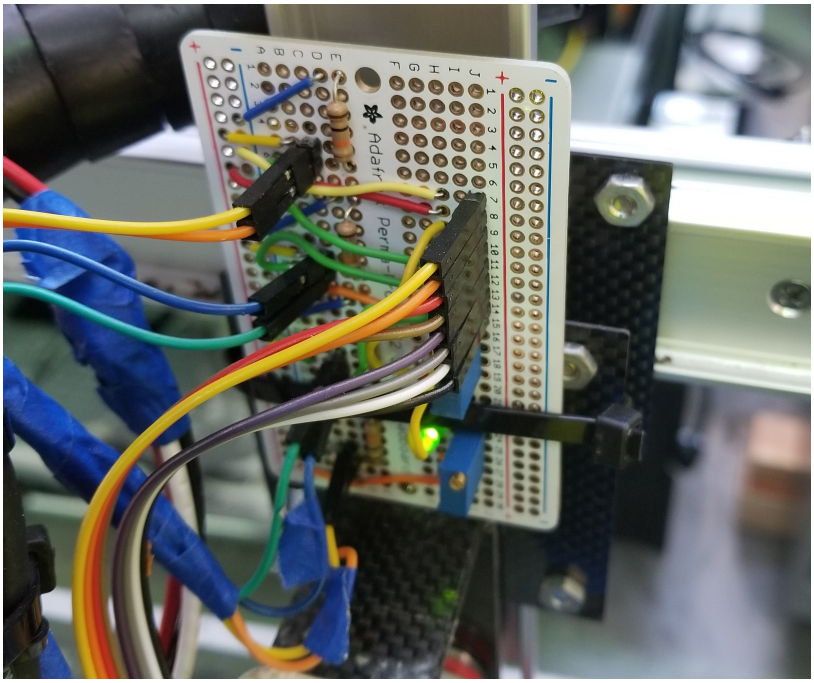

Figure 3.15: Picture showing the power conditioning and distribution circuit used for powering the Firgelli PQ12 Linear Actuators

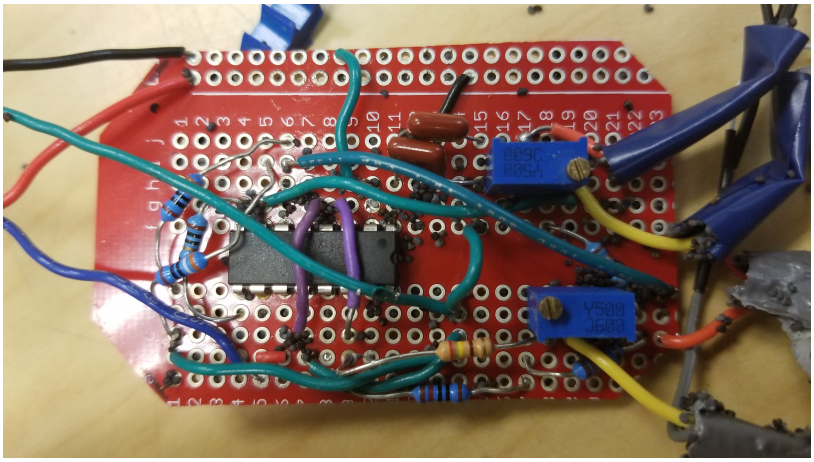

Figure 3.16: A picture showing the design of the strain gauge H-bridge circuit

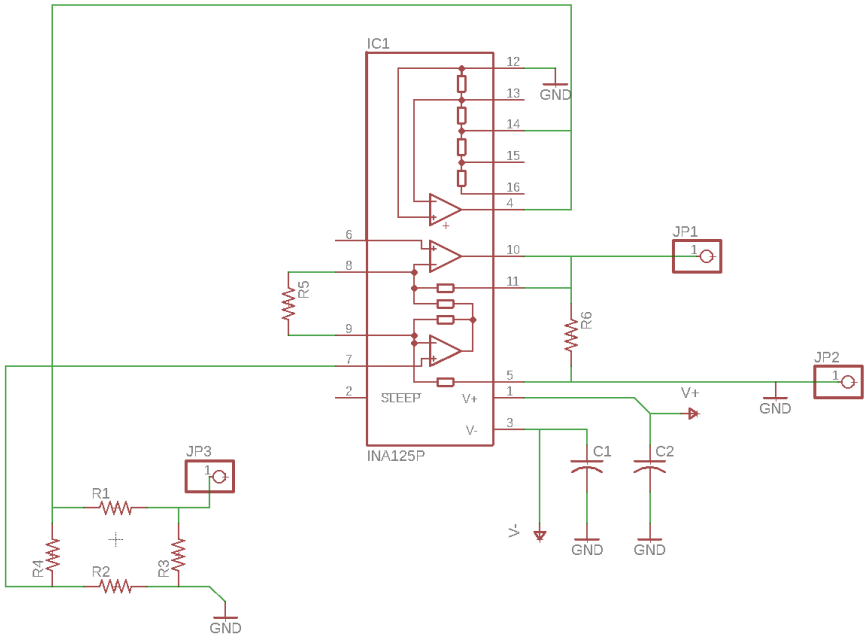

Figure 3.17: An example of a schematic fed into the Eagle CAD system. This particular schematic shows the strain gauge circuit.

tance, and thus force. Thus, a Wheatstone H-bridge system was used, and was connected to an H-Bridge amplifier. However, the bridge does in fact need to be balanced using a variable resistor before it is able to give a proper force reading. During walking, it was quite easy for this balance to be unintentionally adjusted, leading to errors in measurement. This is another one of the reasons that FSR's were favored for this particular application.

3.4.5 EAGLE CAD Design

EAGLE CAD is a circuit design software tool that allows the user to design schematics (Fig. 3.17), and then create a PCB milled circuit board by tracing an intelligent toolpath (Fig. 3.18). Initially this was used in the design and testing of strain gauge circuits, however, because of the lack of complexity involved in the FSR circuit, this system was not necessary for the final product. However, in the future, this software package may prove incredibly useful, especially with the growing need to conserve space on the robot.

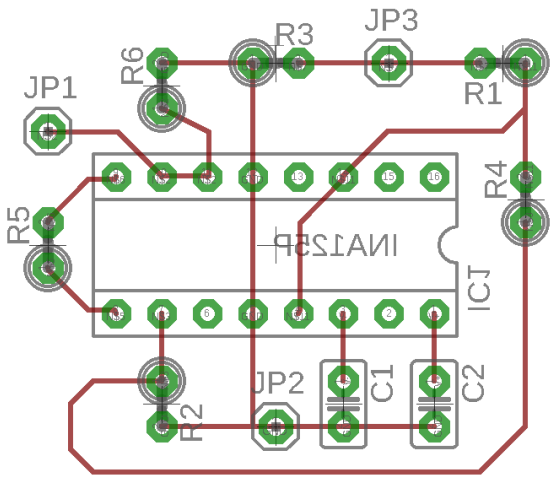

Figure 3.18: An example of a tool path for the schematic above that was generated for the circuit mill. In the future, this will be used to help reduce excess clutter in the biped robot system.

CHAPTER 4
MECHANICAL DESIGN

This chapter discusses the mechanical design and assembly of the biped walking robot. Firstly, we will discuss the approach and inspiration behind the design, and then examine an overview of the system construction.

4.1 Design Approach

As stated in Chapter 2, there were certain design criteria that the purely mechanical aspects of the systems needed to fulfill, particularly in terms of safety, durability, robustness and maintainability. As such, these were considered to be the driving factors when motivating the mechanical design of the biped walker, particularly in terms of material selection and physical geometry.

A Computer Aided Design (CAD) package was used to design all major components of the biped walker that were not available for purchase from major retailers. This proved to be incredibly advantageous in the creation of unique, highly specified parts for the system. Parts created using the CAD software package were able to be virtually tested for stress, fit and tolerance, and could be easily converted to a form that allowed for machining and production.

To effectively meet the design requirements, 3D printing was used as a means of rapid, iterative prototyping. This allowed parts to be uniquely designed and modified according to operator specifications, and allowed for easy maintenance and replacement of parts. To explain, a 3D printer is a piece of machinery that allows three dimensional parts to manufactured through the use of melting a filament of material that is fed in to the system. This melted material is extruded from the machine in the shape and pattern required, then rapidly cooled it for it to hold its form. Typically, these machines use plastic as a filament

material; the printer used to produce parts for the walking robots printed a specific grade of high strength, lightweight plastic called ABS.

These printers are incredibly accurate, with the systems in the lab being able to print with a precision of up to 250 microns. This allowed for the design of very small attachment points for various components. Additionally, a key advantage of the 3D printing system is the ability to print in highly irregular shapes; many of the parts used in the robot walker would be very difficult to effectively produce in a traditional machine shop. In terms of the maintainability of the system, these printers are able to produce exact copies of a given part, which allowed for significantly reduced downtime in the event of mechanical failure. These, along with the added benefit of ABS being a low cost material made 3D printing the ideal solution for the design criteria set forth in this thesis. It should be noted that the models presented in this thesis are the current iteration of the walker, and have built upon previous successes and failures over the course of the project. Even still, the design of the robot is still iteratively adapting and changing based on its operating conditions; this will be further discussed in Chapter 6.

4.2 Design Overview

As stated in the section above, the primary tool for part design was CAD; more specifically in the case of this robot, Solidworks was used. This was used to visualize our robot model, which can be seen in Figs. 4.1 - 4.5.

The robot was 50 cm tall from the ground to the attachment point of the torso, and 68cm overall to the top of the actuated torso. It measured 20cm at the widest point of the foot, and 25cm across the width of the bed, about which it was planarized. The robot, when fully constructed, weighed 1.92kg.

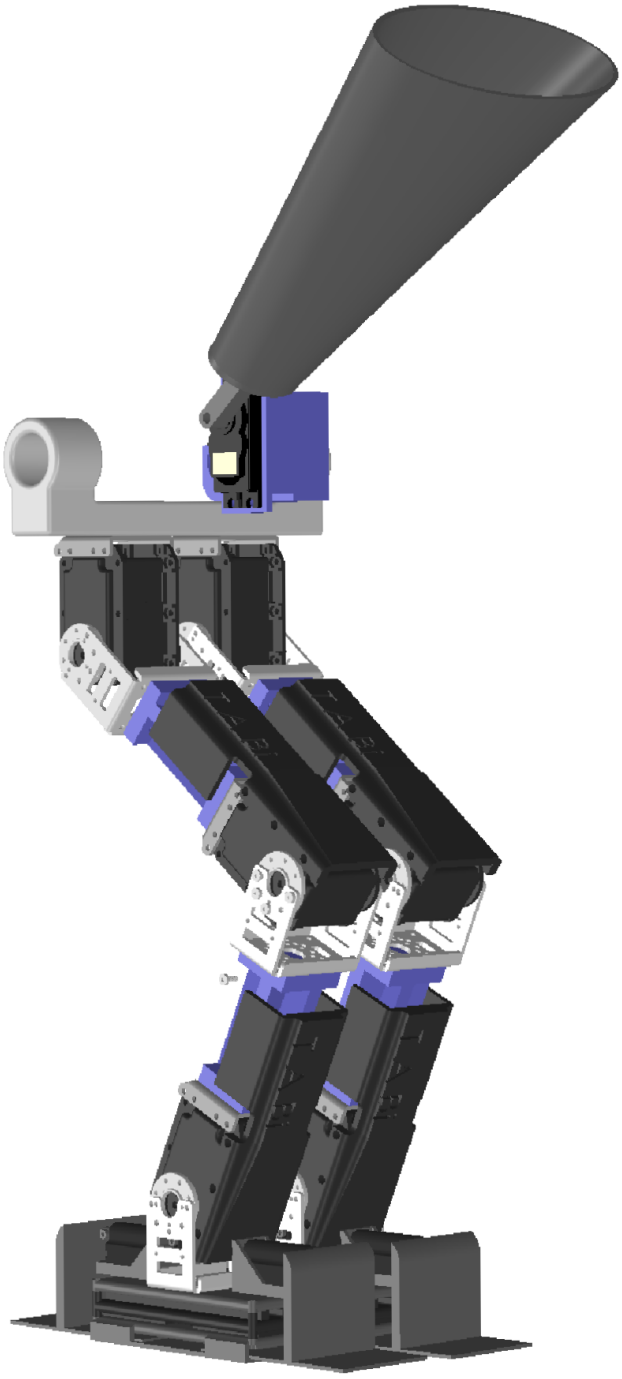

Figure 4.1: An angled front view of the Biped walker Prototype

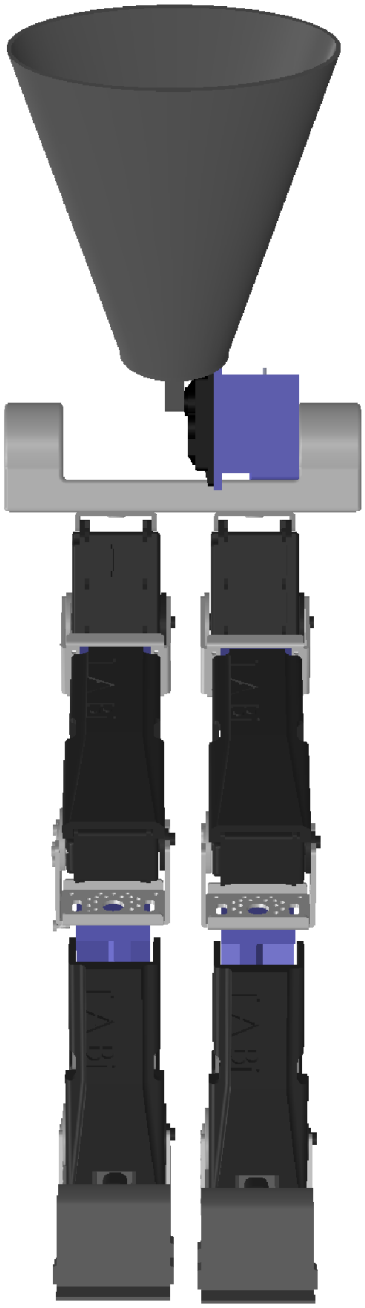

Figure 4.2: A front view of the Biped walker Prototype

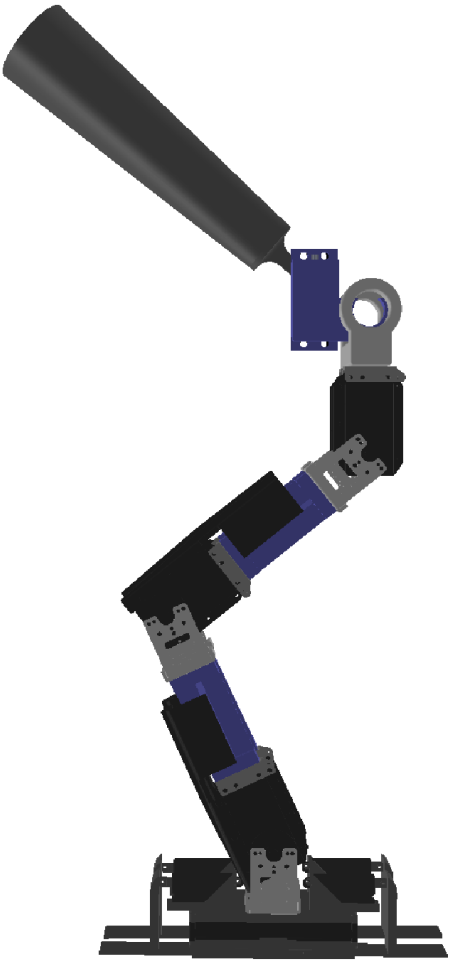

Figure 4.3: A side view of the Biped walker Prototype

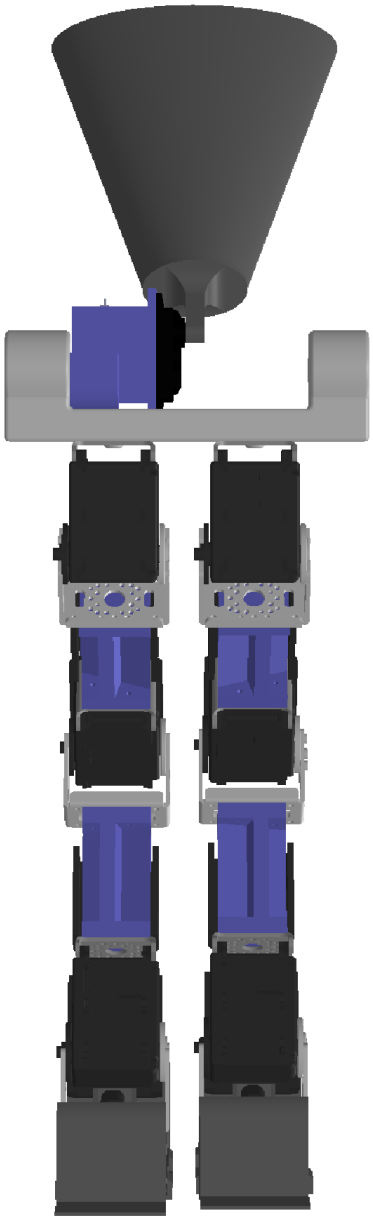

Figure 4.4: A rear view of the Biped walker Prototype

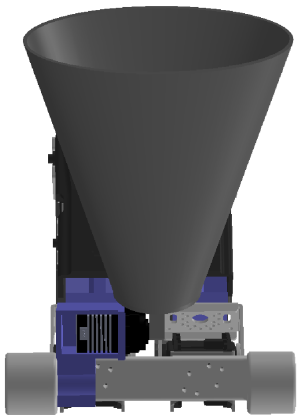

Figure 4.5: A top-down view of the Biped walker Prototype

When building a robot, it is first necessary to start with a main body to which auxiliary parts and limbs may be anchored. As seen in Fig. 4.6, the hip connector served as the key connection between the legs, the torso and the rails of the test bed. The leg brackets and torso servo housing are attached to the hip connector through 2 M6$\times$10 screws each, while the high torque torso servo itself is attached to the housing through 2 M4$\times$5 screws and nuts. This hip connection also served as a point of connection for a diagnostic IMU that gave a readout of hip position, the Arduino UNO that interfaced with the foot and torso system, and the power distribution circuit for the linear actuators on the feet. The circuit and IMU were attached via industrial grade adhesive, and the Arduino was attached through zip ties for easy removal. The actual torso was attached to the torso actuator through a single M2$\times$6 set screw, with torque acting through splines built into the torso attachment point.

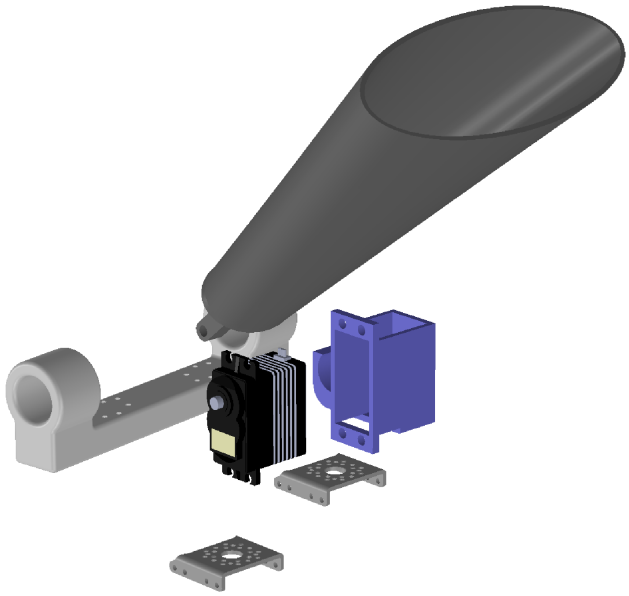

Figure 4.6: An exploded view of the torso of the Biped walker Prototype

When the joints of the legs are examined, the construction was designed to be simple, robust, durable and effective. Figure 4.8 shows a closer look at one of the knee joints. The upper leg extension was anchored to the hip actuators through 4 M2×20 machine screws and nuts. The extension was then connected to the knee actuator bracket through 4 M2×6 machine screws and nuts, with the actuator being affixed to the bracket using another 5 M2×6 machine screws on each side of the actuator shaft. Much like the hip, the other side of the actuator was then attached to another extension through 4 M2×20 machine screws and nuts. to prevent additional wear on the servo motors, two protective plates were also attached to each leg, once again using 4 M2×6 machine screws and nuts to secure each plate to an actuator frame.

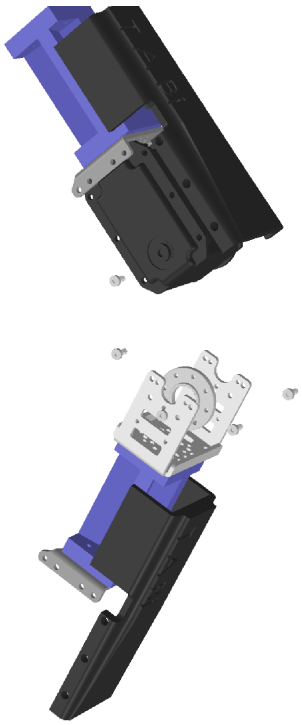

Figure 4.7: An exploded view of a knee joint of the Biped walker Prototype

Perhaps one of the most mechanically interesting parts of the robot system is the foot assembly as seen in Fig. 4.8. Much like before, the ankle actuator was connected to the leg extension from the knee using 4 M2×20 machine screws and nuts. This ankle actuator was also connected to the foot sub-assembly through 5 M2×6 screws that hold the actuator to its bracket, and 4 M2×6 screws that hold the bracket to the foot itself. From here, the top layer of the foot contained a precisely designed press-fit for the Firgelli PQ-12 linear actuator used in the heels and toes. The connection to the Firgelli actuators was reinforced through the use of an M2×6 screw and nut anchoring the non-mobile side of the actuator to the foot structure. Below the top layer of the foot was the middle layer of the foot assembly containing an FSR at the heel and the toe. Below this was the bottom layer of the foot, which contained a hollow frame structure. This hollow frame allowed the housing of extra toe or heel material from the toes and heels whenever the foot had any degree of retraction, while still transmitting force from the ground to the FSR's. The hollow section served as a

guide track for the toes and heels, and also contained a central hole to expel excess granular material that may have adhered to the heel or toe surface during retraction. The three layers of the foot were all connected using a flexible wire bushing, to allow for easy loading of the middle layer FSR's. The toe and heel extenders themselves were anchored to the Firgelli Actuators on the top using an M2$\times$6 machine screw and nut, however, at their base, they were allowed to slide freely in and out of the hollow frame of the base of the foot.

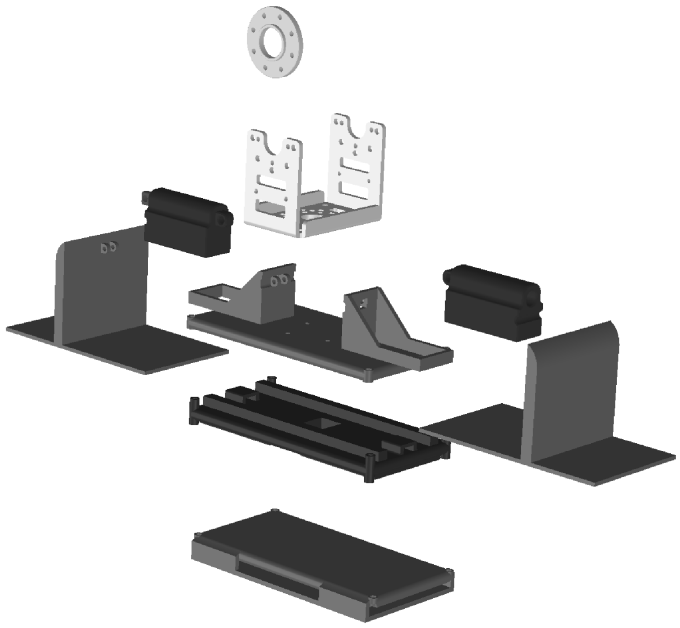

Figure 4.8: An exploded view of the foot of the Biped walker Prototype

When all these sub-assemblies were combined, we were able to build the most current iteration of the walking robot, as seen in Fig. 4.9.

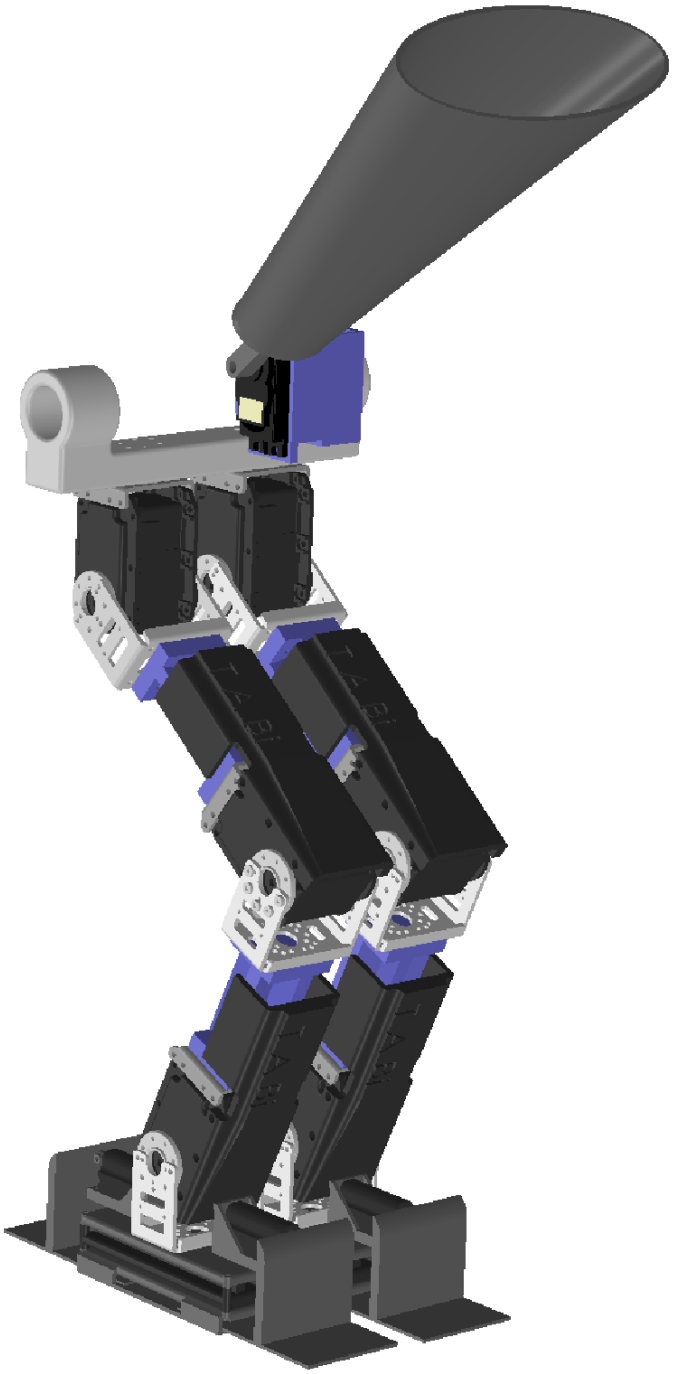

Figure 4.9: A view of the final CAD Prototype

4.3 Assembled Robot

Once the robot system was fully designed, it was possible to construct a physical representation of the CAD models. Various views of the assembled robot can be seen in Figs 4.10 - 4.12.

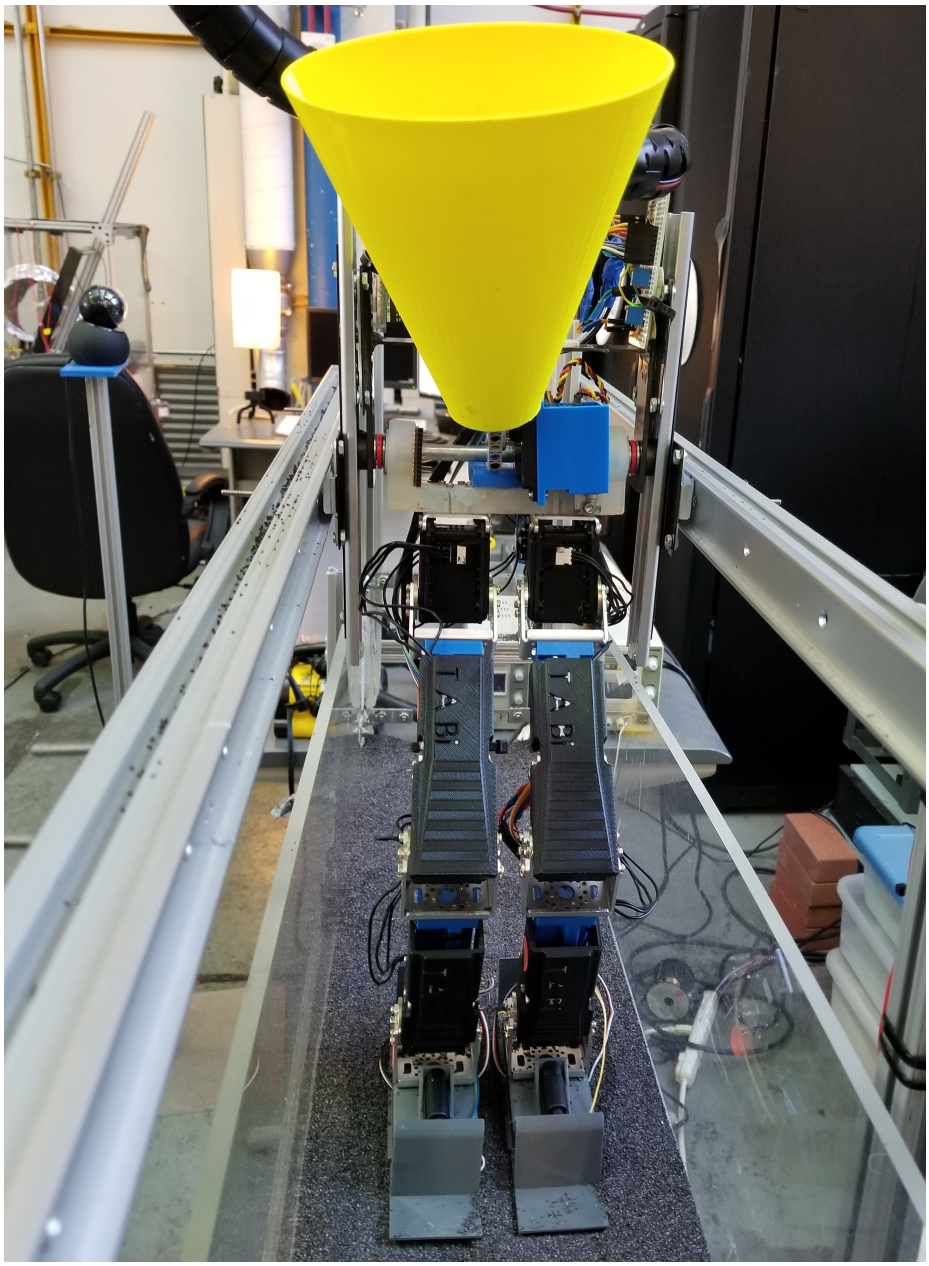

Figure 4.10: A front view of the assembled robot

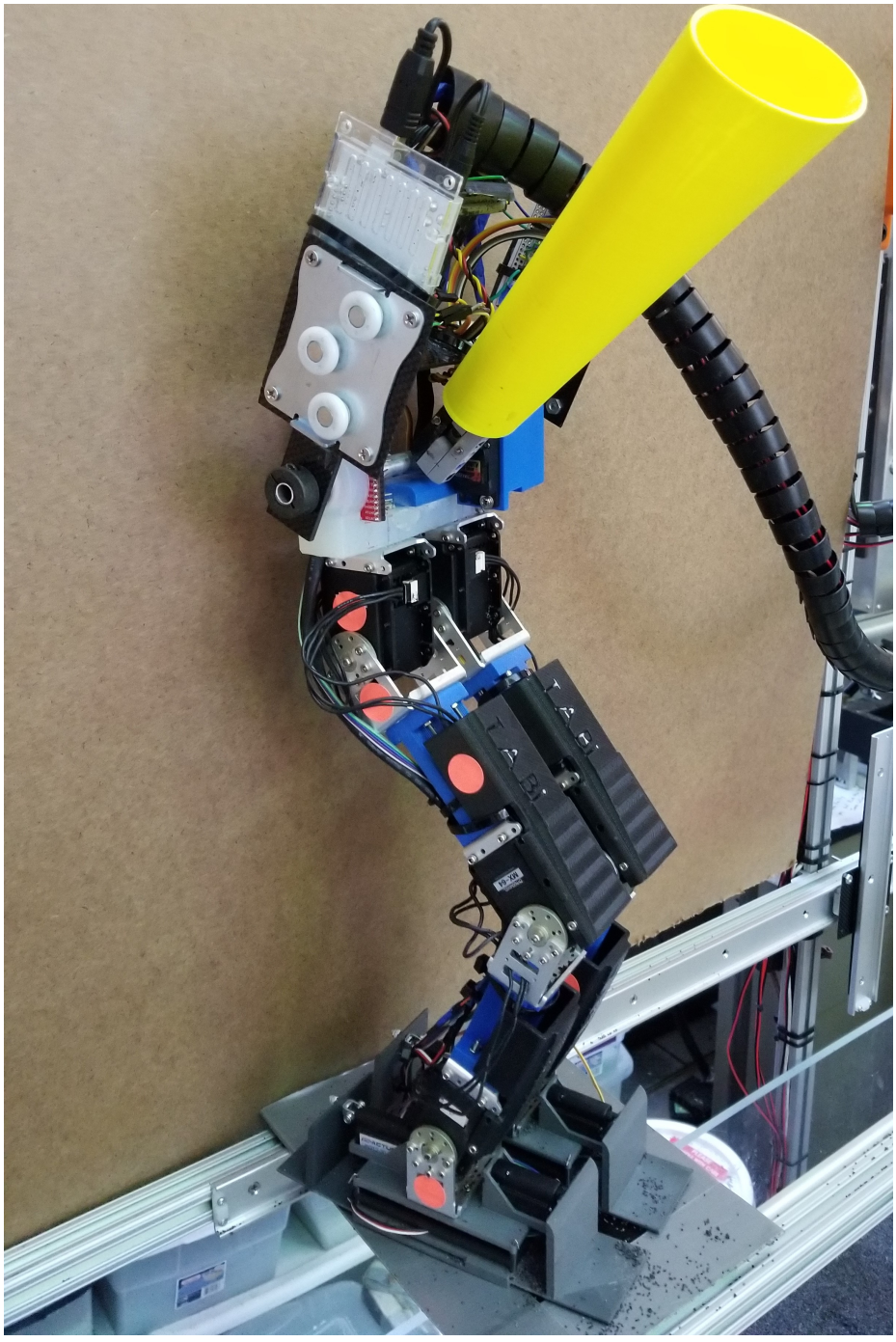

Figure 4.11: An angled view of the assembled robot

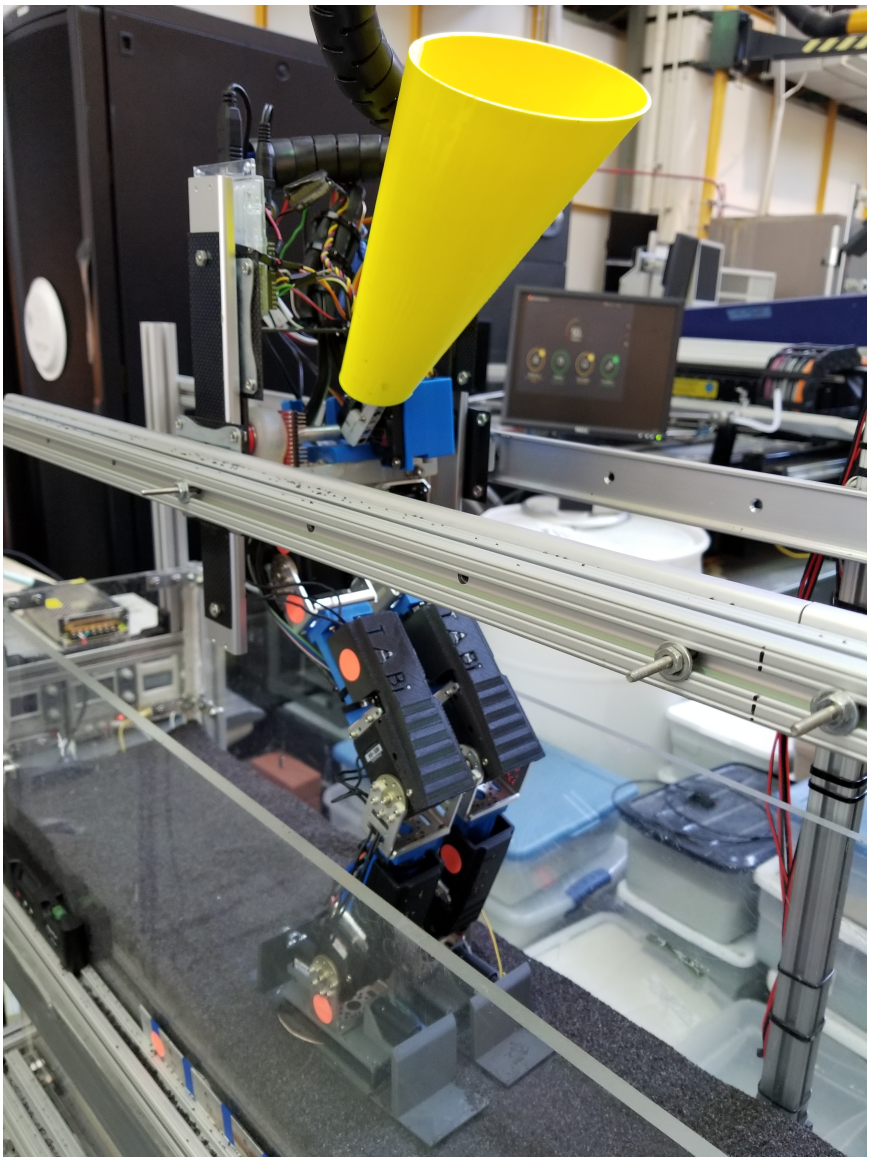

Figure 4.12: An angled view of the assembled robot in the test bed

CHAPTER 5
SOFTWARE OVERVIEW

This chapter discusses the main code structure used in the biped walking project, both in terms of remote desktop and microcontroller architecture. To have an effective robophysical system, it is important to have a set of clear, concise and robust code. Techniques used to implement this are examined below.

5.1 Dynamixel Wizard

Before any low level code implementation, Dynamixel Wizard, a piece of software provided by the leg joint actuator manufacturers, was used to prepare the servos. This program, as seen in Fig. 5.1, has a graphical user interface that allows for intuitive manipulation of servo parameters. Using this, the MX64 actuators were each assigned a numeric identification by the operator, a default baud rate, and suitable Proportional, Integral, and Derivative (PID) gains for a joint level controller as necessary. All these parameters only needed to be set once, however, the wizard proved incredibly useful for troubleshooting and state-level monitoring of the actuators.

5.2 MATLAB

Many modern biped robotic systems tend to receive their joint commands from on-board micro controllers. However, due to size and weight constraints, coupled with the fact that our system would need to recalculate an entirely new joint trajectory system every time the slope angle changed, we found that it was most beneficial, for our purposes, to do heavier trajectory equation calculations through communication with MATLAB on a remote PC. MATLAB, in short, is a matrix-based computation program, and is particularly well suited

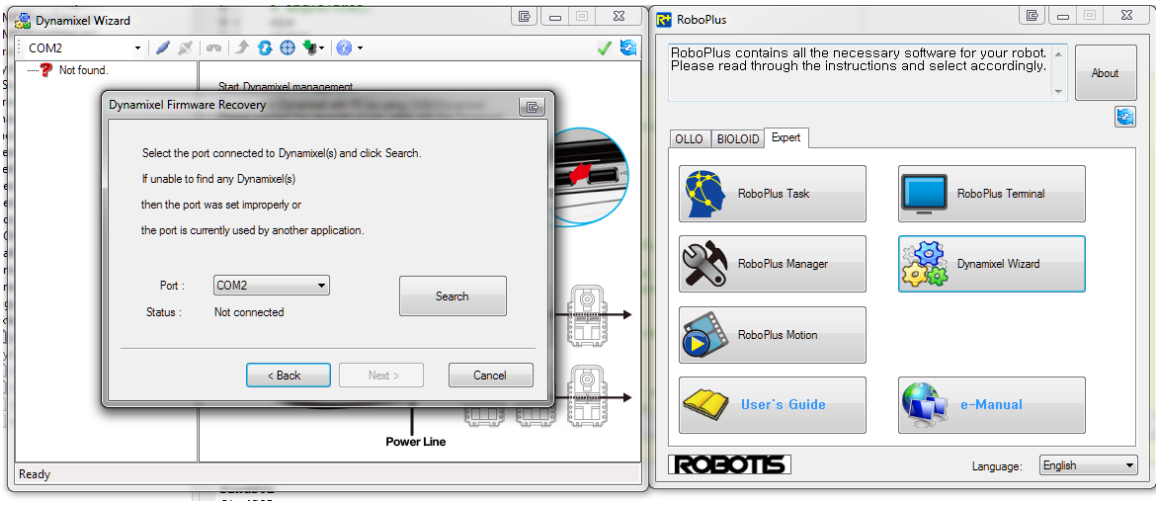

Figure 5.1: A screen capture showing the dynamixel wizard. This was used for initial servo set up, as well as joint level tuning for PID position control.

to applications such as repetitive equation resolution and I/O communication. For this system, we chose to communicate with MATLAB via two way serial.

MATLAB uses its own set of syntax, and it is possible to create scripts, functions and subroutines. Like most other programming platforms, we first begin with a setup or initialization loop, as seen in Fig 5.2. This was used to feed initial parameters into the servos, and prepare them for a set of gait cycles.

After this, the main body of the code, which calls on various sub-functions and subroutines, was implemented as seen in Fig. 5.3. This actually communicates with the on-board microcontroller discussed in section 5.3, after which it uses slope information to generate gait parameters and then combines this with system parameters to develop a single trajectory for the zero moment point. From here, the system then begins calculating joint trajectories based on the number of steps, and cycles until this number is satisfied. Finally, the trajectory is smoothed, and the joint angles are sent back to the actuators.

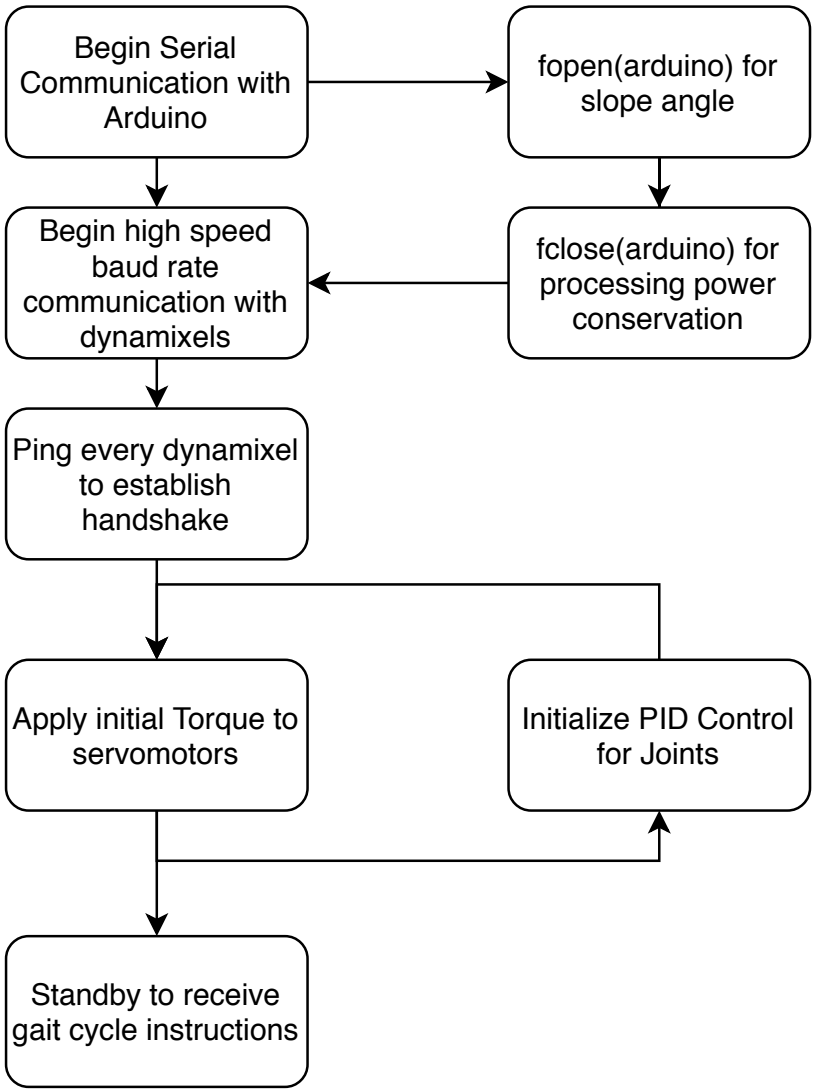

Figure 5.2: A diagram showing the initial setup loop involved in the running of the open loop gait code on MATLAB from the remote PC. This was necessary due to processing power constraints.

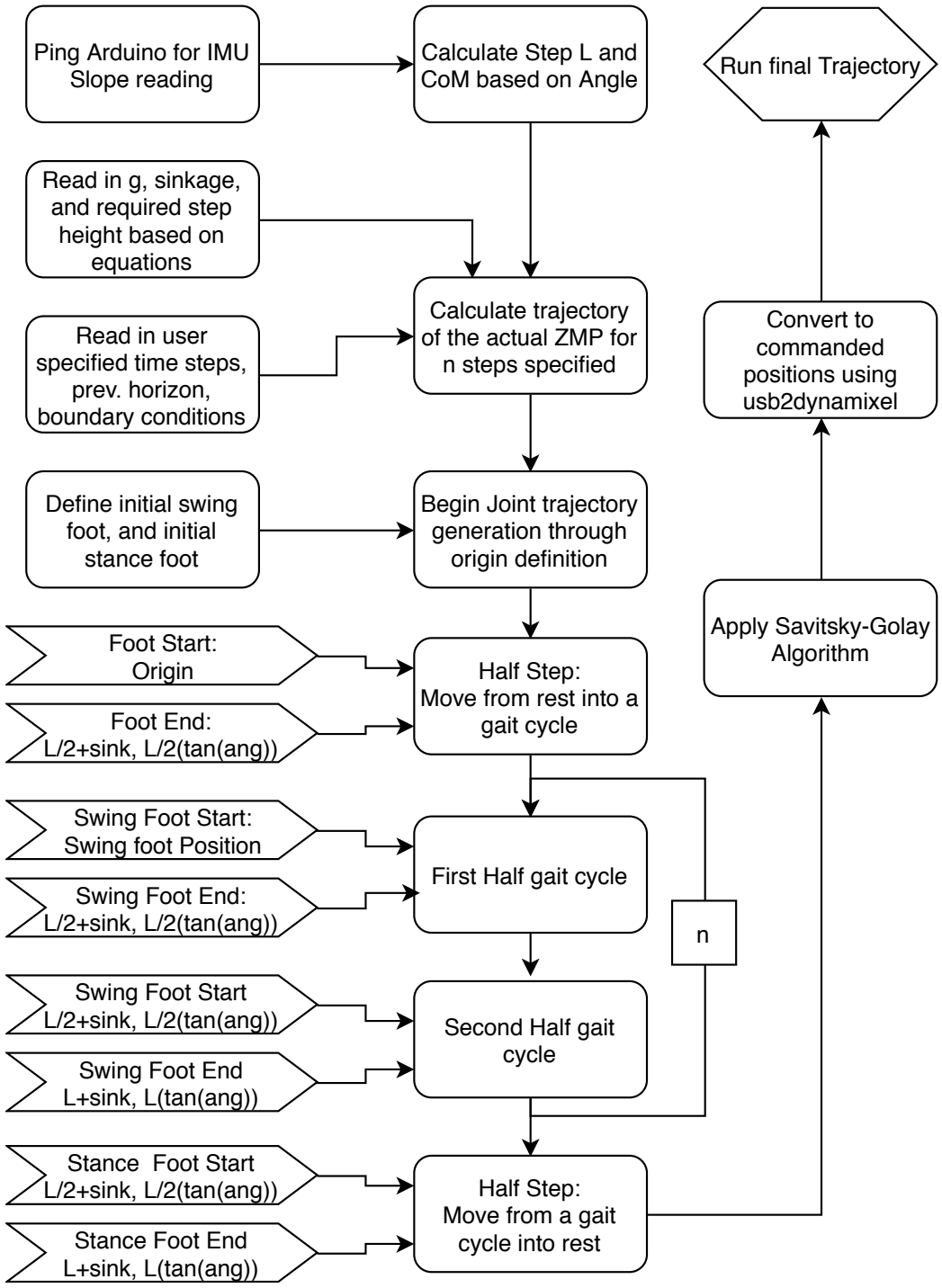

Figure 5.3: A diagram showing the main algorithm used in generation of the optimized open loop gait from MATLAB from the remote PC. Once again, because of the computation power involved in this operation, we were unable to run this process on-board the biped walker.

5.3 Arduino IDE

For the control code, we required a system that could be implemented in-the-loop, without needing to be as computationally robust. As such, the Arduino Uno was chosen, and the Arduino IDE was used to write and compile the torso and foot control code. This code primarily consisted of two loops, the setup (Fig. 5.4) and the main loop (Fig. 5.5). The setup loop runs once at the beginning of a gait trial, and defines all necessary variable and initial conditions. After this, the main loop runs until the operator resets the system, and handles the main controller inputs and outputs.

The torso control for the system was linked directly to the IMU. The raw voltage readings from the IMU were obtained via the SCL and SDA pins on the Arduino, after which they were processed and converted into pitch values. These were then fed as a reference input into the torso servo. This servo used a simple PID control for gradual adjustment, with the absolute position chosen such that it redistributed the weight within the stable boundaries of the feet (this is further discussed in Chapter 6). This was a simple, easy way of contributing to the static stability of the system.

To streamline the flow of information into the control scheme for the feet, comparators and logic were used, as see in Fig. 5.5. When the FSR's relay input in the form of voltage, the system instantaneously converts the signal to force. The differential comparators look at the differences in heel and toe forces, and determine whether the system is leaning too far forward or backward. Additionally, the threshold comparator, looks at the raw force readings of the system to determine whether it is beyond what it should be, given the weight and loading pattern of the robot. The output of these blocks then determines the direction and extent of the expansion of the feet.

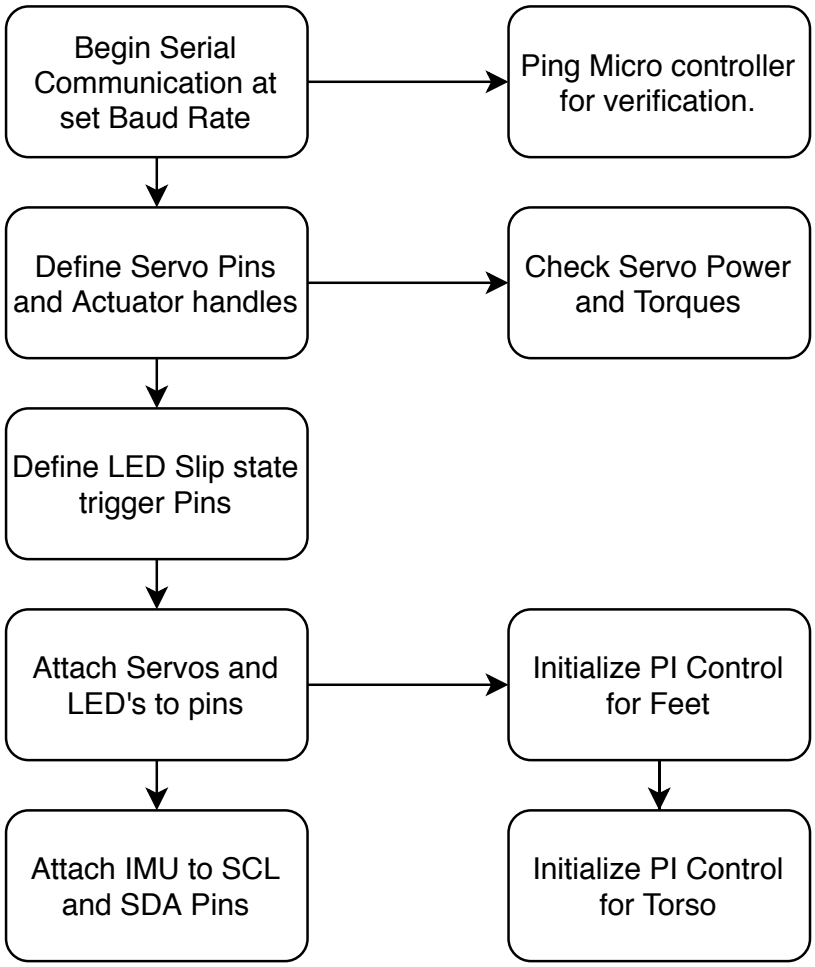

Figure 5.4: A diagram showing the initial setup loop involved in the Arduino based control scheme for the torso and feet. Unlike the gait generation scheme, this portion of the system was run on-board the system.

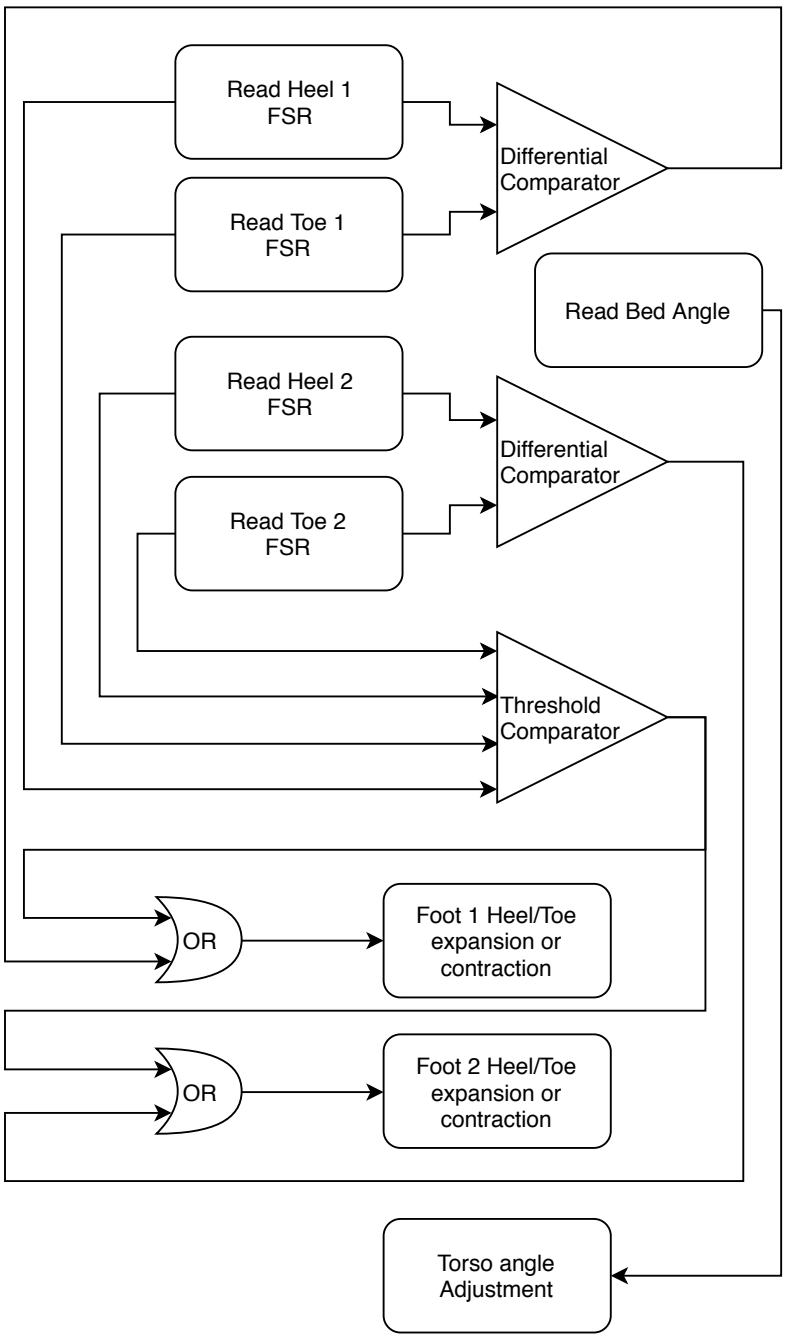

Figure 5.5: diagram showing the high level logic process involved in the Arduino based control scheme for the torso and feet. This was designed to be light and quick to be able to respond in-the-loop when faced with perturbations.

5.4 OBS and Movavi

OBS and Movavi were used to capture and process .mp4 video. This allowed for close examination of frame data and distances, particularly in the case of backward slip and forward locomotion.

CHAPTER 6
RESULTS

In this chapter, we will discuss the experiments conducted using the 7 degree of freedom planar walking biped. We will seek to analyze experimental results, make meaningful observations about the system behaviour, and finally, leverage this knowledge to inform the next iteration of the robot walking system.

6.1 Experimental Design, Observations and Results

When attempting to design and build a robot that efficiently traverses granular inclines, it became apparent that robust experimentation and analysis were required to appropriately quantify our system behaviours. Previous work identified an open loop scheme that encompassed the identification of a stability region for flat footed bipedal walking on level granular material. In order to help the robot walk uphill, we realized that a complete redesign of the open loop gait would have to occur to allow for effective ambulation. After this, we would also need to identify some control scheme to account for deviations from open loop gait.

Before diving into a control scheme, however, it was necessary for the open-loop gait of the system to be adequately characterized and optimized. This was achieved through a number of systematically run experimental trials on a test bed of loosely packed granular material. Firstly, intrusion experiments with the robotic feet were performed to empirically identify foot angles which led to walking without falling. After this, a systematic experimental study in which a staircase biped robotic gait for traversing a sandy slope was empirically designed using Zero Moment Point (ZMP) methods. From these two experiments, results were combined to design, produce and implement gaits that allowed the 7 degree-of-freedom planar biped to ascend slopes of up to 8 degrees, initially using the kine-

matic parameters from past literature. Once the template for an uphill gait was completed, it was then necessary to bolster the robustness of the gait, over a wider range of angles. To achieve this, kinematic parameters from literature were varied experimentally, to produce an interpolated fit for gait, relating the ZMP stability criterion for uphill walking to given slope angles. This was then subsequently put through a series of sensitivity validations at different slope angles.

After this characterization, torso control was implemented to respond to large changes in bed angle, affecting the overall center of mass position of the robot system, and thus the center of pressure of the foot. Concurrently, the force-sensitive feet were then used to provide instantaneous input from the foot surface into a plantar surface area expansion system, which dynamically increased contact area of the robot at the heels or toes, depending on the ground reaction force anomalies of the system. Similar to iterations of open loop gait, the robustness and success rates of these gaits were tested, and the sensitivity was also validated.

Future work discussed in this chapter focuses on a trend that was noticed during gait design: the biped slips backward while maintaining its dynamic stability as it ascends a sandy slope, with a slip distance related to slope angle. In fact, the biped can lose as much as 73% of its expected gait distance to slip at angles of 10 degrees. As such, moving forward, we plan to then expand our control scheme to compensate for the system balance during slip.

6.1.1 Open Loop Staircase Gait Design

ZMP Walking is based on the idea of the Linear Inverted Pendulum Model (LIPM) of bipedal walking, built upon the concept of a stability region in which stable gaits can be generated. Unlike other more dynamical methods of walking, a main characteristic of ZMP is that at any given moment, the trajectory of the gait places the biped within the stable region of the LIPM. Typically, literature for ZMP walking assumes a constant vertical

center of mass (CoM) height and constant foot position, for locomotion on flat surfaces. Thus, for level ground this position is determined using the following equations [9]:

$$P_{x-zmp} = \frac{-\tau_y}{mg} \tag{6.1}$$

$$P_{y-zmp} = \frac{\tau_y}{mg} \tag{6.2}$$

Where τ_x and τ_y are the torques on the ankle of the robot due to inertial effects of the biped, g is acceleration due to gravity, and m is the robot mass. However, once we consider any deviation from walking on regular flat ground with constant center of mass, for instance, walking uphill on soft ground, we need to appropriately modify this equation in order to remain within a stability region. For three dimensional systems, this presents as a series of equation that needs to be controlled about these two axes. Since our biped system is constrained about the x-axis, our system of equations for trajectory can be simplified to:

$$P_{zmp} = P_{y-zmp} = \frac{\tau}{mg} \tag{6.3}$$

If we then consider that the acceleration in the y -direction is given by:

$$\ddot{y} = \frac{g}{z}y - \frac{1}{mz}\tau_x \tag{6.4}$$

where z is the intersection distance from the contact point of the robot with the CoM plane, we can then use this information and substitute (6.2) into (6.4), resulting in:

$$P_{zmp} = P_{y-zmp} = y - \frac{z}{g}\ddot{y} \tag{6.5}$$

This is the governing equation for our planar ZMP walker, and the primary basis on which we begin to modify our gaits.

Once our ZMP position equation has been established, it is necessary to use the properties of the robot to develop the actual joint trajectories of the system. From the literature, previous work demonstrated that the static placement of the foot allowed for the reactive terrain forces to balance the ankle torques. As such, when designing a trajectory, the estimated stability region of the granular material needed to be equivalent to the stability region of the LIPM ZMP model. It was also necessary to design trajectories such that that stability criterion is satisfied for all time [3]. When we factor in the approximate sinkage of the granular matter to be traversed, we arrive at the model to calculate the trajectory of the robot joints T_{ZMP}, which can be given as a function, and is explored further in [3]:

$$T_{ZMP} = f(CoM, L, h, S, g, B_{front}, B_{back}) \tag{6.6}$$

Where CoM is the center of mass height, L is the biped step length, h is the step height, S is the sinkage of the biped, and B_{front} and B_{back} are the stability conditions of the biped for its given mass and size constraints.

Because the surface of the slope is that of granular material, a gait that addresses uphill climbing must be used with the same accommodations made for sinkage and equivalence of the stability regions. When designing our approach to this problem, the following were considered:

1. *Slippage and uniform compaction*: To provide a model of constant sinkage which could be estimated and eventually fed into a ZMP trajectory equation, it is necessary to have predictability of the behavior of the bed. A fluidized bed was built, as discussed in Chapter 2, that allows for the repeatable preparation of uniform and loosely packed granular material, in this case poppy seeds [7]. Blowing air up through the base of the bed fluidizes the substrate when turned on, and after deactivating the blowers and letting the grains settle, a loosely packed and uniform granular surface remains. To accurately feed sinkage information into our ZMP trajectory generation

Table 6.1: Robot and bed sinkage parameters for the 7 degree of freedom planar walker

Quantity	Value
Robot Mass	1.86 kg
Plantar Surface Area	100 cm3
Intrusion Depth	1.8 cm
Foot Length	20 cm
Foot Height	5 cm

algorithm, we first needed to know what the sinkage of the robot would be at a given weight. to address this, a simple measurement of parameters was conducted, as seen in table 6.1. If the sinkage is not properly accounted for in situations where complex, nonlinear ground is considered, we find that the robot gait will, of course, not compensate for the extra sink distance, and thus cause dragging and tipping during the gait cycle.

2. *Failure of the substrate itself*: Another key challenge that we face when walking uphill on granular material is the failure of the surface itself, due to the effects of gravity, frictional forces, and lateral forces applied by the surface of the robot foot [25]. These complex interactions have been found to occur in slopes as low as 6° for the robot,

Staircase gaits have been studied with respect to ZMP trajectories for many years [14, 15]. Similarly, ZMP trajectories over uneven or complex terrain have also been very thoroughly explored, due to the fact that biped robots rarely operate in perfectly ideal situations [3, 13]. We seek to combine much of the work that has been done in order to allow for the development of a robust uphill walking uphill over granular material, to serve as a foundation for any control scheme.

When deviating from flat ground, inconsistencies in the ZMP position generation scheme tend to arise, due to the fact that the equation assumes transfer of this point along a plane during the double support phase (DSP). As such, even though we are interested in a staircase-type gait, in which each foot lands slightly higher than the other, we quite simply use a virtual slope model [15]. Thus, our flat walking ZMP equation derived in 6.5 can be modified, leaving us with an expression for stair climbing up a virtual slope that was implemented as our ZMP staircase equation [15]:

$$P_{zmp}\frac{k\ddot{y}+g}{g} = y - \frac{z}{g}\ddot{y} \tag{6.7}$$

This equation allows the trajectory of the foot to follow a staircase pattern, while allowing it's CoM to ascend the slope in a linear manner. However, implementation of a staircase gait by itself is not sufficient to implement on a slope with sinkage. Two major modifications were made to the trajectory generation to provide a novel, robust, and stable gait. Because the differences in slope angles are trigonometrically related to the "height of the stairs", the slope angle and intrusion angle of the foot were necessary augmentations of (6), such that the function to generate T_{ZMP} must include θ and ϕ as inputs:

$$T_{ZMP} = f(CoM, L, H, S, g, B_{front}, B_{back}, \theta, \phi) \tag{6.8}$$

Where θ is the slope angle of the sand,and ϕ is the intrusion angle of the foot. A kinematic playback of this can be seen in Fig. 6.1. Once this gait was developed, it was found that a traditional spline fit [3] of the ZMP trajectory path was sufficient only up to the point in the gait cycle that the robot seeks to compensate for sinkage (at the end of two full steps, or one full gait cycle). Because of this, a Savitsky Golay [18] criteria, or piece-wise spline with history, was designed and used to generate a smoothed staircase trajectory for the robot to follow.

Table 6.1.1 outlines the algorithm for the calculation of the joint trajectories. The pro-

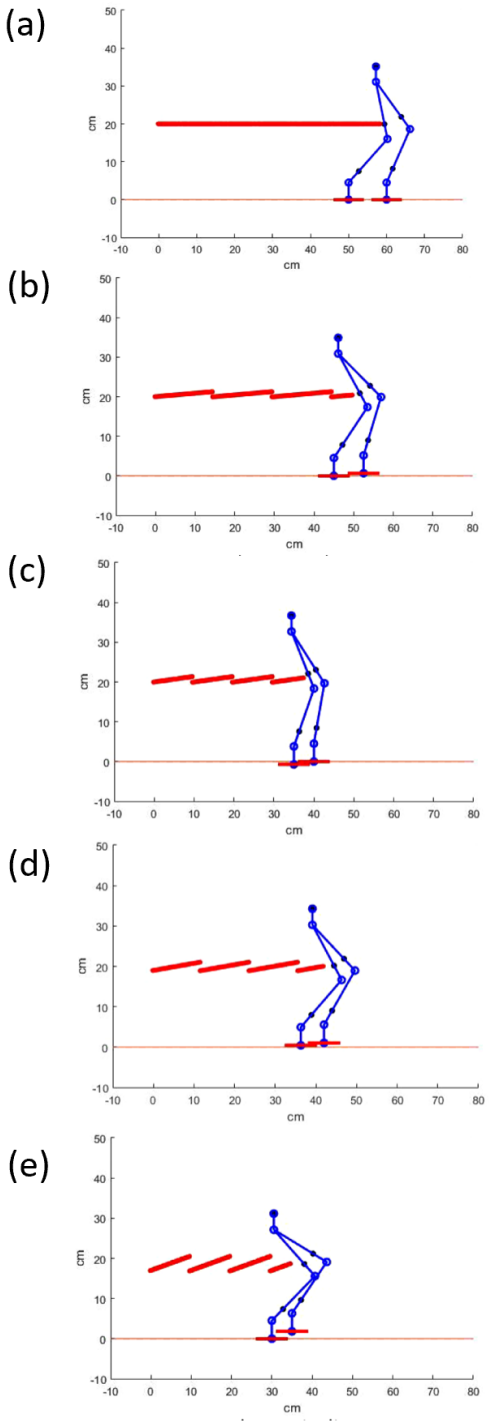

Figure 6.1: When the gait was being tested, a kinematic playback environment was used to test feasibility before bench-top implementation on the robot. The figure shows CoM trajectory at (a) 0 degrees, (b) 5 degrees, (c) 10 degrees, (d) 15 degrees, and (e) 20 degrees.

cess of Preview Control [3, 9, 14, 15] was used to generate ZMP references, which are then converted to joint angles through inverse kinematics. The necessary intrusion angle of the foot is represented by ϕ, and the forward hip posturing can be given as $\phi/2$. s_{DSP0} is the set number of initial double support samples, s_{DSP}, is the number of double support samples, s_{SSP} is the number of single support samples, n_{steps} is the number of steps, $Q_{initial}$ is the initial joint position matrix, Q_{SSP1} is the first SSP joint position matrix, Q_{DSP1} is the first DSP joint position matrix, Q_{SSP2} is the second SSP joint position matrix, Q_{DSP2} is the second DSP joint position matrix, $Q_{SSPFinal}$ is the final SSP joint position matrix, $Q_{DSPFinal}$ is the final DSP joint position matrix, $Q_{intermediate}$ is the pre-processed joint position matrix, Q_{final} is the final joint position matrix, and H is the preview horizon.

6.1.2 Open Loop Staircase Parameter Choice

To quantify our foot size, and thus B_{front} and B_{back} [3], we adapted the idea of the "polygon of stability" for locomotion on hard ground for use on granular media [3]:

$$d_c = \frac{L}{2}(1 - \frac{1}{\gamma}) \tag{6.9}$$

where we consider relationship of the planar foot length, L, to intrusion depth d_c and γ is the force overshoot ratio, which factors in force and velocity of the intrusion into the granular material, and can be obtained from literature.

Apart from this, the parameters used at the beginning of the process were those from previous literature that fell within the stability criterion for flat footed, carefully controlled locomotion on granular material [3]. These gave us somewhat of a starting point for the experiments detailed in this section, and were given as a *CoM* height of 20.5cm, swing foot height h of 3cm, sinkage S of 1.8cm (table 6.1, B_{front} and B_{back} being taken from (6.9)), and a step length L of 15cm.

Table 6.2: Joint trajectory generation for the planar walker

	Algorithm for Joint Trajectory generation
1)	Slope angle read in; L and CoM computed: $L, CoM = (\theta)$
2)	ZMP Trajectory Reference computed: $ZMP\ Ref = (s_{DSP0}, s_{DSP}, s_{SSP}, n_{steps}, B_{front}, B_{back}, L)$
3)	ZMP Ref used to calculate CoM trajectory from Preview Control: $CoM\ Traj = (ZMP\ Ref, H, CoM, T, g, \theta)$
4)	CoM Traj used to plug into the robot inverse kinematics In general: $Q = (CoM\ Traj, backgoalposition, frontgoalposition)$ $Q_{initial} = (CoM\ Traj, 0, 0)$ $Q_{SSP1} = (CoM\ Traj, 0, sink+(L/2)tan(\theta))$ $Q_{DSP1} = (CoM\ Traj, 0, sink+(L/2)tan(\theta))$ $Q_{SSP2} = (CoM\ Traj, sink+(L/2)tan(\theta), sink+(L)tan(\theta))$ $Q_{DSP2} = (CoM\ Traj, sink+(L/2)tan(\theta), sink+(L)tan(\theta))$
5)	Repeat for n_{steps} if n_{steps} is complete: $Q_{SSPFinal} = (CoM\ Traj, sink+(L)tan(\theta), sink+(L)tan(\theta))$ $Q_{DSPFinal} = (CoM\ Traj, sink+(L)tan(\theta), sink+(L)tan(\theta))$
6)	Applying smoothing and adjustments: $Q_{intermediate} = (Q_{initial} + n_{steps}(Q_{SSP1}+Q_{DSP1}+Q_{SSP2}$ $+Q_{DSP2})+Q_{SSPFinal}+Q_{DSPFinal})$ Q_{Final} = Savitsky-Golay($Q_{intermediate}, \phi$)

6.1.3 Intrusion into Granular Material

We first sought to experimentally determine the ideal angle of foot intrusion for our system. From a systematic experimental sweep of foot angles, we found that the optimal foot angle was:

$$\theta = \phi. \tag{6.10}$$

The results of this experiment can be seen in Fig. 6.2, and was conducted as following:

1. *Establishing of Reference Frames*: The lab frame was used as reference, with the floor being 0°. The bed of poppy seeds was elevated to 5°.

2. *Sweep of Angles of Intrusion*: For N=5 trials for each foot angle between -5° and 10°, the walker was run for n= 4 steps, and a success was defined as the walker standing upright on two feet at the end of the trial, else the experimental trial was recorded as a failure. This gave an experimental data set size of 96 total trials.

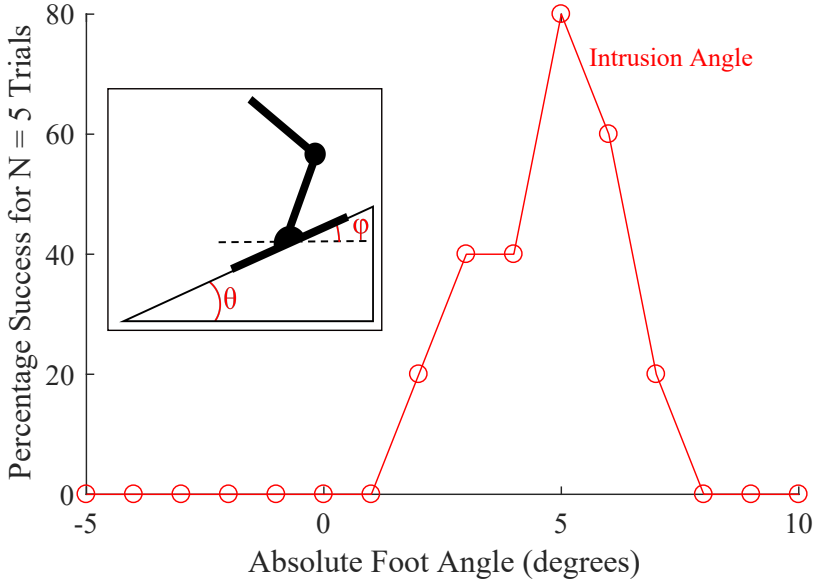

Figure 6.2: Results of varying the intrusion angle of the foot on the slope surface where $\theta = 5$ is the slope angle, and ϕ is the absolute angle of the foot, measured in the lab frame. The highest rate of success was found to be tangent to the surface of the slope.

When we consider a low-mass, low speed system like the biped walker, this result made intuitive sense to us, since the robot did not have enough mass or velocity during a given gait cycle to intrude effectively into the granular material. Instead, much like the sidewinder rattlesnake [6], we achieved the greatest success when we attempted a normal foot surface placement to a given slope angle. Thus, we hypothesize that a "placing" instead of a "digging" foot motion was more successful due to the relatively low mass and plantar pressure of the walker, compared to the "digging" behavior of humans which are significantly heavier and more effective at intruding beyond the granular surface [5].

6.1.4 Open Loop Characterization and Interpolation of Gaits Parameters

Previously, the relationship in (6.8) was considered, and through systematic experimentation, a set of parameters was identified that allowed for a stable gait at $\theta = 0^\circ$. However, our end goal required that our system would be able to traverse inclines of up to 10°. Thus, to achieve this, we began with these same parameters: the *CoM, L, H, S*, B_{front} and B_{back} that worked for the previous iteration of the biped system to operate on undisturbed, level ground. These were chosen because we knew that they intrinsically fulfilled the stability requirements for the ZMP equation. From here, it became apparent that these parameters became increasingly ineffective at higher slope angles, and thus, we sought to design an experiment that could quantify our successes and failures, allow for exploration of more suitable uphill parameters, and then juxtapose the successes and failures of our new parameters to those previously used. The experimental methods employed in this process were as follows:

1. Since the robot was required to climb a slope of from 0° to 10°, we first sought to identify a "best average" gait formulation. To achieve this, the bed was raised to 5°, the average of the slope angles that would be traversed by the walker.

2. Since S, B_{front} and B_{back} were geometric properties of the system that could not be changed, and h had negligible effect on the stance stability, we sought to modify

the remaining variables in the trajectory generation algorithm, namely *CoM* and *L* through systematic exploration. To do this, we began with the initial parameters that worked at 0°, and gradually lowered the *CoM* and *L* in 0.5cm decrements until a gait was achieved that allowed for a success rate above 80% for a set of $n = 5$ runs. This gave us our general climbing parameters.

3. These parameters then needed to be fully characterized. The newly obtained values of *CoM* and *L* that allowed for successful trials at θ=5 were used to generate a trajectory for n = 4 steps. Similar to before, a success was defined as the walker completing all 4 steps and returning to an initial double support (DSP) position. The bed was leveled and the ground was re-fluidized and reset before each trial.

4. A sweep of trials was conducted with bed angles from θ=0 to θ=10°, with $\phi = \theta$. Ten trials were run at each bed angle (n= 10) trials. This gave an experimental data set size of 100 total trials.

The successes and failures of the experiment can be seen on Fig. 6.4, where as expected, the gait generation mechanism is the most robust at θ=5°, with a success rate of 80%. However, for just a 2° increase, the success rate falls drastically to 30%, and with a 4° increase, the success rate drops all the way down to 0%. Thus, it became necessary to formulate a gait generation scheme that could improve performance at these inclines. The method used to do this was as follows:

1. Just as before, a success was defined as the walker completing 4 steps and returning to an initial double support (DSP) position. The bed was leveled and the ground was re-fluidized and reset before each trial. Through systematically incrementing and decrementing our values by 0.5cm, starting at θ=5°, at each angle, a set of parameters *CoM, L* were also established from θ=0° to θ=10°, with a success being defined as the largest values of *L* and *CoM* to allow for at least 50% success during N = 10 gait trials at a given θ. This metric of success was chosen due to the fact that we are

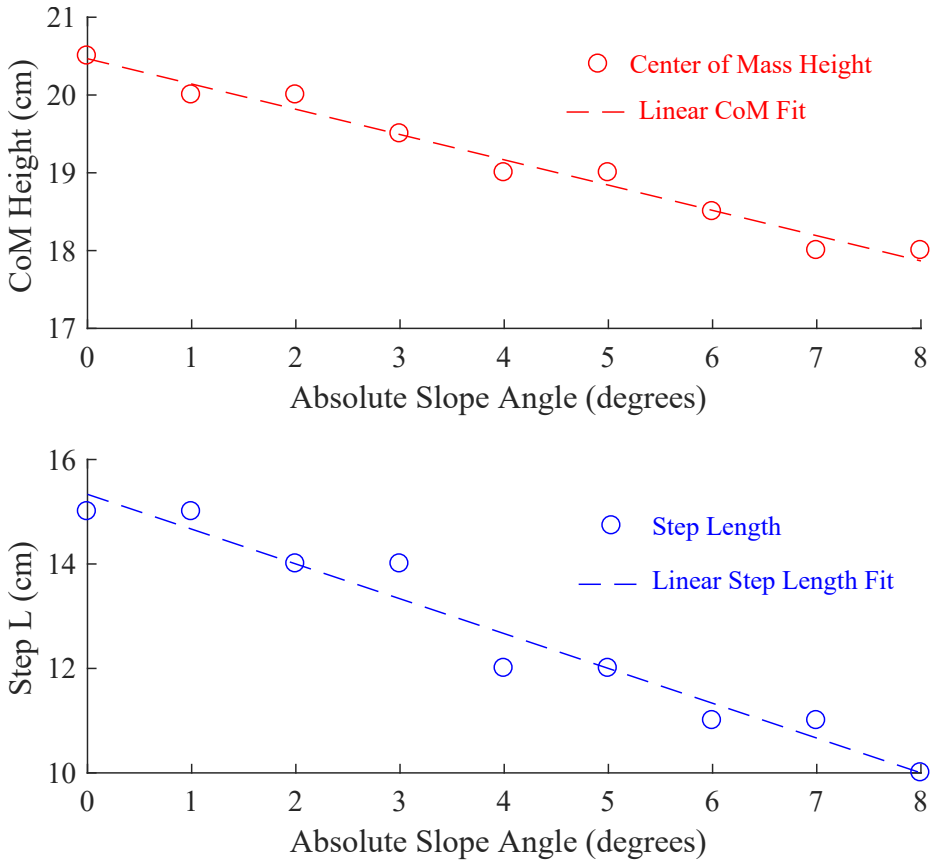

Figure 6.3: Manually tuned gaits for specific slopes. These were then used to formulate a parameterized policy through the use of a linear fit. In (a), we see the results for Vertical CoM height, and in (b) we see the same experiment for step length. In order to accommodate increasing slope angles, we found that decreasing the Step Length and CoM height was necessary.

primarily concerned with the locomotion of the robot on a granular incline, and as such, a larger L and CoM were favored.

2. The successful parameters from $\theta = 0°$ to $\theta = 10°$ were then fit with a linear regression, and functions that related all parameters to slope angle were identified for the planar walker. (Fig. 6.3).

3. A sweep of trials was again conducted with bed angles from θ=0 to θ=10°, with $\phi = \theta$. This time, however, instead of constant parameters, the CoM and L angle-dependent functions were used to generate the corresponding gaits. Ten trials were

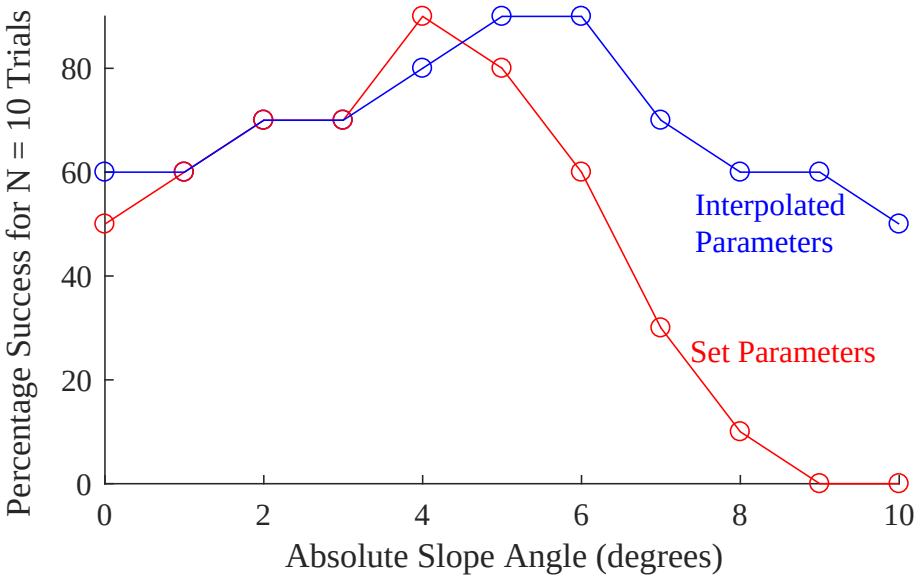

Figure 6.4: Results of trials for set (L = 15cm, CoM = 20.5cm) and interpolated parameters using the staircase gait. When the same set parameters of L and CoM were used, there was a higher failure rate than when interpolated (connected) parameters were used. The similarity in the curves at angles lower than 6° is likely due to the fact that the gait was designed around a 5 degree incline, and then adapted to other slope angles accordingly.

run at each bed angle (n= 10) trials. This gave an experimental data set size of 100 total trials.

At this point, because the step length and CoM were both related through a system of continuous linear equations, the robot had a specific gait for each slope angle within the limits of the hardware setup (angles of $0-10°$, with a resolution of $0.01°$). Once this parameterization was applied, we found that the robot was significantly more successful at traversing the sandy slope, due to the specificity of each gait to a particular incline. The results of this can be seen in Fig. 6.4. These results are encouraging, since we were able to improve our success rates at $\theta = 9°$ and $\theta = 10°$from 0% to 60% and 50% respectively; a substantial improvement over our initial trial.

6.1.5 Testing Gait Sensitivity

Once the gait was parameterized to be slope-specific, it then became necessary to augment the walking to become more resistant to perturbations. To quantify this, we tested the robustness of the parameterized gaits of the walker [6] using systematic sensitivity experiments that modelled this disturbance as a deviation from the commanded slope angle. This served as a practical test of our method to mis-estimations of the slope angle by sensors or operators. In order to do this, another experiment was designed:

1. A slope angle of $\theta = 2^\circ$ was input into the gait code, for $n = 6$ steps. A success was defined as the walker completing all 6 steps and returning to an initial DSP position. The bed was leveled and the granular terrain was reset through the air fluidized before each trial.

2. The bed was raised to the corresponding θ input into the code, and the robot was run $N = 3$ times, each time recording the distance, and at the end of the third trial, establishing an average distance. This was considered to be our benchmark distance, or our relative distance of 1.

3. The bed was then lowered to an angle of $(\theta – 1^\circ)$, while keeping then same input angle of θ in the code. The robot was run $N = 3$ times, each time recording the distance, and at the end of the third trial, establishing an average distance. This distance was then divided by the average distance at θ to obtain a relative distance traveled. This is important due to failure and slippage of the robot.

4. Once more, the bed was lowered to $(\theta – 2^\circ)$ and the robot was run $N = 3$ times, each time recording the distance, and at the end of the third trial, establishing an average distance. This distance was once again divided by the distance traveled at slope θ in order to obtain a relative distance traveled.

5. This process was further repeated another 2 times, this time increasing the bed angle

beyond that of the commanded angle. Thus, for a commanded angle of θ, the actual bed angles would have been $(\theta + 1^\circ)$ and $(\theta + 2^\circ)$ respectively.

6. After the relative distances were analyzed for a commanded gait angle of θ=2°, the entire process was then repeated for θ=4°, 6°, 8° and 10°, giving a grand total of 150 experimental trials.

For low angles, $(\theta < 6^\circ)$ we find that there is a reasonable level of robustness to perturbation in the open loop gait (Fig. 6.5). This is indicated by the high relative distances(fraction of distance covered at a particular offset angle, compared to the distance traveled when the slope angle is accurate to the gait) at lower inclines. However, at higher granular inclines, we observe large drop-off on either side of the sensitivity curve, once the gait is not specifically designed for that particular incline. It is this key fact that highlights the need for some sort of control scheme, as will be discussed later in the chapter.

6.1.6 Failure Methods

Over the course of hundreds of experimental trials, it became apparent that two major types of failure occur. These are described below.

Tipping

At lower angles, typically for $\theta < 6^\circ$, the main method of failure is through tipping, or unintended intrusion of the biped into the granular media. This is usually as a result of unresolved moments that cause forward or backward rocking. These in turn cause a slight intrusion of the heel or toe into the granular media. At this point, when the robot attempts to take another step, if the extra resistive and frictional forces are sufficiently high, the robot will fail, and fall either back or forward.

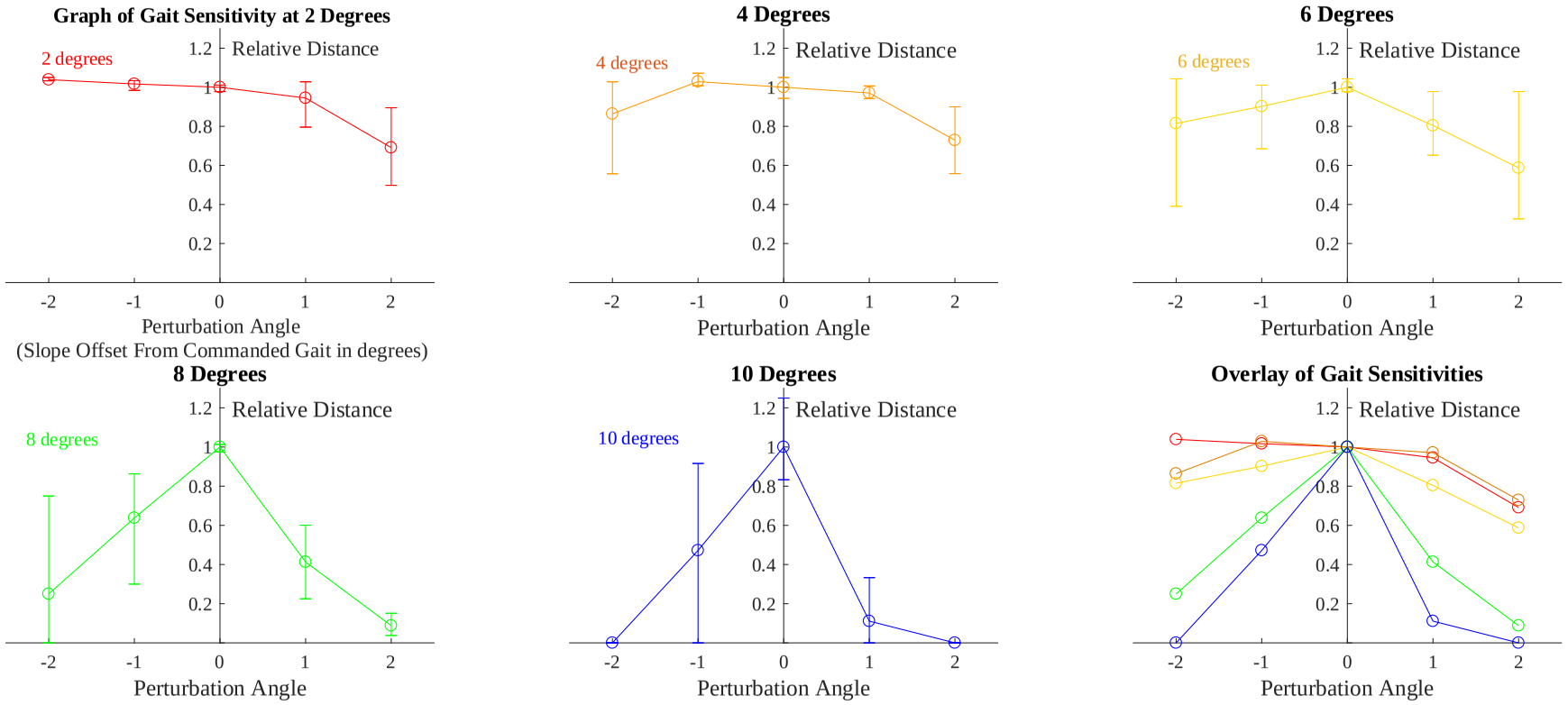

Figure 6.5: Gait sensitivity plots for biped staircase ZMP gait from 2 to 10°. relative distance was used instead of absolute distance because of varying step lengths when climbing the slope. We see that as we deviate from the expected distance, we observe a significant decline in performance. This is especially apparent at steeper inclines. For a slope angle of 2°, the plan biped was still able to achieve a relative distance of over 0.6 for a perturbation of 2° in either direction. However, at 10°, this falls to 0.0.

Slipping

At higher angles ($\theta > 6^{\circ}$), the primary form of failure was observed to be slipping of the material itself. This will be discussed further in subsection 6.1.7, however, the main cause for failure is the yielding of the granular material itself. From our elementary observation and analysis, we hypothesize that lateral forces of the foot placement and the gravitational effects of the poppy seeds above and below the stance position of the robot on the bed agitate the granular material from a state of rest, to that of an 'avalanche' effect. This yielding of material causes instability at the foot surface, and thus makes the robot itself fall over.

Loosely Packed and Compacted Material Variations

One ongoing area of exploration is that of locomotion on loosely packed granular media versus compacted material. We hypothesize that because of more aeration in loosely packed media, and less required force to cause some degree of intrusion, failure by tipping is more likely in loosely packed granular media. This is intuitive, in that the more compact the granular material, the closer it begins to model hard ground [3].

6.1.7 Backward Slip and the "Granular Treadmill" Problem

Another aspect that we explored was that the actual commanded distance did not always equate to traveled distance on a slope of granular material (Fig. 6.6). After inspection of videos of the foot-substrate interaction and flow, we hypothesized that this was due to slippage during the DSP, in which the robot is stable, but still slides incrementally backward as it positions its second foot. This is seen in Fig. 6.7.

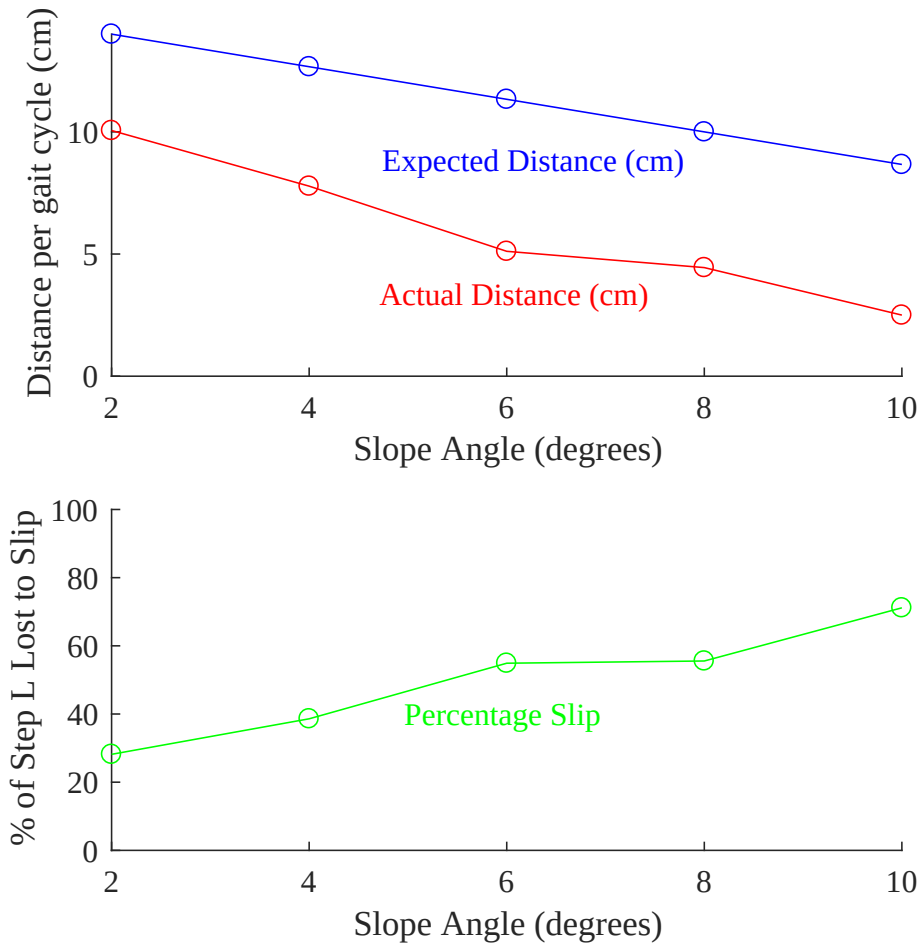

Figure 6.6: Graph showing the actual and commanded distance for slope angles between 2° and 10°.This allows us to better understand and characterize the slipping (backward motion of the robot foot due to sliding on the granular surface) of the robot for each slope angle. As can be seen, the robot slips more as the slope becomes steeper

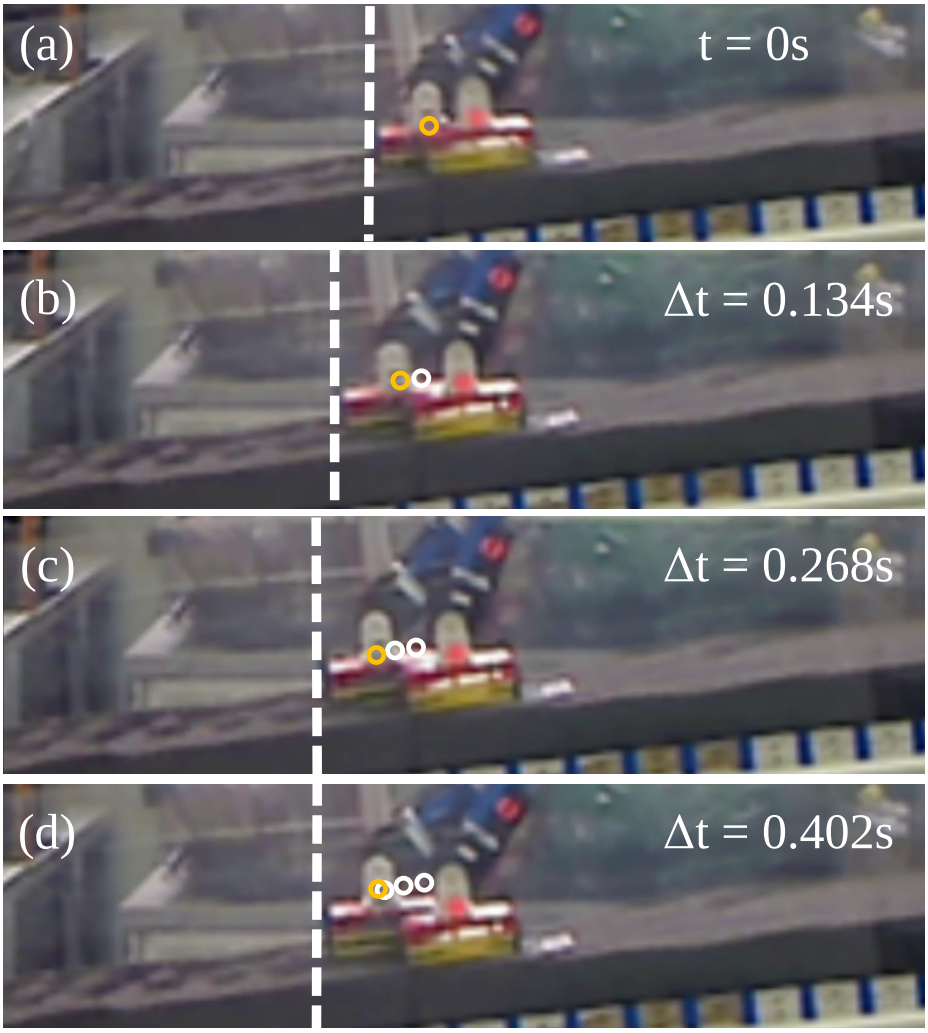

Figure 6.7: A zoomed in profile of the foot slip during walking on a slope of granular material, where the dashed lines signify the back of the robot foot, the orange circles mark the current position of the ankle joint, and the white circles mark the cumulative positions for the displayed frames. In (a), the foot makes initial contact for a DSP with the sandy slope. In (b), the back foot begins to slide backward, instead of staying fixed on the ground as expected. in (c), the foot has arrived at its furthest position, and the robot begins another SSP as seen in (d).

6.1.8 Constant Parameter Experiments

Once the above experiments were conducted, it became necessary to verify which of the main manipulated parameters, namely CoM or L, that had the most significant impact on success rates and distance travelled. To test this, an experiment was designed that firstly held the step length of the robot constant at the average value of the ZMP permissible range (12.5 cm) while varying the CoM height. After this, the CoM height was held constant, and step length was varied. A similar experiment to subsection 6.1.4 was used:

1. A success was defined as the walker completing 4 steps and returning to an initial double support (DSP) position. The bed was leveled and the ground was re-fluidized and reset before each trial.

2. N = 10 gait trials were conducted at $\theta = 2$ and the lowest possible CoM height for a constant step length of L = 12.5cm. After this, the CoM height was raised by 1cm. N = 10 gait trials were again conducted at the new CoM height. The entire process was repeated until achieving a CoM height of 20cm at $\theta = 2$.

3. After this, the process in step 2 was repeated for angles of $\theta = 4, 6, 8$ and 10°. This gave an experimental data set size of 170 total trials for constant step lengths.

4. N = 10 gait trials were conducted at $\theta = 2$ at the lowest possible step length for a constant center of mass height of CoM = 18.75cm. After this, the step length was increased by 1cm. N = 10 gait trials were again conducted at the new step length height. The entire process was repeated until achieving the longest step length in the permissible region of our equations at $\theta = 2$.

5. After this, the process in step 2 was repeated for angles of $\theta = 4, 6, 8$ and 10°. This gave an experimental data set size of 230 total trials for constant center of mass heights, and a grand total of 400 constant parameter identification trials.

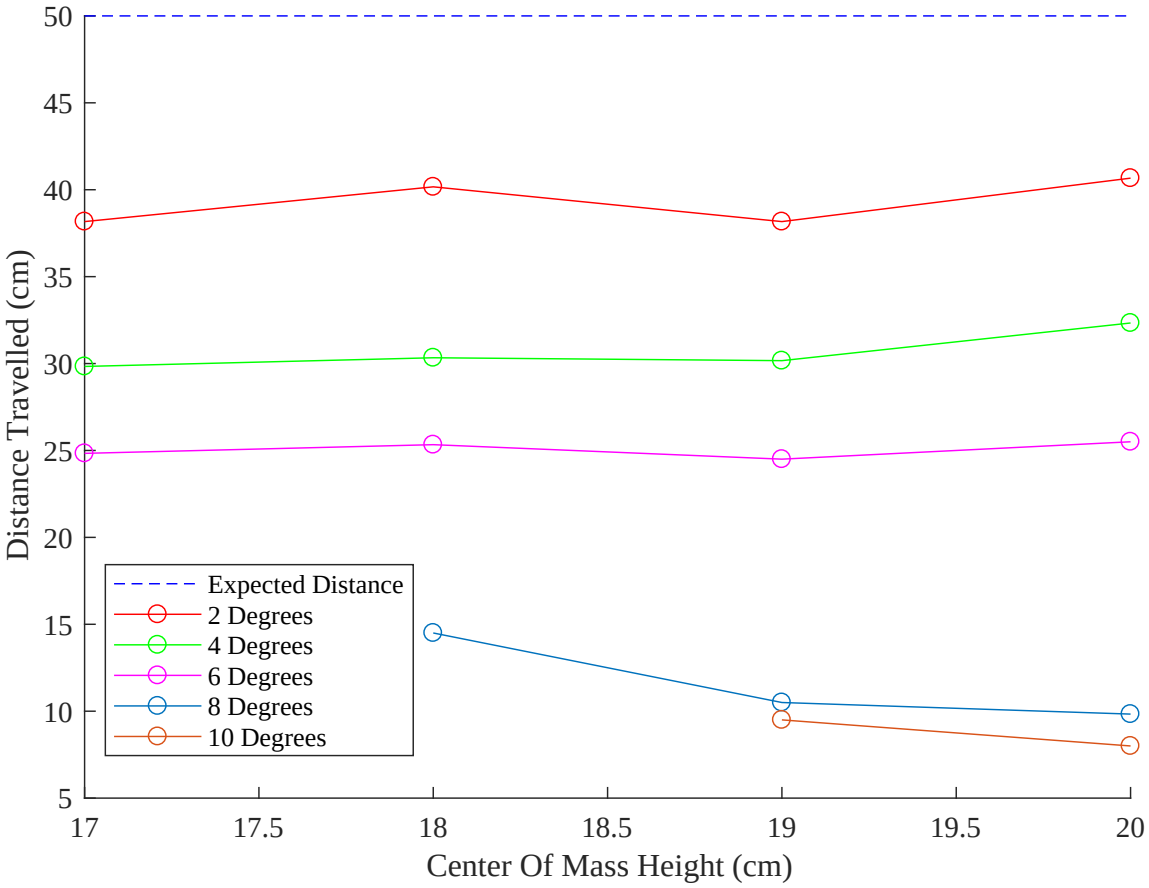

Figure 6.8: Graph showing the expected and actual distance for slope angles between 2° and 10° when the Step Length is held constant at an average of 12.5cm. This study allowed us to better understand which of our two key postural parameters, CoM or L, played a more significant role in locomotion. With the exception of the 8° graph, the graphs are offset from the expected distance by some value, but retain a similar gradient.

As seen in Figs. 6.8 and 6.9, the slippage referenced in subsection 6.1.7 accounts for an offset from our expected values for distance. For the case where the step length is held constant (6.8), we see that, with the exception of the 8° graph, the curves have similar shapes to that of the expected distances. However, in the case of a constant center of mass height, (Fig. 6.9), we find that increasing the step length actually increases the magnitude of the offset at any given angle. This leads us to the conclusion that the kinematics and dynamics involved in shortening or lengthening a step are largely the dominant parameter when considering low mass, low speed, stable walking on granular material.

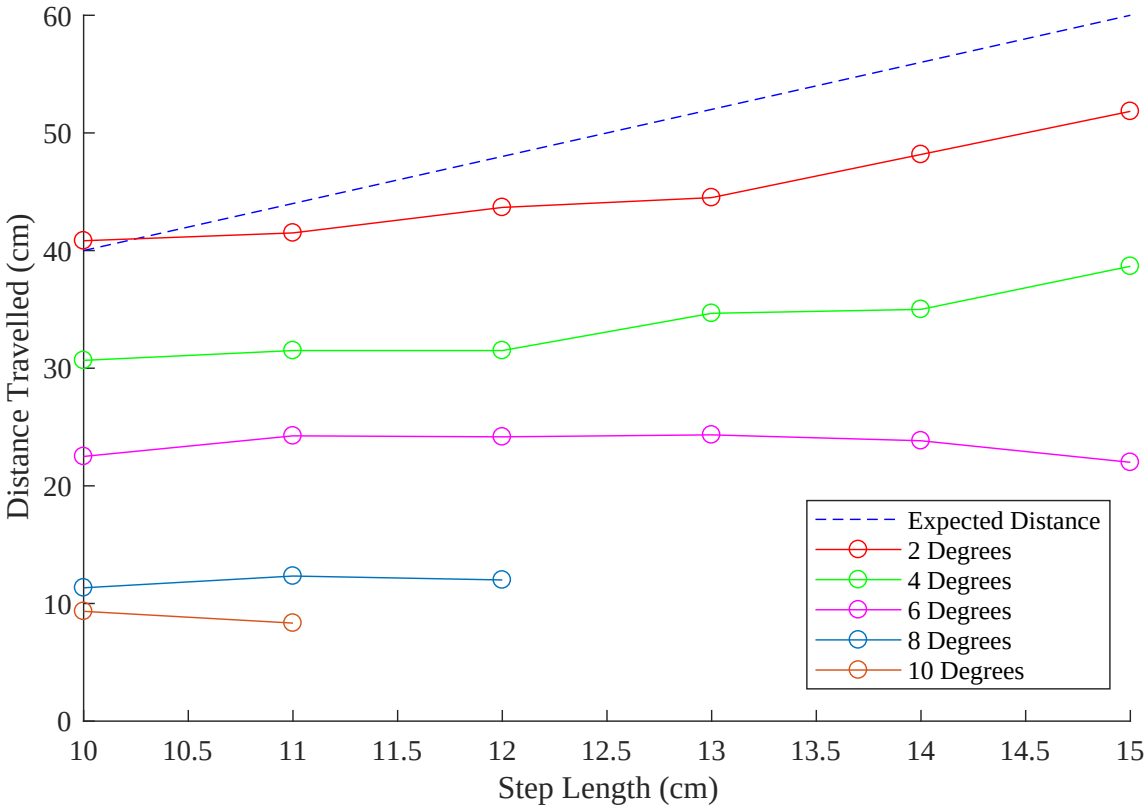

Figure 6.9: Graph showing the expected and actual distance for slope angles between 2° and 10° when the CoM Height is held constant at an average of 18.75cm. This study allowed us to better understand which of our two key postural parameters, CoM or L, played a more significant role in locomotion. We find that like Fig. 6.8 the angles are offset, however, the gradients of the curves become increasingly negative as slope angle is increased.

6.1.9 Torso Servo Control and Linear Actuator Installation

As seen in 6.4 and 6.5, through the use of a simple linear fit, we were able to increase success rates from from 0% at $\theta = 9$ and $\theta = 10$ to 60% and 50% respectively. We theorize that this is due to the significant re-posturing of the 7- DOF system according to slope angle to remain within the polygon of stability. Similarly, this explains why the sensitivities drop off quite sharply at higher angles. If we consider that the support length normal to the lab frame is given by $Lcos(\theta)$ (Fig. 6.2), we find that the polygon of stability becomes smaller as θ increases, thereby leading to more sensitive gaits.

As we examine the sensitivity curves, it becomes evident that the given scheme of gait generation is effective when the walker receives an accurate slope angle as input. However, for smaller perturbations, modeled as small offsets in slope angle from expected angle, we see that the gait effectiveness falls significantly – as much as 100% for 2 degree perturbations. Because of the nonlinear properties of granular material [25], we needed to understand the force profiles at the foot-material boundary [7]. Unlike conventional balance control, to optimize biped walking over granular material it is necessary to characterize how the substrate itself actually yields. Once this was done, we initially hypothesized that through simple inertial control, for instance, in-the-loop torso re-positioning, we could begin to improve sensitivity by combining the IMU and force feedback as a more bioinspired approach to biped walking on complex media.

Because the ZMP walking mechanism is flat footed, we were able to take advantage of the heel and toe differentials to develop a reference force differential input to our control signal. The reasoning behind this was that it would be able to help us model the effect of small bumps or non-uniformities in the context of planar granular surface. We proposed that using simple instantaneous numerical differentiation on the heel and toe differentials would provide a basis on which we augment the control of this system.

In general, this can be modeled as:

$$\dot{F} = \frac{f(F+h) - f(F)}{h} \tag{6.11}$$

Where F is the difference of the instantaneous force feedbacks from the heel and toes, and h is the change in F [16, 17].

Thus, once the gait sensitivity and parameterization experiments were complete, we sought to incorporate torso servo control into the design of the robot. We initially began to use in-the-loop dynamic positioning of the torso to compensate for failure. However, this yielded very little success. In fact, it was found that dynamic, rapid re-positioning actually

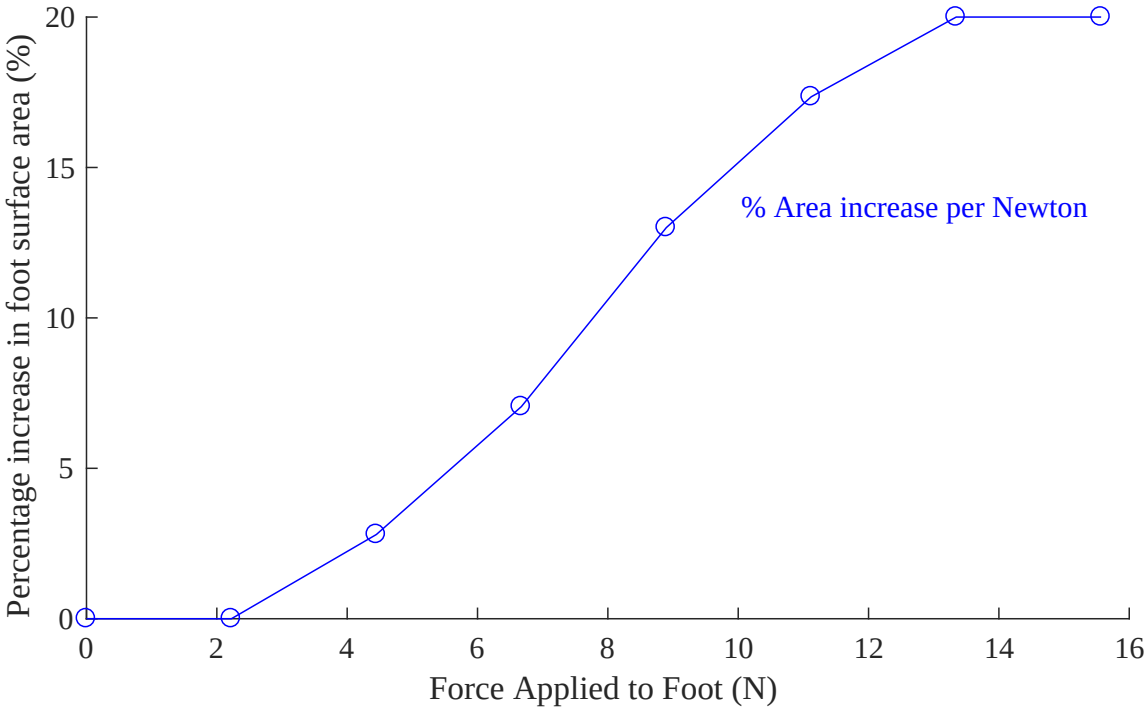

Figure 6.10: Graph showing the total potential increase in foot surface area given an applied force. Maximum potential extension is achieved at 16N, while the total weight of the robot, and thus the maximum potential loading force, is 18N.

created additional moments around the foot-surface boundary, leading to intrusion into the granular material, and hereby creating a higher rate of failure. Thus, we decided to use the torso as a way of redistributing center of mass that was dependent only on the on the angle of the incline. In order to achieve this, we decided to use actual slope angle based feedback into the system for the torso. As seen in Chapters 2 and 3, an IMU was installed on the bed to automatically input an angle to the biped code, at which point it would generate a trajectory accordingly. We therefore adopted this mechanism to feed an input into the position controller, according to the real time bed angle.

To truly develop a novel control scheme based on force profile, we once again looked to nature. As stated in Chapter 1, the biped walker, for the purposes of this thesis, is considered to be a low mass, low speed system. We began examining different biological systems, but perhaps the most interesting case was that of the Sidewinder Rattlesnake,

Crotalus cerastes. This organism expands the contact length of its body up to 40% when ascending slopes of up to 20°. This served as the bio-inspiration that led to the installation of heel and toe actuators that expanded the foot surface up to 20% for slopes up to 10°. (Fig. 6.10). We sought to use the force differential as input, with a case based control system governing the expansion of the foot. If the force differential between the heel and toe indicated that the pressure on one side of the foot was more than 1.25 times higher than undisturbed walking, it was found that this was typically a good indicator that the robot would intrude into the granular media and fail to complete its gait cycle [4]. Thus, in that scenario, the side of the foot close to the high pressure area would expand, thereby distributing pressure and increasing contact area. We hypothesized that this bio-inspired scheme would have significant impact on the success rates and sensitivities of our gaits, and thus, sought to run a second set of systematic experiments examining this. These experiments, as well as their implications, are examined in the remaining subsections of this chapter.

6.1.10 Controlled Gait Success Rates

As stated above, one of the first steps to investigating the effect of the bio-inspired foot design was to test the raw effectiveness of the system. This was done through conducting the same set of experiments as subsection 6.1.4, with the same sets of initial conditions and controlled variables. The process is once again detailed below:

1. As in the previous two iterations of the experiment, a success was defined as the walker completing 4 steps and returning to an initial double support (DSP) position. The bed was leveled and the ground was re-fluidized and reset before each trial.

2. The successful parameters from $\theta = 0^\circ$ to $\theta = 10^\circ$ were then fit with a linear regression, and functions that related all parameters to slope angle were identified for the planar walker.

3. A sweep of trials was again conducted with active foot and torso control,and bed angles from θ=0 to θ=10°, with $\phi = \theta$. Ten trials were run at each bed angle (n= 10) trials. This gave an experimental data set size of 100 total trials.

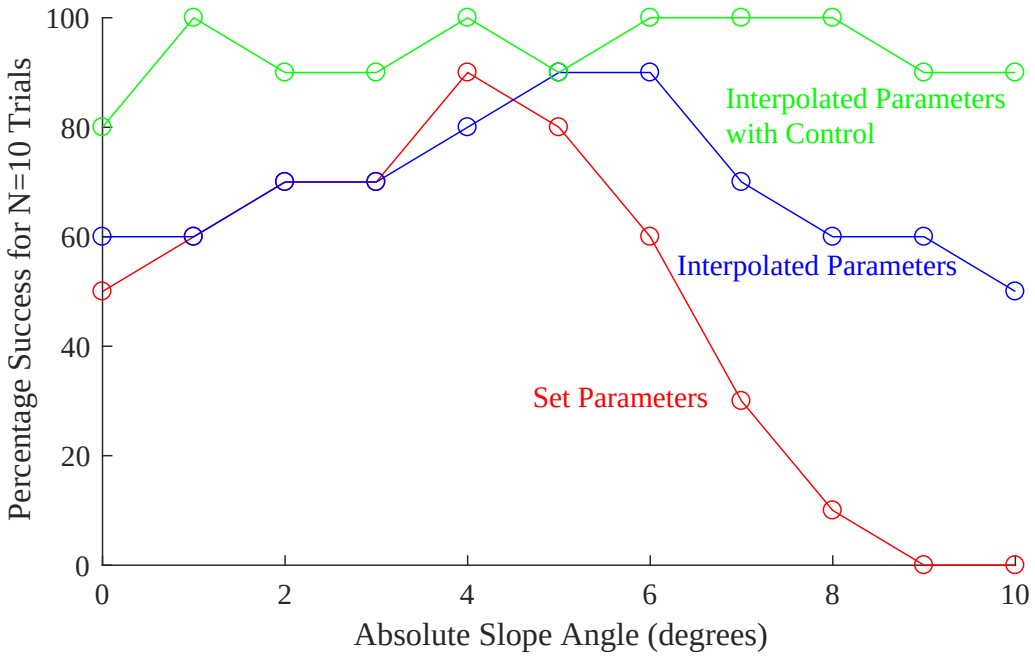

Figure 6.11: Results of trials for set parameter (L = 15cm, CoM = 20.5cm), interpolated parameters, and interpolated parameters with control using the staircase gait. There was an enormous increase in success rates when the control was used, particularly at angles higher than 6°.

when Fig. 6.11 is considered, we see a significant improvement for almost every angle within the limits of the hardware. For angles of θ=10°, we were able to achieve as much as a 40% increase in success rates over interpolated parameters, and an increase of 90% when compared to the set parameter trials. This confirmed our initial hypothesis that this bio-inspired scheme would have significant impact on the success rates, due to the process of stopping the uncontrolled intrusion of the heel or toes, and instead distributing the forces over a wider surface area. Given our success, we then set out to investigate the robustness of this gait through sensitivity testing.

6.1.11 Controlled Gait Sensitivities and Slip

Once the gait was augmented with torso and foot control, we once again tested sensitivities in a similar manner as before. This allowed us to get a fuller picture of the robustness of the controller, since the open loop gait, by design, was specialized to perform at specific slopes. We hypothesized that the sensitivity curves seen in Fig. 6.5 would become more flattened, and less sensitive to perturbation as raw success rates increased. As before, used systematic sensitivity experiments that modelled this disturbance as a deviation from the commanded slope angle.The process followed was the same as before:

1. A slope angle of $\theta = 2^\circ$ was input into the gait code, for n = 6 steps. A success was defined as the walker completing all 6 steps and returning to an initial DSP position. The bed was leveled and the granular terrain was reset through the air fluidized before each trial.

2. The bed was raised to the corresponding θ input into the code, and the robot was run N = 3 times, each time recording the distance, and at the end of the third trial, establishing an average distance. This was considered to be our benchmark distance, or our relative distance of 1.

3. The bed was then lowered to an angle of (θ–1°), while keeping then same input angle of θ in the code. The robot was run N = 3 times, each time recording the distance, and at the end of the third trial, establishing an average distance. This distance was then divided by the average distance at θ to obtain a relative distance traveled. This is important due to failure and slippage of the robot.

4. Once more, the bed was lowered to (θ–2°) and the robot was run N = 3 times, each time recording the distance, and at the end of the third trial, establishing an average distance. This distance was once again divided by the distance traveled at slope θ in order to obtain a relative distance traveled.

5. This process was further repeated another 2 times, this time increasing the bed angle beyond that of the commanded angle. Thus, for a commanded angle of θ, the actual bed angles would have been $(\theta + 1^\circ)$ and $(\theta + 2^\circ)$ respectively.

6. After the relative distances were analyzed for a commanded gait angle of θ=2°, the entire process was then repeated for θ=4°, 6°, 8° and 10°, giving a grand total of 150 experimental trials.

When compared to the underlay of 6.5, we find that the sensitivity experiments conducted using the foot and torso control (Fig. 6.12) yield results that indicate a far more robust gait. we find that for angles of $\theta < 6^\circ$, the gait is almost flat - an excellent indication of gait robustness. at higher angles, especially $\theta = 8^\circ$ and $\theta = 10^\circ$, there is significant drop off on the right side of the sensitivity curves. It should be noted that this was not caused by robot failure, but by failure of the material itself; the robot would continually slide backward, unable to continue forward progress. As such, it became necessary to analyze the slip patterns with the controller.

Upon investigation of slip with the robot, it was found that when the controller was turned on, there was no appreciable improvement for undisturbed gait (6.13). This is due to the fact that when the commanded gaits and the actual gaits of the slope are in agreement, the controller does not have to contribute as much to the overall stabilization of the system. It then became necessary to conduct a set of "pseudo-sensitivity" trials where the bed was offset by -2° and $+2^\circ$. This yielded an interesting set of results, which can be seen in Figs. 6.14 and 6.15. In Fig. 6.14, the bed has a negative offset, and we observe that at higher angles, the open loop gait is unable to move the system forward. However, when the foot controller is introduced, the robot is able to move forward more, even at higher slope angles. We hypothesize that this is due to the dispersion of the forces through the expanding feet. This limited the magnitude of the pressures transmitted to the granular surfaces, therefore making it more difficult to start the process of granular flow.

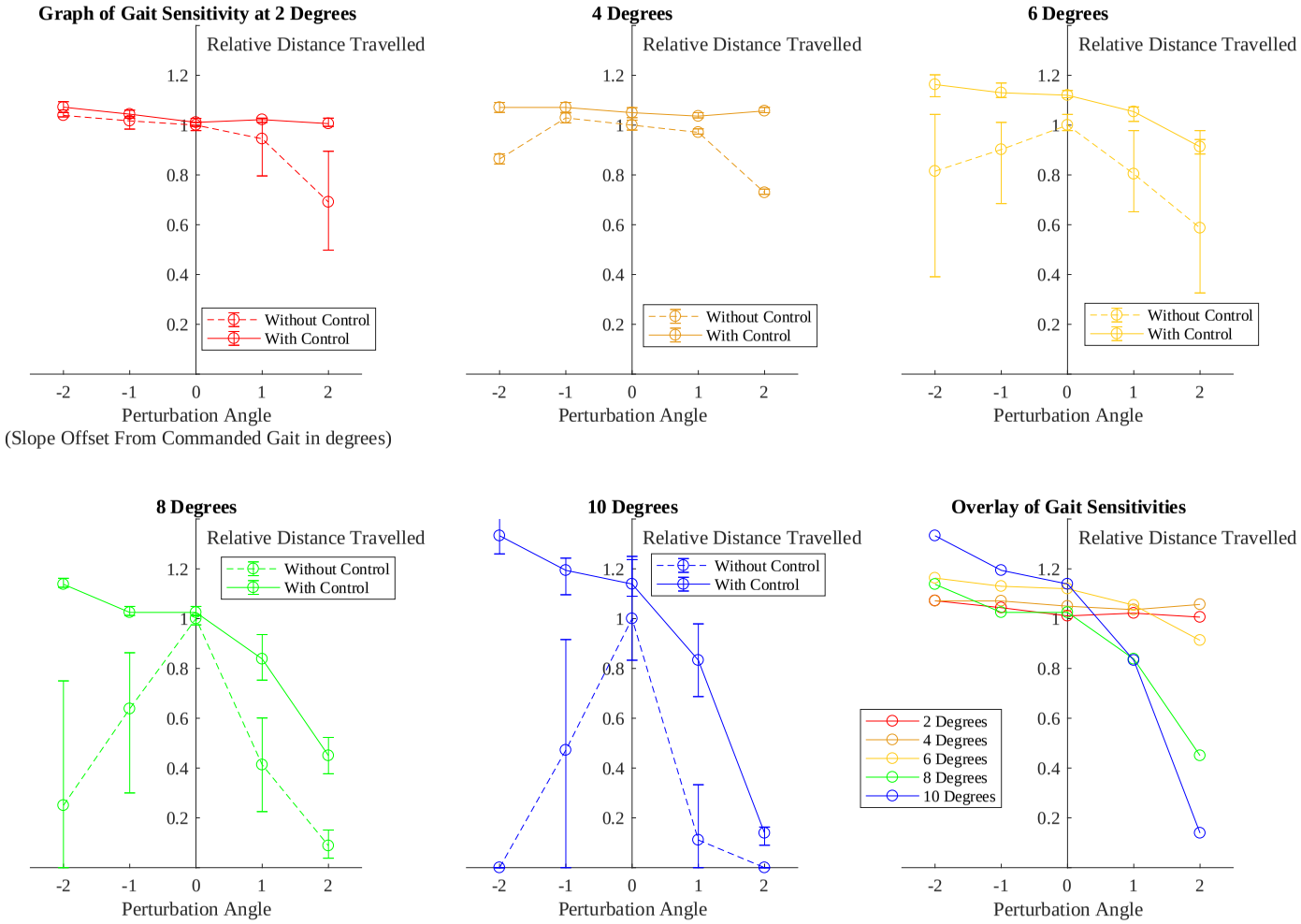

Figure 6.12: Gait sensitivity plots for biped staircase ZMP gait with torso and foot control from 2 to 10°. As before, relative distance was used instead of absolute distance because of varying step lengths when climbing the slope. The initial sensitivity trials are under-laid in dashed lines. We see a significant increase in robustness, especially at lower gaits. At higher gaits, such as 10°, there is an improvement in sensitivity, however, the robot is then sliding backward too much to achieve forward progress, resulting in small relative distances.

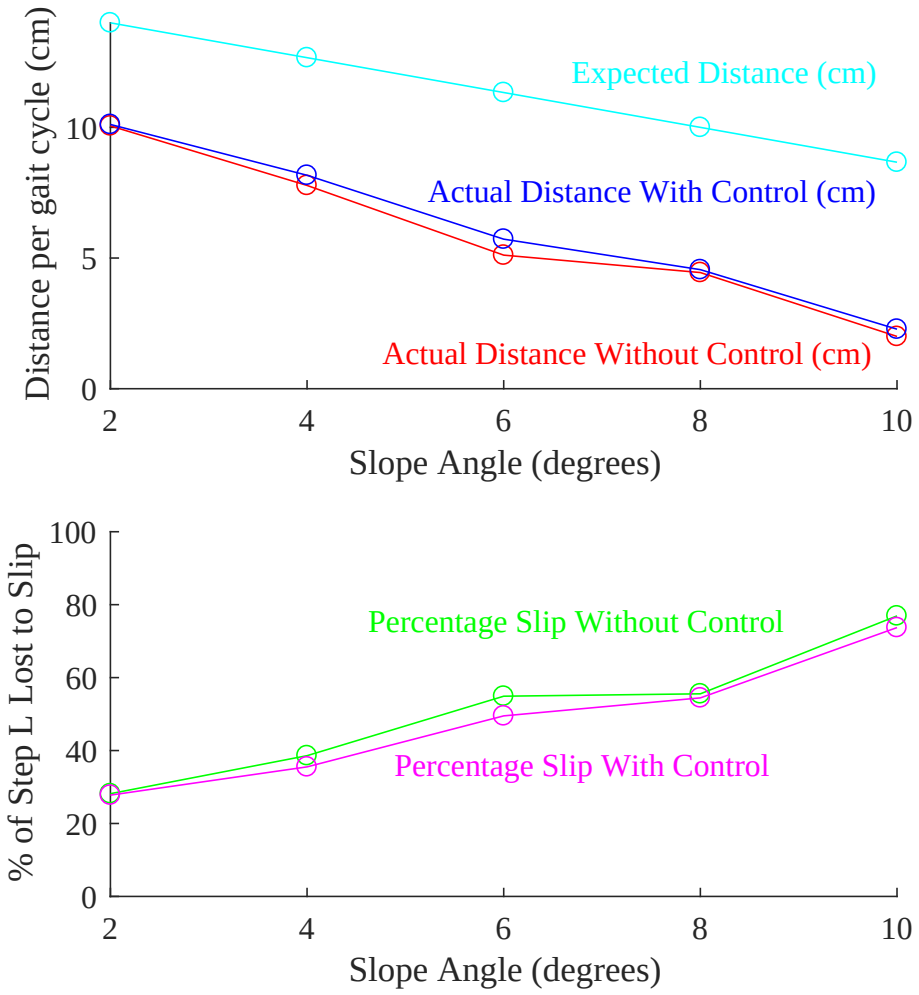

Figure 6.13: Graph showing the actual and commanded distance for slope angles between 2° and 10°, with and without control. This graph shows undisturbed gait, as as such, without the need for much control, the slip distances with and without the controller are quite similar.

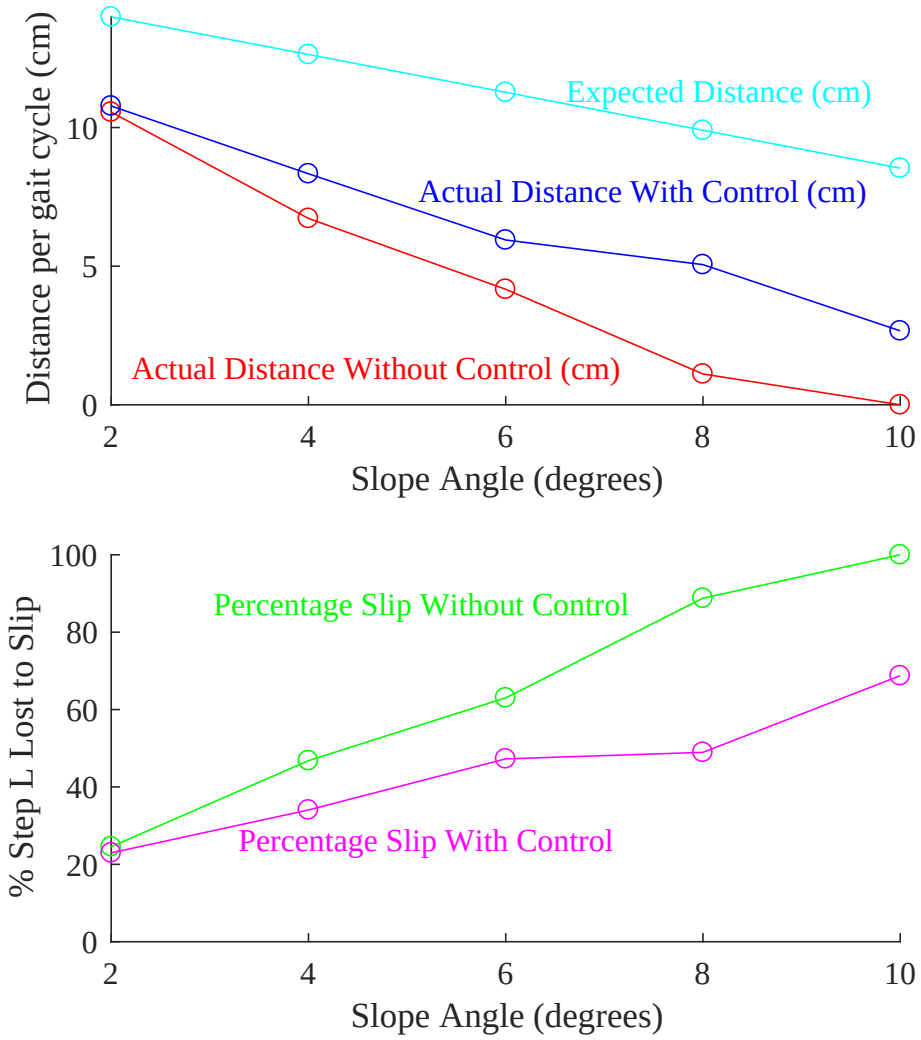

Figure 6.14: Graph showing the actual and commanded distance for slope angles between 2° and 10°, with and without control. This graph shows a negative offset of 2°. In this scenario, at higher angles, the open loop gait is unable to make any forward progress, but with the controller on, the system performance improves. This is credited to the dispersion of forces through the expanding feet, making it less likely that the surface will 'avalanche'.

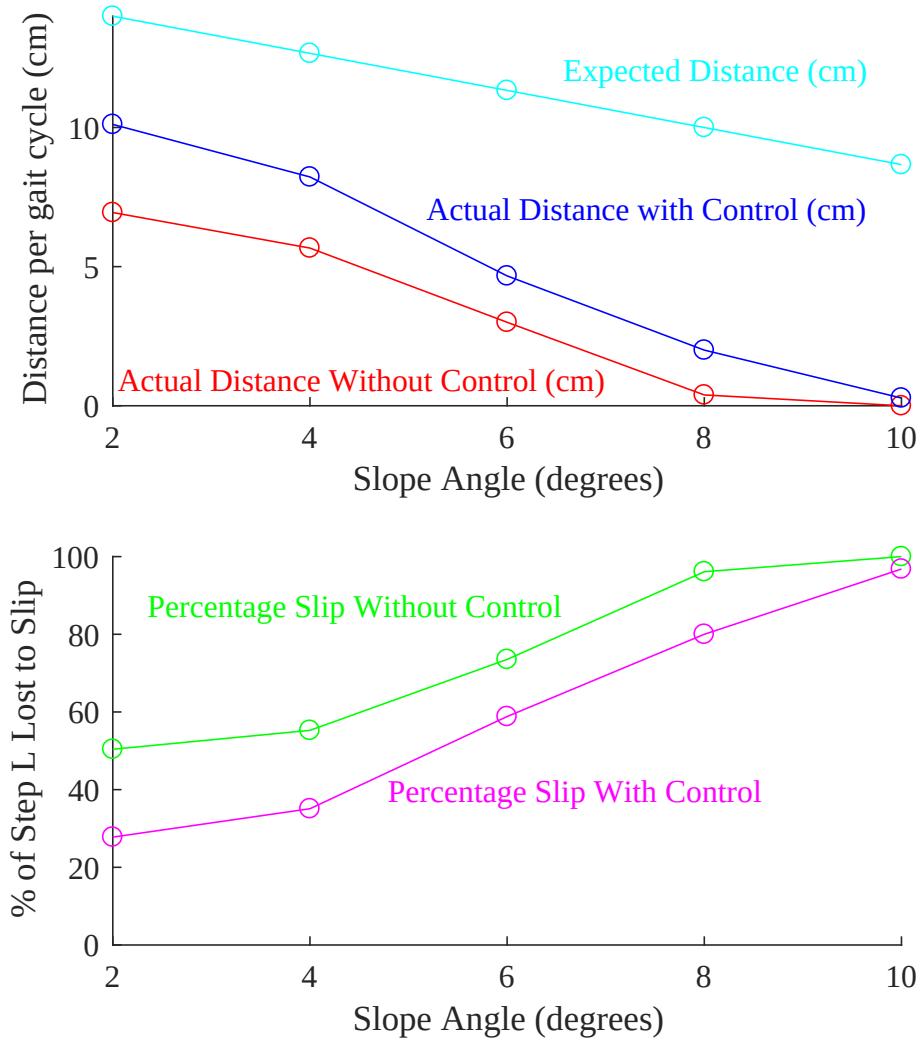

Figure 6.15: Graph showing the actual and commanded distance for slope angles between 2° and 10°, with and without control. This graph shows a positive offset of 2°. In this scenario, at higher angles, the controlled gait starts with an advantage, but the curves converge at higher angles.

In Fig. 6.15, we observe an interesting trend where the controlled gait initially has an advantage, we hypothesize, due to the process of force dispersion as mentioned above. However, amount of slip associated with the controlled and uncontrolled gaits become convergent, and finally meet at 10°. We hypothesize that this is due to the existence of a 'zero stiction point' for low mass systems. For those systems that walk along the surface of the sand, this 'zero stiction point' is that angle where the friction of contact, or stiction, is completely overcome by gravitational and reactionary lateral flow forces of the granular media. This is a key area that will be investigated in our future work.

6.1.12 Robot Limitations and Processing Capability

Over the course of the experiments described above, most of the low level joint position control was done on the embedded micro-controllers on the MX-64 servos, while the trajectory generation was done using a remote PC. This and the Arduino Uno used for the torso and foot control continue to serve their purposes quite well. However, these schemes are implemented on top of open loop gait. Thus, to fully integrate the gait trajectory and with real-time control regulation, we require a system that is fully on-board the robot itself. Currently, the time delay and synchronization errors associated with making real time gait adjustments on the remote PC are far too high for a controller to be reasonably implemented. This will require a more powerful micro-controller, such as a BeagleBone or Arduino Due, that can process trajectory, torso and foot control simultaneously.

6.2 Conclusions and Future Work

This thesis outlined the design and and implementation of a robust uphill gait scheme on a low mass, planar biped walking system using a specialized test bed of granular material. We were able to show that through the optimization of open loop gait, variation of inertial properties, and development of contact area control, a robust locomotion system for biped robotic locomotion on granular media can be identified and implemented. In order

to achieve this, project, we performed a series of systematic design implementations, trials and experiments to enable a 7 degree-of-freedom planar biped walker to robustly traverse granular inclines. In addition to the actual implementation of our control scheme, we were also able to investigate the dominant parameters when faced with low speed, non-intrusion based gait on granular media, as well as the effects and magnitude of backward slip on the system.

In the future, we will focus on the problem of slip at higher angles. We propose the augmentation of the current gait scheme and foot control to allow for the reduction of backward slip. This is important, due to the fact that the current control scheme, while maintaining stability, does not ensure forward progress of the biped at any given angle. At higher angles, this begins to enter the realm of climbing robots, at which point, the idea of using a strictly bipedal system may not be entirely feasible, and a ”pseudo-quadrupedal” gait may need to be implemented.

Another future direction will be the expansion of the gait scheme to allow for a full range of inclines and declines. Even though the current scheme has proven to be translatable to declines based on initial qualitative analysis, negative slopes present a new set of challenges. Foremost among these is the idea of amplification of the backward slip problem during inclined gait. We have called this the ”ski” problem, in which the robot loses traction, and while remaining dynamically stable, slips all the way down a given incline.

Apart from this, there are a few long term additions to the system that we seek to implement. We plan to fully automate the test bed system to allow for a high number of experiments to be conducted within a relatively short time frame, without the need for operator input. This is the limiting factor in terms of the amount of data collected, as well as the times at which the robot is able to be operated. Additionally, we intend to begin the investigation of the system when operated at high speed, to see what the differences in controller needs may be.

All in all, this thesis has highlighted the iterative design and systematic experimentation

on a biped robotic system, in order to devise a scheme for low mass walking on granular material. We hope that this in turn, will then lay the foundation for even more exciting, thought provoking, and groundbreaking work to come.

Appendices

APPENDIX A

PART DRAWINGS

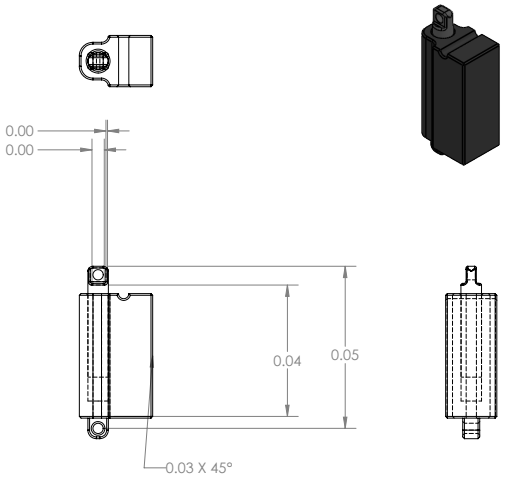

Figure A.1: Firgelli Linear Actuator. All dimensions in inches

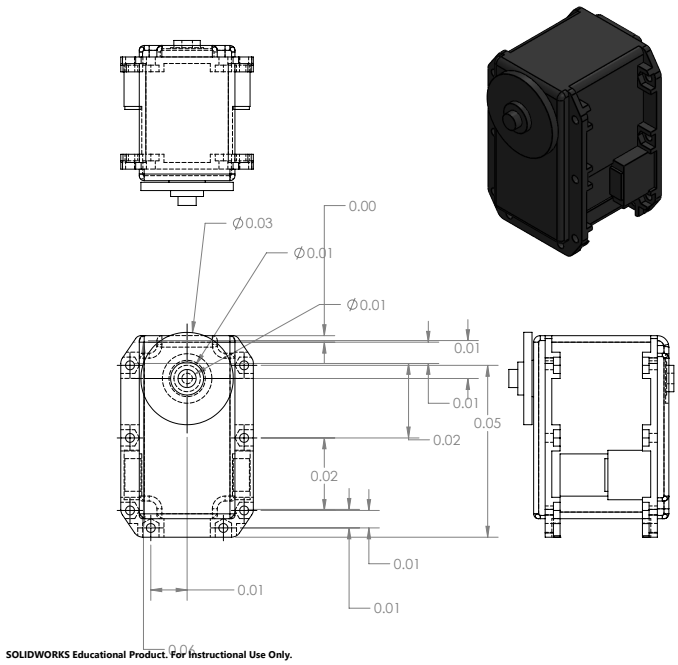

Figure A.2: MX-64T Servo Motor. All dimensions in inches

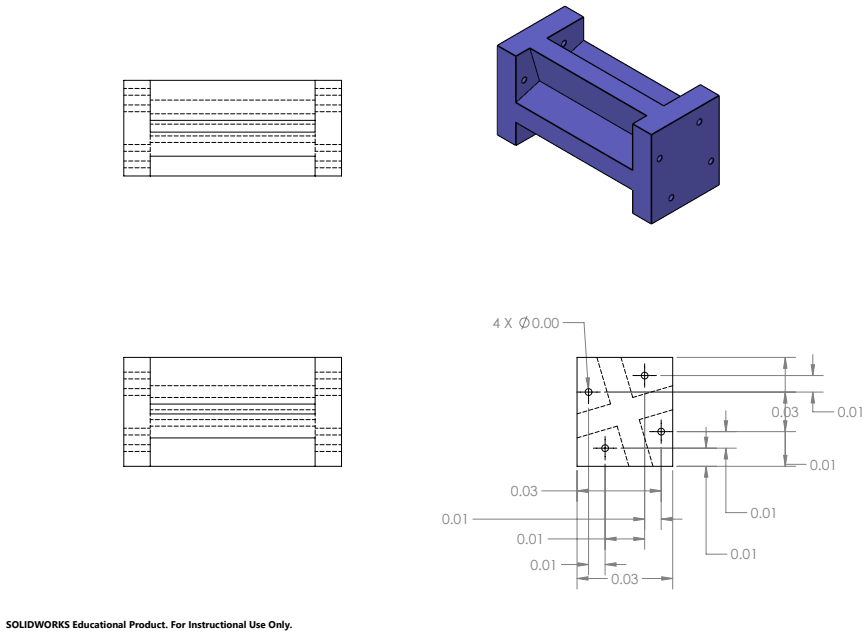

Figure A.3: Leg Connection. All dimensions in inches

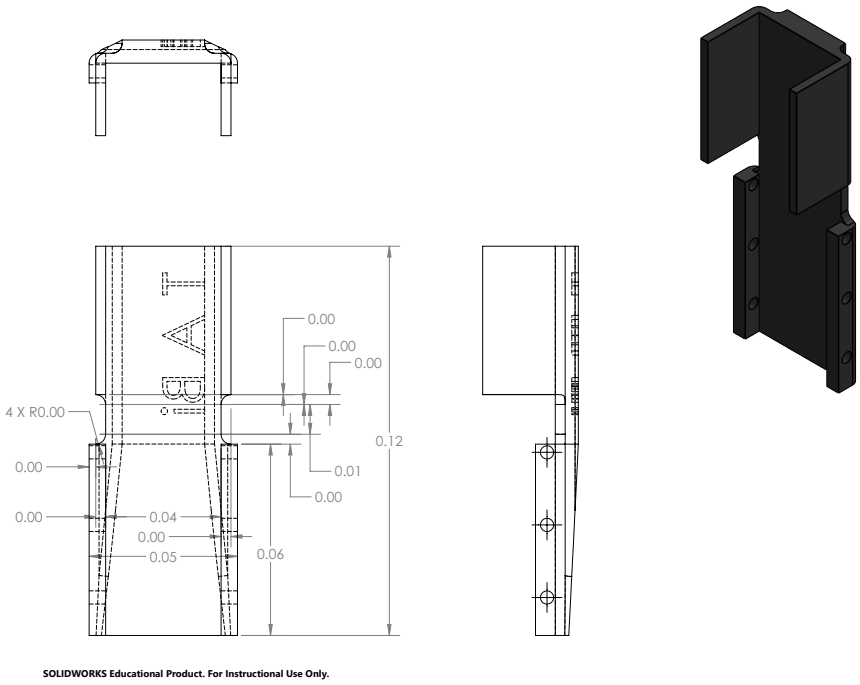

Figure A.4: Protective Cladding for Legs. All dimensions in inches

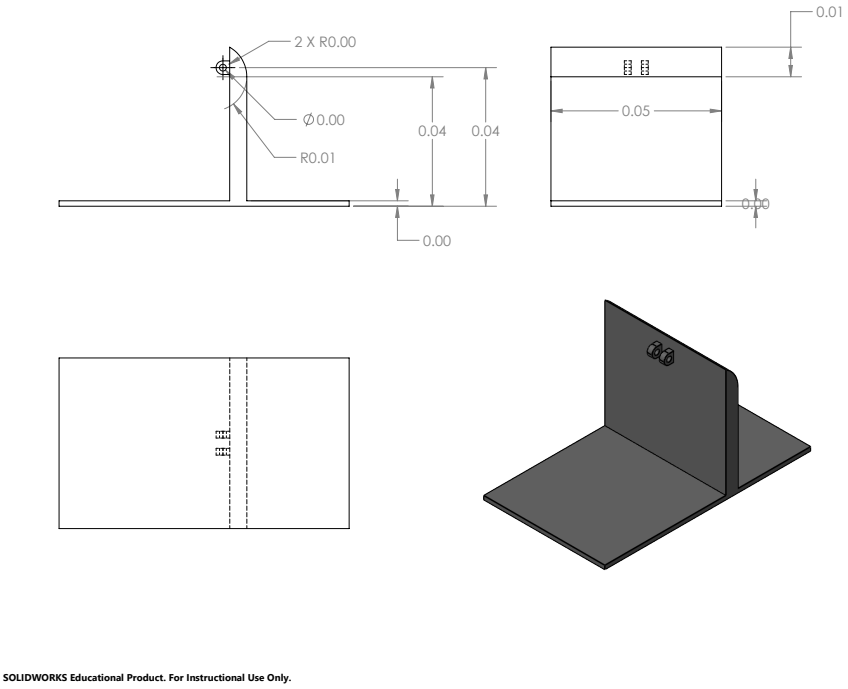

Figure A.5: Heel and Toe Foot Components. All dimensions in inches

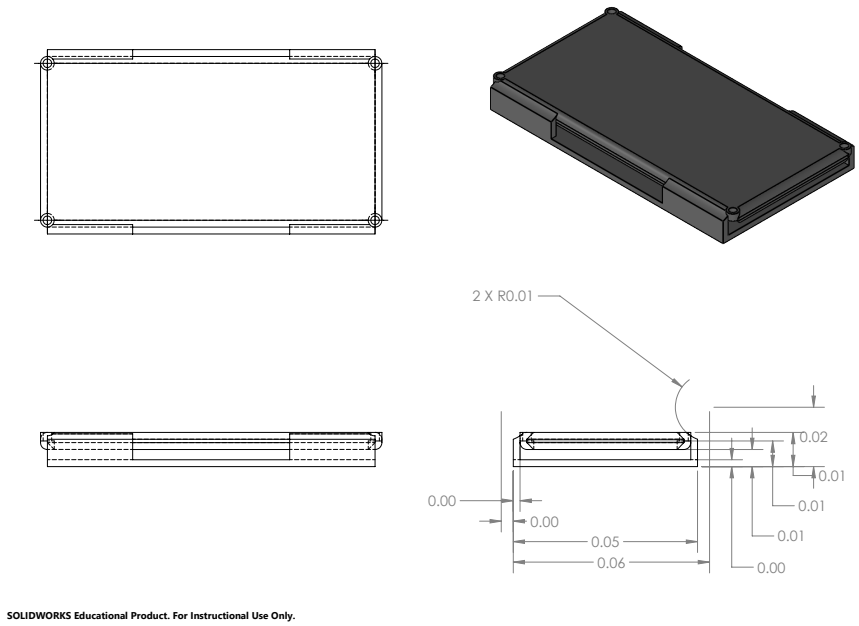

Figure A.6: Base of Foot. All dimensions in inches

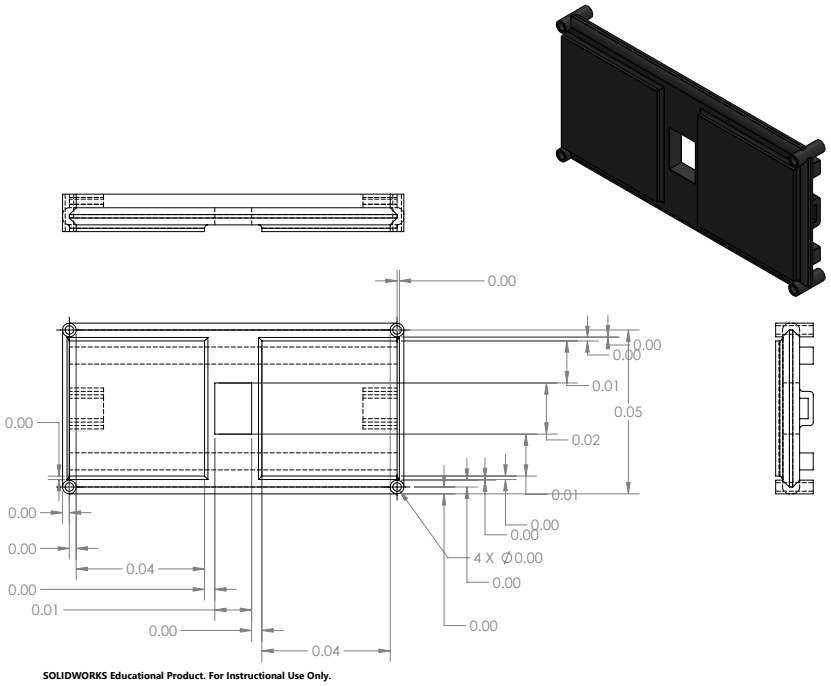

Figure A.7: Middle Of Foot. All dimensions in inches

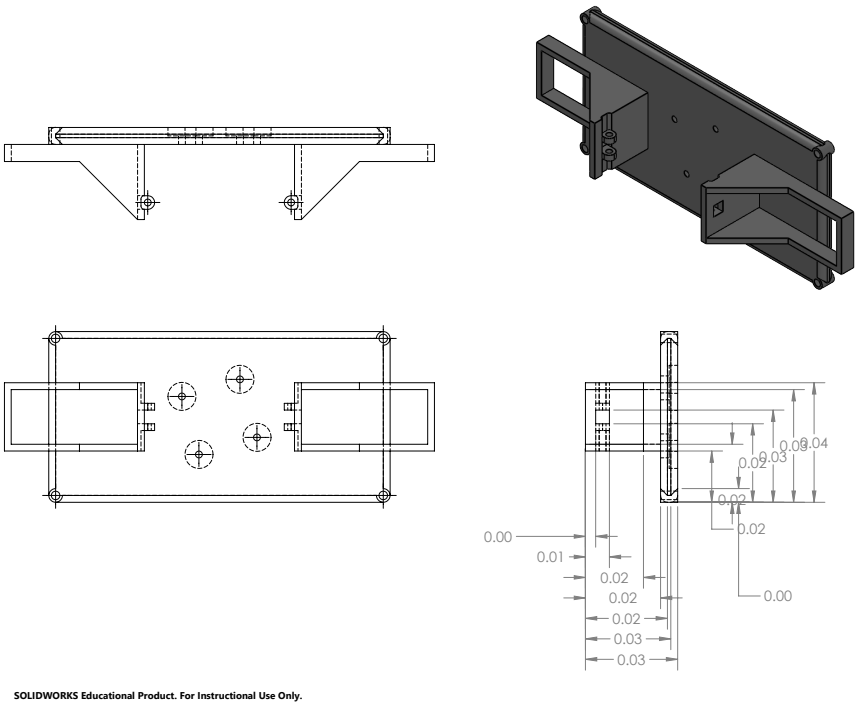

Figure A.8: Top of Foot with Actuator Attachments. All dimensions in inches

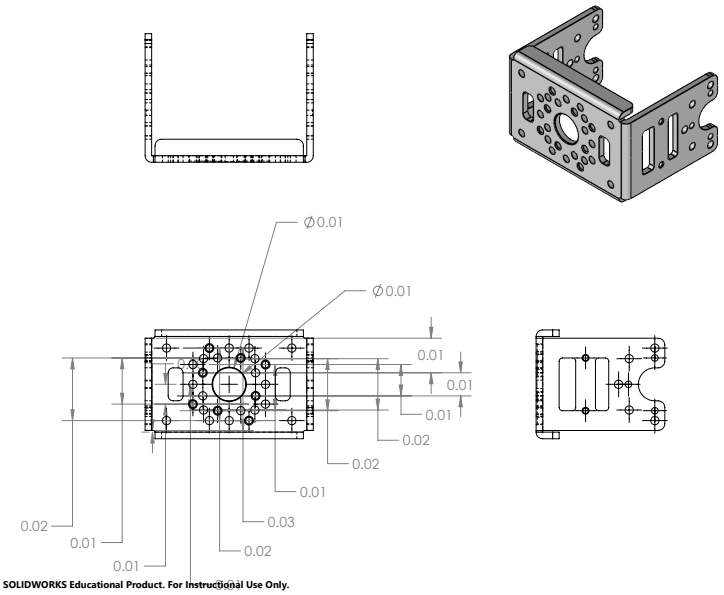

Figure A.9: Joint Bracket for Actuators. All dimensions in inches

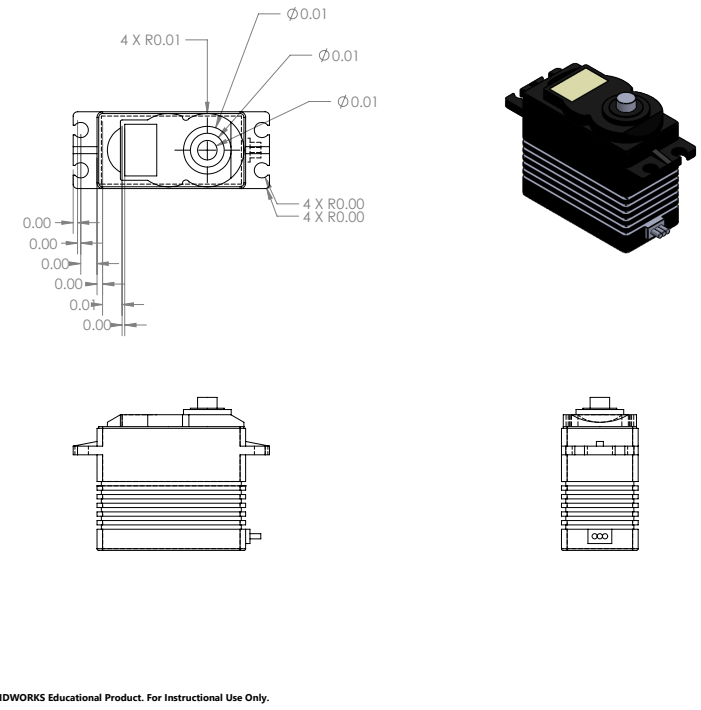

Figure A.10: Hi-Tech High Torque Servo. All dimensions in inches

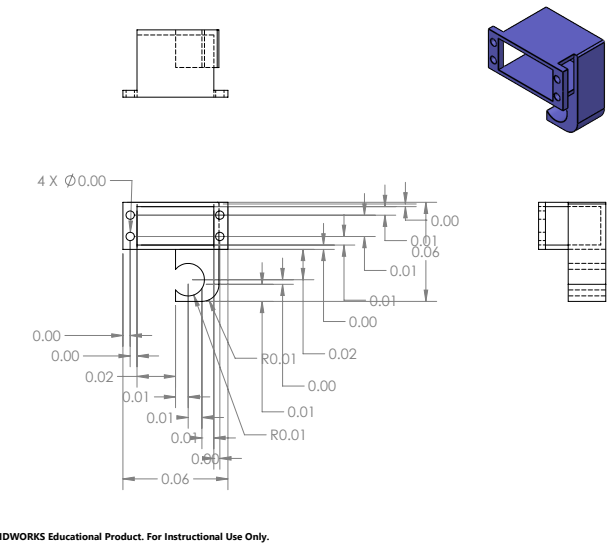

Figure A.11: Bracket for High Torque Servo. All dimensions in inches

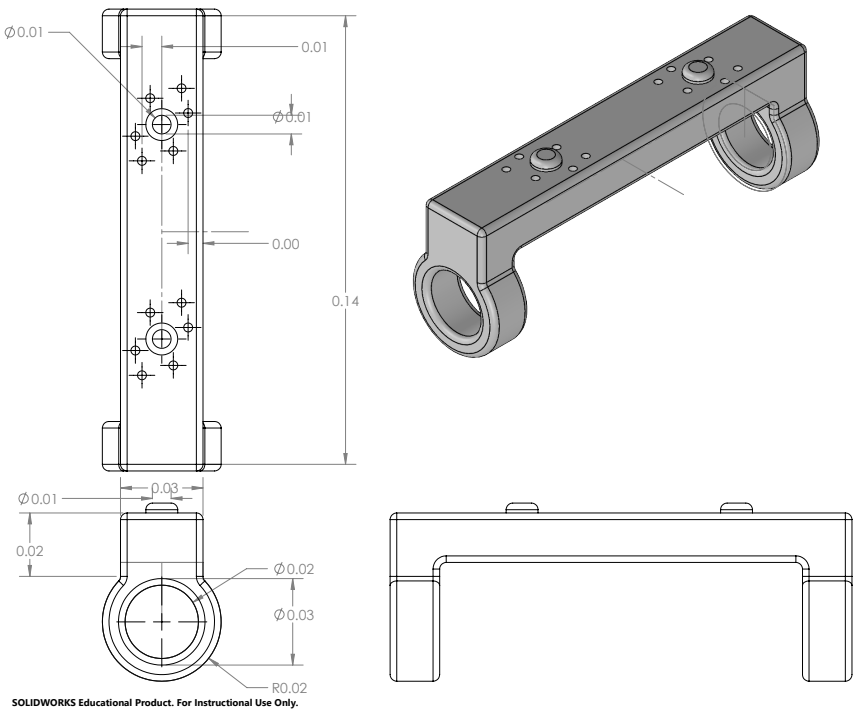

Figure A.12: Main Torso Servo Attachment Point. All dimensions in inches

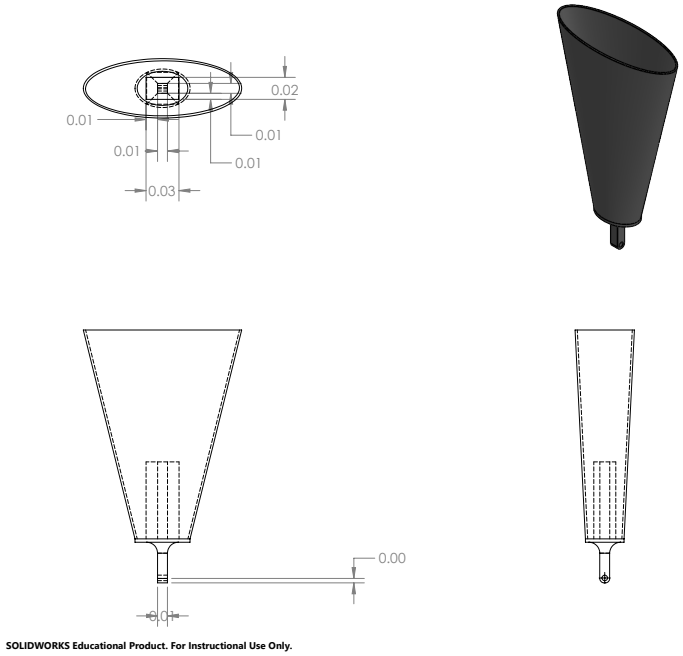

Figure A.13: Weighted Torso. All dimensions in inches

APPENDIX B

MINIMUM PARTS LIST

All prices in the Bill of Materials on the following page are in USD. The total cost of the experimental setup was calculated to be $6,237.05. It should be noted that this does not account for small materials available through the lab, such as wiring, resistors, LED's and protoboards, which may prove useful in the design and implementation of the robotic walker.

Item	Vendor	Part Number	Qty.	Cost
Varable DC Power Supply Unit	Amazon	KPS3010D	2	84.99
9DOF IMU	Sparkfun	LSM9DS0	2	9.94
Toro Ultra Blower/Vacuum	T.H.D.	51619	2	69.97
10 Foot Aluminum T-Slot Rail	McMaster Carr	47065T101	4	30.54
Aluminum Corner Bracket	McMaster Carr	47065T236	30	5.21
Aluminum Surface Bracket	McMaster Carr	47065T255	20	6.07
Zinc Plated Steel Mounting Screw	McMaster Carr	47065T142	30	2.29
Low Friction Rail (sold per mm)	McMaster Carr	972K5K3	2500	0.38
Rail Carriage Bearing Assembly	McMaster Carr	972K5K2	4	43.33
1/4” Clear Acrylic sheet, 48”x48”	McMaster Carr	8560K436	1	181.19
Rubber Sealant for Air Chamber	McMaster Carr	5546K42	25	1.72
Ducting Hose for Blowers	McMaster Carr	5152k44	12	4.83
Aluminum Honeycomb Filters	McMaster Carr	2150K12	4	27.83
3M Silicone Sealant	McMaster Carr	74955A54	1	16.64
V-Groove Top Reading Level	McMaster Carr	2151A45	2	10.46
Ball Bearings for Carriage Rod	McMaster Carr	2342K186	2	14.84
12 Inch Rotary Shaft	McMaster Carr	2342K186	1	8.43
Carbon Fiber Sheet	McMaster Carr	8181K12	1	36.58
Structural Acrylic Sheet	McMaster Carr	8589K84	1	62.45
Remote control Transmitter	McMaster Carr	8129A83	1	43.08
Remote control Receiver	McMaster Carr	8129A59	1	68
Firgelli Heavy Duty 40” Actuator	Firgelli	FA-200-IP66-12	2	249.99
Unwashed Poppy Seeds	Spices Inc	100139 013	1	174.56
Spiral Cable Wrap	Amazon	14625	1	7.49
Robotis MX-64AT Servo Motors	Robotis	902-0060-000	6	299.99
X3P Robot Cable	Robotis	903-0249-000	1	15.9
Stratasys Dimension Cartridge	AET Labs	340-21203	2	130
Hitech HS-7980TH Servo	ServoCity	37980S	1	174.99
Arduino Uno Starter Kit	Amazon	ARD22_LCD	1	53.99
Robotis Side Frame Set	Trossen	RO-903-0160	6	11.9
Robotis Hinge Frame Set	Trossen	RO-903-0159	6	27.9
Servo Manager Kit	Trossen	KIT-DXL-MGR	1	90.95
Bioloid Nut and Bolt Set	Trossen	RO-903-0055	1	23.4
Force Sensitive Resistors	Adafruit	FSR406	4	8.94
Firgelli PQ12 MicroActuators	Firgelli	PQ12-P	4	65

REFERENCES

[1] Q. Huang, Y. Nakamura, and T. Inamura, "Humanoids walk with feedforward dynamic pattern and feedback sensory reflection," in *Robotics and Automation, 2001. Proceedings 2001 ICRA. IEEE International Conference on*, IEEE, vol. 4, 2001, pp. 4220–4225.

[2] J. Aguilar, T. Zhang, F. Qian, M. Kingsbury, B. McInroe, N. Mazouchova, C. Li, R. Maladen, C. Gong, M. Travers, *et al.*, "A review on locomotion robophysics: The study of movement at the intersection of robotics, soft matter and dynamical systems," *Reports on Progress in Physics*, vol. 79, no. 11, p. 110 001, 2016.

[3] X. Xiong, A. D. Ames, and D. I. Goldman, "A stability region criterion for flat-footed bipedal walking on deformable granular terrain," in *Intelligent Robots and Systems (IROS), 2017 IEEE/RSJ International Conference on*, IEEE, 2017, pp. 4552–4559.

[4] J. Gosyne, C. Hubkici, X. Xiong, A. Ames, and D. Goldman, "Bipedal locomtion up sandy slopes: Systematic experiments using zero moment point methods," *Humanoid Robots (Humanoids), 2018 18th IEEE-RAS International Conference on*, 2018.

[5] T. M. Lejeune, P. A. Willems, and N. C. Heglund, "Mechanics and energetics of human locomotion on sand.," *Journal of Experimental Biology*, vol. 201, no. 13, pp. 2071–2080, 1998.

[6] H. Marvi, C. Gong, N. Gravish, H. Astley, M. Travers, R. L. Hatton, J. R. Mendelson, H. Choset, D. L. Hu, and D. I. Goldman, "Sidewinding with minimal slip: Snake and robot ascent of sandy slopes," *Science*, vol. 346, no. 6206, pp. 224–229, 2014.

[7] C. Li, T. Zhang, and D. I. Goldman, "A terradynamics of legged locomotion on granular media," *Science*, vol. 339, no. 6126, pp. 1408–1412, 2013.

[8] E. R. Westervelt, J. W. Grizzle, and D. E. Koditschek, "Hybrid zero dynamics of planar biped walkers," *IEEE Transactions on Automatic Control*, 2003.

[9] S. Kajita, F. Kanehiro, K. Kaneko, K. Fujiwara, K. Harada, K. Yokoi, and H. Hirukawa, "Biped walking pattern generation by using preview control of zero-moment point," in *ICRA*, vol. 3, 2003, pp. 1620–1626.

[10] C.-C. Huang, "Biped robot with a vestibular system," PhD thesis, Virginia Tech, 1991.

[11] D. A. Winter, A. E. Patla, and J. S. Frank, "Assessment of balance control in humans," *Med Prog Technol*, vol. 16, no. 1-2, pp. 31–51, 1990.

[12] A. V. Cuppone, V. Squeri, M. Semprini, L. Masia, and J. Konczak, "Robot-assisted proprioceptive training with added vibro-tactile feedback enhances somatosensory and motor performance," *PloS one*, vol. 11, no. 10, e0164511, 2016.

[13] K. Hashimoto, Y. Takezaki, H. Motohashi, T. Otani, T. Kishi, H.-o. Lim, and A. Takanishi, "Biped walking stabilization based on gait analysis," in *Robotics and Automation (ICRA), 2012 IEEE International Conference on*, IEEE, 2012, pp. 154–159.

[14] W. Huang, C.-M. Chew, Y. Zheng, and G.-S. Hong, "Pattern generation for bipedal walking on slopes and stairs," in *Humanoid Robots, 2008. Humanoids 2008. 8th IEEE-RAS International Conference on*, IEEE, 2008, pp. 205–210.

[15] T. Sato, S. Sakaino, E. Ohashi, and K. Ohnishi, "Walking trajectory planning on stairs using virtual slope for biped robots," *IEEE transactions on industrial electronics*, vol. 58, no. 4, pp. 1385–1396, 2011.

[16] K. Kondak and G. Hommel, "Control algorithm for stable walking of biped robots," in *Proceedings of the International Conference on Climbing and Walking Robots (CLAWAR)*, 2003, pp. 119–126.

[17] A. Hereid, S. Kolathaya, M. S. Jones, J. Van Why, J. W. Hurst, and A. D. Ames, "Dynamic multi-domain bipedal walking with atrias through slip based human-inspired control," in *Proceedings of the 17th international conference on Hybrid systems: computation and control*, ACM, 2014, pp. 263–272.

[18] A. Polanski, A. Switonski, H. Josinski, K. Jedrasiak, and K. Wojciechowski, "Estimation system for forces and torques in a biped motion," in *International Conference on Computer Vision and Graphics*, Springer, 2010, pp. 185–192.

[19] J. Aguilar and D. I. Goldman, "Robophysical study of jumping dynamics on granular media," *Nature Physics*, vol. 12, no. 3, p. 278, 2016.

[20] P. F. Meyer, L. I. Oddsson, and C. J. De Luca, "The role of plantar cutaneous sensation in unperturbed stance," *Experimental brain research*, vol. 156, no. 4, pp. 505–512, 2004.

[21] Y. Wang and S. Wang, "A new directional-intent recognition method for walking training using an omnidirectional robot," *Journal of Intelligent & Robotic Systems*, vol. 87, no. 2, pp. 231–246, 2017.

[22] P.-B. Wieber, "Trajectory free linear model predictive control for stable walking in the presence of strong perturbations," in *IEEE-RAS international conference on humanoid robots*, 2006.

[23] C. G. Atkeson and B. Stephens, "Multiple balance strategies from one optimization criterion," in *Humanoid Robots, 2007 7th IEEE-RAS International Conference on*, IEEE, 2007, pp. 57–64.

[24] M. Morisawa, S. Kajita, F. Kanehiro, K. Kaneko, K. Miura, and K. Yokoi, "Balance control based on capture point error compensation for biped walking on uneven terrain," in *Humanoid Robots (Humanoids), 2012 12th IEEE-RAS International Conference on*, IEEE, 2012, pp. 734–740.

[25] N. Gravish and D. I. Goldman, "Effect of volume fraction on granular avalanche dynamics," *Physical Review E*, vol. 90, no. 3, p. 032 202, 2014.

[26] Ell, Miskatonic, and Chelsea, *Sparkfun electronics*.

[27] H. Geyer, A. Seyfarth, and R. Blickhan, "Compliant leg behaviour explains basic dynamics of walking and running," *Proceedings of the Royal Society of London B: Biological Sciences*, vol. 273, no. 1603, pp. 2861–2867, 2006.

[28] A. D. Kuo, J. M. Donelan, and A. Ruina, "Energetic consequences of walking like an inverted pendulum: Step-to-step transitions," *Exercise and sport sciences reviews*, vol. 33, no. 2, pp. 88–97, 2005.

[29] A. D. Ames, "Human-inspired control of bipedal walking robots.," *IEEE Trans. Automat. Contr.*, vol. 59, no. 5, pp. 1115–1130, 2014.

[30] B. McInroe, H. C. Astley, C. Gong, S. M. Kawano, P. E. Schiebel, J. M. Rieser, H. Choset, R. W. Blob, and D. I. Goldman, "Tail use improves performance on soft substrates in models of early vertebrate land locomotors," *Science*, vol. 353, no. 6295, pp. 154–158, 2016.

[31] J. Pratt, J. Carff, S. Drakunov, and A. Goswami, "Capture point: A step toward humanoid push recovery," in *Humanoid Robots, 2006 6th IEEE-RAS International Conference on*, IEEE, 2006, pp. 200–207.

[32] D. J. Farris and G. S. Sawicki, "The mechanics and energetics of human walking and running: A joint level perspective," *Journal of The Royal Society Interface*, rsif20110182, 2011.